



Universitat Autònoma de Barcelona

ADVERTIMENT. L'accés als continguts d'aquesta tesi queda condicionat a l'acceptació de les condicions d'ús establertes per la següent llicència Creative Commons:  http://cat.creativecommons.org/?page_id=184

ADVERTENCIA. El acceso a los contenidos de esta tesis queda condicionado a la aceptación de las condiciones de uso establecidas por la siguiente licencia Creative Commons:  <http://es.creativecommons.org/blog/licencias/>

WARNING. The access to the contents of this doctoral thesis it is limited to the acceptance of the use conditions set by the following Creative Commons license:  <https://creativecommons.org/licenses/?lang=en>



DOCTORAL THESIS

Non-invasive
imaging of the
metabolic state of
oocytes, cumulus
cells and embryos

MARTA VENTURAS PEDRO

Universitat Autònoma de Barcelona
Doctoral program in Cellular Biology

UAB



HARVARD
UNIVERSITY

 BOSTON IVF

 UNIVERSITY OF
OXFORD

 BRIGHAM AND
WOMEN'S HOSPITAL

**UNIVERSITAT AUTONOMA DE
BARCELONA**

DOCTORAL THESIS

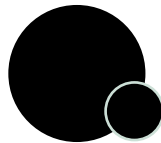
**Non-invasive imaging of the
metabolic state of oocytes,
cumulus cells and embryos**

Author
Marta Venturas Pedro

Director
Dan Needleman

Tutor
Joan Blanco

A compendia of publications doctoral thesis presented for the PhD program in
Cellular Biology at the Universitat Autònoma de Barcelona



Work presented in this thesis was undertaken in The Needleman Lab, department of
Molecular and Cellular Biology at Harvard University, Cambridge, Massachusetts, USA.



HARVARD
UNIVERSITY

Dr. Daniel Needleman, Principal Investigator of The Needleman Lab, Department of molecular and cellular biology at Harvard University,

certifies that:

Marta Venturas Pedro has performed all the work presented in this thesis manuscript under my supervision to obtain the title of PhD in Cellular Biology at the Universitat Autònoma de Barcelona

Boston, January 2022

A handwritten signature in black ink, appearing to read 'Daniel Needleman', followed by a long horizontal line extending to the right.

Dr. Daniel Needleman

*“At the end of the day, we can endure much more than we think we can”
Frida Kahlo*

Acknowledgements

First and foremost, to my advisor, Dan Needleman. Thank you for believing in me and giving me the opportunity to do this amazing work at your lab. For teaching me so much and for all the great advice you have given me throughout the PhD. I would also like to thank my tutor, Joan Blanco, for all your help.

M'agradaria dedicar aquesta tesi als meus pares, Carme i Francesc. Perquè sense la vostra confiança i constant suport res d'això hagués sigut possible. I a la Laura, la millor germana que es pot tenir. Gràcies família per estar sempre al meu costat, per cuidar-me i estimar-me tant des de la distància.

To Denny Sakkas and Catherine Rackowsky, thank you for your incredibly useful advice and support. I look forward to collaborating with you many times more. And to Emily Seidler and Tim Sanchez, thanks for your support, mentorship, and friendship.

A special mention should be given to all the members of the Needleman lab, in particular to Xingbo Yang, thank you for being an amazing colleague and mentor; and to Colm, Che-Hang, Will and Maya, thank you all for your valuable advice and friendship.

To the Oxford University collaborators Dagan Wells and Kishlay Kumar, and to Brigham and Woman's IVF embryologists, especially Jay Patel, and Boston IVF embryologists for having all the patience to teaching me and coordinating with me.

To Artemis, Krista, Fred, and Jeremy. Because getting to know you was the best thing that happened during my experience in Boston, even in the middle of a global pandemic. Thank you for being my family. Without your friendship, laughs, chats, surfs, and trips this would have been much harder. To all my friends in Boston, thank you for showing me all the US traditions and making me feel so welcome and loved here. And to the celiacos, for bringing a bit of my culture here.

A tots els Shaiets per fer-me sentir a casa cada cop que torno a Barcelona. En especial a les Chonis, per ser un pilar imprescindible a la meua vida. Gràcies pels 27 anys d'amistat inseparable. I a la Julia, per ser-hi sempre, per tot i en tot, lluny però a prop. I al Roger i Bernat, perquè no es pot tenir millors cosins. A tots ells per demostrar-me que l'amistat realment no té fronteres.

And to you, Tim, the biggest thank you. For always blindly believing in everything I do. Your vision of life makes one think everything is possible. (Even surfing). Thank you for being my best friend and for building an incredible team with me. T'estimo.

Thank you all for being there.

Boston, February 2022

Summary

Abstract	6
Abbreviations	8
List of included publications	9
Chapter 1. Introduction	10
1. <i>Infertility</i>	11
1.1 Assisted reproductive technologies.....	12
2. <i>Oocyte and embryo development</i>	13
2.1 Cumulus-oocyte complex development	13
2.2 Embryo development	14
3. <i>Quality assessment</i>	15
3.1. Techniques of oocyte quality assessment	15
3.2. Techniques of embryo quality assessment.....	16
4. <i>Metabolism of human COCs and embryos</i>	17
4.1 Cumulus- oocyte metabolism	17
4.2 Preimplantation embryo dynamic metabolism	18
5. <i>Assessment of cellular metabolism</i>	20
5.1 Techniques to evaluate metabolic state	20
5.2 Fluorescence Lifetime Imaging Microscopy.....	21
Chapter 2. Thesis Objectives	24
Chapter 3. Results	26
6. <i>Publication 1: Combined non-invasive metabolic and spindle imaging as potential tools for embryo and oocyte assessment</i>	27
7. <i>Publication 2: Metabolic imaging of human cumulus cells reveals associations among metabolic profiles of cumulus cells, patient clinical factors and oocyte maturity</i>	50
8. <i>Publication 3: Metabolic state of human blastocysts measured by fluorescence lifetime imaging microscopy</i>	71
Chapter 5. General Discussion	102
Chapter 6. Conclusions	108
References	110
Annex	116

Abstract

Embryo metabolism has long been linked to embryo viability, suggesting its potential utility to aid in selecting high quality embryos in assisted reproductive technologies (ART). Despite new advances to assess oocyte and embryo metabolism to determine their quality, non-invasive methods to robustly measure metabolic state are still lacking.

Fluorescence lifetime imaging microscopy (FLIM) is a non-invasive method for measuring the metabolic state of cells. FLIM measures the autofluorescence of nicotinamide adenine (phosphate) dinucleotide (NAD(P)H) and flavine adenine dinucleotide (FAD+), intracellular coenzymes essential for cellular respiration and glycolysis. FLIM enables measures of not only the fluorescence intensity of these molecules, which correlates with their concentration, but also the fluorescence lifetimes, that provides information on enzyme engagement. A metabolic measurement produces 9 quantitative parameters for characterizing the metabolic state of cells. Along with FLIM, second harmonic generation (SHG), which allows imaging of polarized structures such as the spindle, can also be obtained.

The first study of this thesis aimed to explore the feasibility, sensitivity, and safety of FLIM and SHG to be used for oocyte and embryo assessment. This study showed that FLIM in combination with SHG can detect sensitively meaningful changes in metabolism through mouse embryo development. FLIM detected changes in the metabolic state due to metabolic perturbations and does not significantly impair mouse embryo development.

Metabolic cooperativity between the oocytes and its surrounding cumulus cells is essential for correct oocyte and embryo development. The aim of the second study was to determine whether FLIM could detect differences in the metabolic state among human cumulus cell clusters. FLIM enabled quantitative measurements of the metabolic state of cumulus cells and detected variations between clusters, with greater variance among clusters from each patient than between patients. Additionally, cumulus cell metabolic parameters were associated with patient age and anti-Mullerian hormone levels, but not with BMI. Variations between cumulus cells associated with mature and immature oocytes were also found, suggesting the potential utility of this technique in ART assessments.

Mammalian embryos undergo variations in metabolism over the course of preimplantation development. Embryo metabolism has long been linked to embryo viability, suggesting its potential use in selecting high quality embryos in ART. Nonetheless, the metabolism of human embryos is not fully characterized yet, probably due to a lack of non-invasive methods to measure their metabolic state. The third study sought to determine whether non-invasive FLIM could detect variations in metabolic profiles of human discarded blastocysts. FLIM revealed extensive changes in the metabolic state of discarded human blastocysts associated with

blastocyst development over 36h, the day after fertilization and blastocyst developmental stage. Significant metabolic heterogeneity was observed within individual blastocysts, between the inner cell mass and the trophectoderm, and between the portions of hatching blastocysts within and without the zona pellucida. These results further demonstrate the highly dynamic and plastic metabolism of preimplantation embryos and the potential utility of measures of metabolic state to aid in embryo selection in ART.

This thesis has sought to deepen the knowledge of non-invasive assessments of oocyte, cumulus cell and embryo metabolism. Taken together, the results of the present thesis present that FLIM in combination with SHG can provide detailed biologically relevant information and could be promising approaches to assess oocyte and embryo developmental competency through non-invasive quantitative measures of their metabolism and spindle morphology.

Abbreviations

AMH	Anti Mullerian hormone
ART	Assisted reproduction techniques
BMI	Body mass index
CC	Cumulus cells
COC	Cumulus oocyte complex
FAD+	Flavine adenine dinucleotide
FLIM	Fluorescence lifetime imaging microscopy
FSH	Follicle stimulating hormone
GnRH	Gonadotropin hormone releasing hormone
GV	Germinal vesicle
ICM	Inner cell mass
ICSI	Intra cytoplasmatic sperm injection
IVF	In vitro fertilization
LH	Luteinizing hormone
MI	Metaphase I oocytes
MII	Metaphase II oocytes
mtDNA	Mitochondrial DNA
NADH	Nicotinamide adenine dinucleotide
NADPH	Nicotinamide adenine phosphate dinucleotide
PGT-A	Preimplantation genetic testing - aneuploidy
TE	Trophectoderm
SHG	Second harmonic generation
TCSPC	Time correlated single photon counting
TZPs	Transzonal projections

List of included publications

1. Sanchez T, Venturas M, Aghvami SA, Yang X, Fraden S, Sakkas D, Needleman DJ. Combined noninvasive metabolic and spindle imaging as potential tools for embryo and oocyte assessment. *Hum Reprod.* 2019 01;34(12):2349–61
2. Venturas M, Yang X, Kumar K, Wells D, Racowsky C, Needleman DJ. Metabolic imaging of human cumulus cells reveals associations among metabolic profiles of cumulus cells, patient clinical factors, and oocyte maturity. *Fertil Steril.* 2021 Sep 1;S0015-0282(21)01808-2.
3. Venturas M, Shah J, Yang X, Sanchez T, Conway W, Sakkas D, Needleman DJ. Metabolic state of human blastocysts measured by fluorescence lifetime imaging microscopy. *Hum Reprod* 2022; deab283.



Chapter 1. Introduction

1. Infertility

Compared to other mammalian species, the human reproductive system is relatively inefficient (1). Leading to approximately one in six couples suffering from infertility worldwide (2). Infertility is defined as a disease of the female or male reproductive system that prevents the conception of a child or the ability to carry a pregnancy to deliver after 12 months or more of regular intercourse (3). There are multiple factors that can impact human reproductive function like: both maternal and paternal age, body mass index (BMI), timing of intercourse, duration of attempting to conceive or lifestyle, and probably

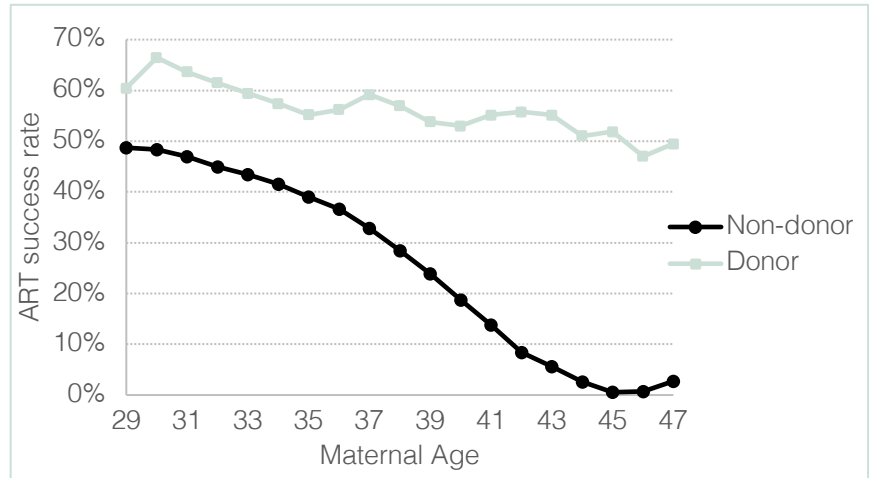


Figure 1: CDC, 2015 IVF Statistics of success rate for IVF treatments (assessed by the presence of a fetal heartbeat per embryo transferred) with maternal age for non-donor patients (black) and when donor eggs are used (grey).

more unknown factors (3). Amongst them, maternal age is thought to be the most important factor influencing human fertility (4,5). Female fertility starts to decline at age 24, showing a dramatic decline at around 37 years old (6). This decline is accompanied by a reduction of the number of total follicles, also known as ovarian reserve, which results in a decrease in Anti-Müllerian hormone (AMH) levels (7).

Additionally, success rates achieved through assisted reproductive technologies (ART) decline as maternal age increases. Older patients undergoing ART with their own oocytes show

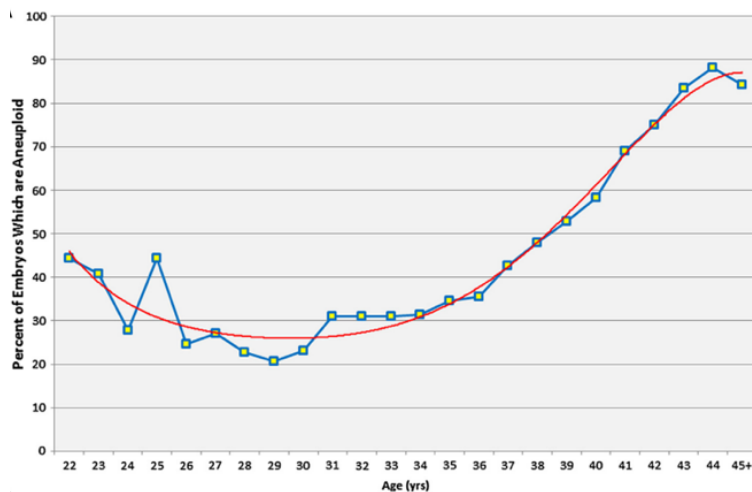


Figure 2: Percentage of embryos with aneuploidies with maternal age (Franasiak et al., 2014).

a significant decrease in implantation rates compared to patients using donor oocytes (Figure 1). Therefore, maternal age not only impacts the quantity but also the quality of the eggs of a patient. Together with the age-related reduction in female fertility, there is an increase of the risk of other disorders that may affect female fertility like, the rate of chromosomal abnormalities in preimplantation embryos and spontaneous

abortions (5,8). The aneuploidy rates increase from around 25% at age 30 to an 80% at age 42 (Figure 2)(5,9,10). Additionally, levels of AMH are also known to negatively impact oocyte quality (11). To overcome human fertility inefficiency, treatments like ART are continuously evolving. ART are all treatments that include the handling of eggs, sperm and/or embryos. Approximately 2.5 million ART cycles are performed per year, and its current success rates are around 33% (2). Constant advances in ART treatments are increasing the hope of millions of people suffering infertility worldwide.

1.1 Assisted reproductive technologies

During an ART cycle, exogenous hormones are administered to a patient to stimulate the ovaries to produce multiple mature oocytes rather than a single one. These oocytes are retrieved by aspiration from the follicles in the ovaries and its quality is evaluated (see 3.2). Then, those oocytes that are mature can be fertilized using two well established methods(12): either via in vitro fertilization (IVF), where motile sperm are placed together with the oocytes and incubated overnight, or intra cytoplasmic sperm injection (ICSI), where a single sperm is directly injected using a micropipette system into the mature egg. The subsequent embryos are then cultured up to five or six days since they were fertilized. The quality of the surviving embryos is assessed at day three, five and/or six, in order to rank the best ones. The final embryo or multiple embryos may be transferred back to the uterus once the endometrium is prepared (Figure 3).

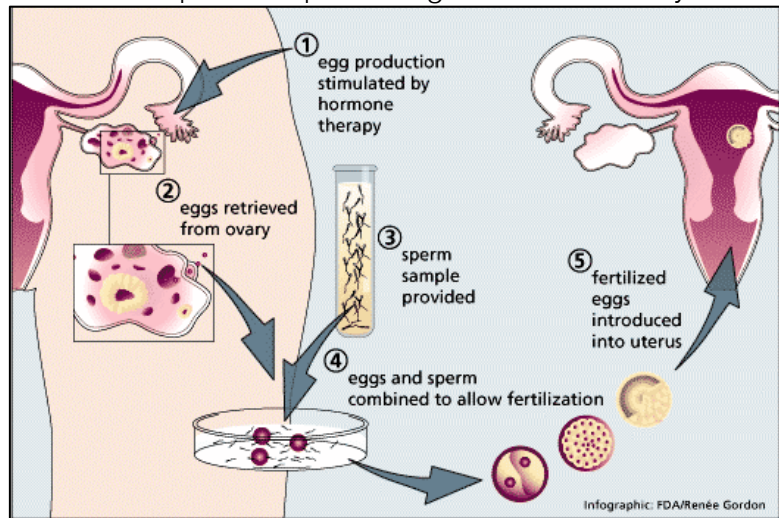


Figure 3: Depiction of an ART procedure. It starts with the hormonal stimulation of a patient to produce several mature eggs (1), the eggs are then retrieved from the ovary via aspiration (2). After the retrieval of the sperm sample (3), those eggs that are mature are fertilized (4). The successfully developed embryos are then transferred into the uterus (5) (Picture taken from *Infographic, R Gordon*)

once the endometrium is prepared (Figure 3).

The overarching goal of ART treatments is to transfer a single embryo to reduce the risks associated with multiple pregnancies (13) while maintaining the pregnancy rates (14). For this reason, choosing the right oocyte and embryo has been a focus of IVF research for a long time (15,16). Selecting the optimal embryo with high implantation potential will reduce the number of embryos to transfer, decreasing the risk for the mother and child (13) and, in turn, the associated emotional and economic impact (17,18). Therefore, developing techniques to select the oocytes and embryos with the highest quality and implantation potential has been of great importance in ART.

2. Oocyte and embryo development

2.1 Cumulus-oocyte complex development

At the fourth month of gestation human oogenesis begins with primordial follicles starting to develop until 20 weeks of fetal life. Human females are born with a finite reserve of primordial follicles, which are composed by oogonia surrounded by a single layer of somatic cells, called theca cells (19). Oogonia are arrested at the prophase stage of the first meiotic division (20), also known as germinal vesicle (GV). AMH is the growth factor responsible for maintaining the primordial follicles in this resting state (21,22).

At the start of puberty, oogenesis resumes, following a surge of follicle stimulation hormone (FSH), which releases several primordial follicles from their resting state and triggers the start of their growth and development. At this moment, the oogonia start to grow and the layer of somatic cells starts to proliferate into the granulosa layer, which marks the formation of the primary follicle (Figure 4). Then, the proliferation of granulosa cells create a second layer and give rise to the secondary follicle and the formation of a fluid filled cavity marks the development of the antral follicle (23). One of these antral follicles becomes dominant whereas the rest become atresic.

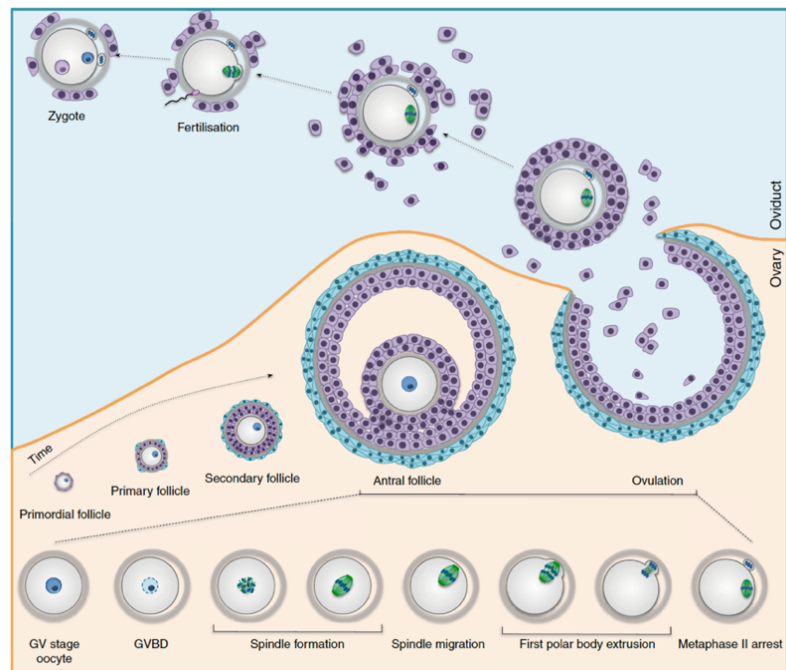


Figure 4: Follicle and oocyte development until fertilization. Oocyte in grey, cumulus cells in purple, theca cells in blue and spindle in green and chromosomes in dark blue (Picture taken from Mihajlović and FitzHarris, 2018).

A spike of both hormones FSH and luteinizing hormone (LH) triggers ovulation, where the dominant oocyte completes meiosis I, extruding the first polar body with half of the genetic material, and arrests again at the metaphase stage meiosis II, called metaphase II oocyte (MII). The developmental process from the GV to the MII stages is called oocyte maturation and in humans takes approximately 36 hours to complete (24). At this point, the follicle enlarges and ruptures at the surface of the ovary, releasing the MII oocyte surrounded by a matrix of granulosa cells, a structure called cumulus-oocyte complex (COC)(19,23,24). The oocyte will then complete meiosis II, releasing the second polar body, only if a sperm fertilizes it (Figure 4).

The specialized granulosa cells that enclose the oocyte are called cumulus cells (CC). The CC extend transzonal projections (TZPs) through the zona pellucida, the layer of glycoprotein that surrounds the oocyte, all the way to the surface of the oocyte (24,25) (Figure 5). The existence of a bidirectional crosstalk between the oocyte and its surrounding cumulus mass through gap junctions within the TZPs and paracrine signals has been previously observed (26,27). CC-oocyte interaction is essential for successful oocyte growth, maturation and subsequent embryo development (28–31). Hence, a better understanding of oocyte growth regulation and the role of CCs throughout this process would provide new insights in the principles of germ cell development.

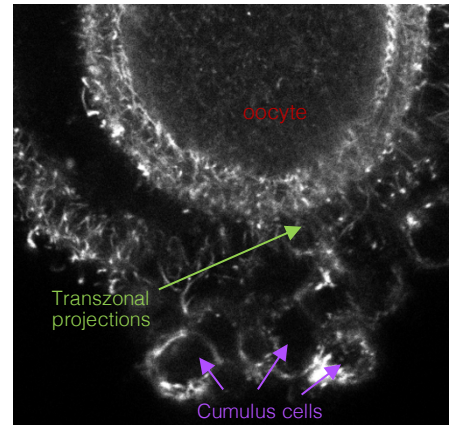


Figure 5: Confocal section of a mouse COC stained using Sir-Actin to label actin to observe the actin-rich transzonal processes (green) from CCs (purple), traversing the zona pellucida until the cortex of the oocyte (red). (Image taken by me).

2.2 Embryo development

After the embryo is fertilized by a sperm, it becomes a 1 cell diploid embryo surrounded by the zona pellucida. The zygote then undergoes several mitotic cleavage divisions, consecutively dividing into a number of smaller cells or blastomeres (20). Until the 16-cell stage, where blastomeres flatten against each other and the boundaries between them become undistinguishable. This compacted structure is called morula (Figure 6).

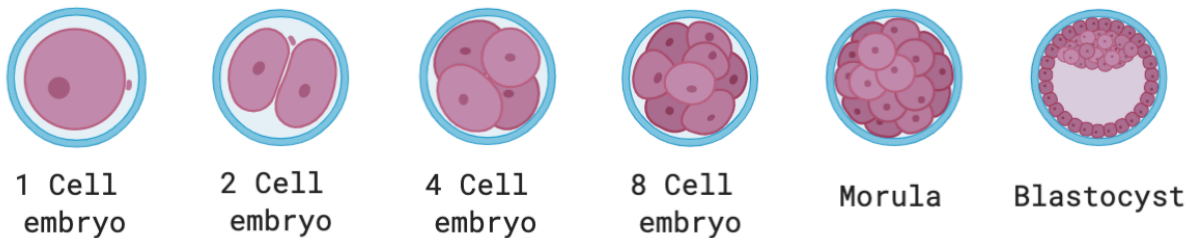


Figure 6: Depiction of mammalian preimplantation development from one cell to the formation of a blastocysts. Images created with BioRender.com

After, the sodium-potassium ATPase pumps of the outer blastomere layer start to pump sodium into the central area, followed by an osmotically driven movement of water, which forms a fluid-filled cavity, the blastocoel (Figure 6). This structure is called blastocyst and it comprises a layer of cells on the outside called trophoblast (TE) that will give rise to the placenta and the inner cell mass (ICM) that will become the foetal tissues. In humans, four/five days after fertilization, the blastocyst starts a process of expansion over the following day or two (Day five or six after fertilization).

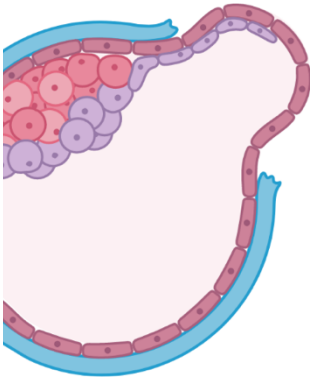


Figure 7: Depiction of the embryo hatching process, where the embryo frees itself from the zona pellucida to implant in the uterus wall. Image created with BioRender.com

Throughout these stages of embryo preimplantation development, the zona pellucida acts as a protective barrier. The blastocyst then undergoes a process called hatching, where the embryo escapes from the zona pellucida (32)(Figure 7). The hatched blastocyst is then ready to implant in the wall of the uterus.

The molecular mechanisms involved in the ability of an embryo to develop and implant successfully are not yet fully understood. For this reason, methods to study embryo preimplantation development non-invasively and the acquisition of developmental competency would perhaps provide helpful tools to improve IVF treatments.

3. Quality assessment

3.1. Techniques of oocyte quality assessment

Traditionally the evaluation of oocyte quality has been based on the morphological classification of the expansion and thickness of the COCs and the presence of a polar body (33–35) (Figure 8). Despite the valuable information this approach provides, it is quite subjective and can be imprecise, and may not relate to the intrinsic competence of the enclosed oocyte (36,37). For this reason, other assessments have been developing in order to increase the accuracy of oocyte evaluation, like maturation score grading, removing the CCs to better visualize the oocyte or non-invasive spindle imaging using polarized light microscopy(38).

Evaluation of oocyte quality entails cumulus oocyte complex morphological evaluation. Oocytes are categorized as: mature (Metaphase II oocyte), when the COC is expanded.; metaphase I oocyte, when they have a less expanded COC; and highly compacted COC is associated with an immature oocyte or GV.

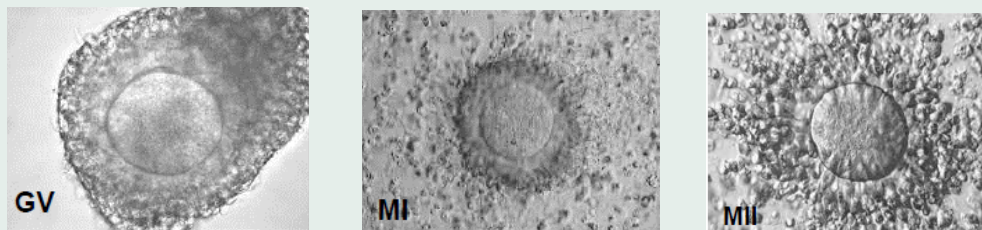


Figure 8: Images of human cumulus oocyte complexes at GV stage (immature), MI stage, and at MII stage (mature) (Images taken from Brigham and Woman's Hospital).

However, oocyte maturation not only requires nuclear maturation, which entails the completion of meiosis I until metaphase II, but also involves cytoplasmic maturation (34). Oocyte cytoplasmic maturation includes: rearrangement of organelles, accumulation of mRNA, proteins, substrates and nutrients that are needed to achieve acquisition of developmental competency (40). Both nuclear and cytoplasmic maturity are essential for the acquiring better oocyte quality and successful embryo development (40,41). However, the essential underlying steps necessary to achieve cytoplasmic maturity and its relationship with nuclear maturity are not yet fully understood.

In addition, the bidirectional crosstalk between the oocyte and its CC mass is essential for the resumption of meiosis (42) and they help maintain the oocyte in meiotic arrest at prophase I until ovulation is triggered (28). Given the essential role of CCs for oocyte maturation and the acquisition of developmental potential (43–48) and that these cells are typically removed or trimmed before IVF treatments; they have the potential to be used in non-invasive assays of oocyte developmental competency.

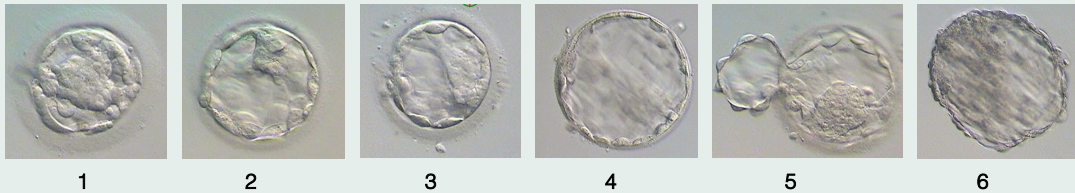
3.2. Techniques of embryo quality assessment

The assessment of embryo quality has been a key goal in ART for trying to optimize embryo selection to improve success rates. Currently, embryo selection is based in the evaluation of the morphological appearance of the embryo (49). This evaluation is normally performed at the one cell stage, with the evaluation of the pronucleus, at day three and at day five and/or six after fertilization. This morphological score entails the grading of blastocyst expansion stage and ICM and TE morphology (Figure 9). This scoring system has been associated with implantation and live birth rates (50–52). Despite its widespread use, embryo morphological scoring has limited predictive power, it does not provide direct measures of the physiology of the embryo (53) and the contributions of both the ICM and TE are not yet fully understood (54,55).

Promising innovations in techniques of embryo selection are shedding some light but have yet to be proven successful. Monitoring morphological changes through embryo development using time lapse microscopy has provided great knowledge on embryo dynamics but shown limited evidence of its clinical benefit (56–58). Recently, the use of artificial intelligence to provide predictive algorithms of time-lapse imaging to improve embryo selection have shown some promise in ART (59). Moreover, preimplantation genetic testing for aneuploidy (PGT-A) to determine the ploidy status of an embryo has been widely used for improving embryo selection. PGT-A has shown increased success in pregnancy rates (60), but mainly in older patients (61,62). Additionally, there is still up to 40% of euploid embryos that fail to implant (60) possibly due to other factors or perhaps metabolic dysfunctions. Despite the promising findings in all these studies and novel techniques, IVF success rates remain low.

Blastocyst morphological grading is based on the expansion stage of the embryo and the consistency of the cells within inner cell mass (ICM) and trophoctoderm (TE). Embryos are scored with a number corresponding to their expansion stage:

- 1- **Early blastocyst:** the blastocele occupies less than half of the embryo's volume
- 2- **Blastocyst:** the blastocele is more than half of the embryo's volume
- 3- **Full blastocyst:** the blastocele fills the entire embryo but the zona pellucida remains thick.
- 4- **Expanded blastocyst:** the volume of the blastocele is larger than the embryo and the zona pellucida starts to thin.
- 5- **Hatching blastocyst:** the TE starts to herniate through the zona pellucida.
- 6- **Hatched blastocyst:** the blastocyst has completely escaped the zona.



Additionally, blastocysts are categorized with two letters, the first grades the ICM then the TE grade. Following this system(49):

ICM:

- A:** many cells and tightly packaged
- B:** several cells and loosely grouped
- C:** few scattered cells

TE:

- A:** cohesive epithelium formed by multiple cells
- B:** less cells forming a loose epithelium
- C:** few and large cells

Figure 9: Current scoring of blastocyst morphology. (Images taken by me).

4. Metabolism of human COCs and embryos

4.1 Cumulus- oocyte metabolism

In addition, the intimate communication between oocytes and its CCs via TZPs is bidirectional (24,46,63,64): CC produce growth factors and hormones, nutrients, metabolic precursors, and other small molecules for oocyte maturation and development (65,66); oocyte secreted factors enable CCs differentiation and formation of the hyaluronan matrix (67,68) (Figure 10). This crosstalk between the oocyte and its surrounding cumulus mass supports oocyte maturation, growth and embryo development (26,28,29,31). Inhibiting the GAP junctions and blocking the TZPs leads to a reduction in oocyte intracellular ATP (69). This indicates that CCs play a role in maintaining the energy levels of the oocyte (46,70). Pyruvate consumption by COCs has been positively associated with oocyte maturation (67,70).

Mitochondria play key roles in supplying energy in the form of ATP for the maturation and growth of the oocytes (71,72). Dysfunction of oocyte mitochondria has been associated with oocyte quality (73–75), but the molecular mechanisms associated remain unknown (76,77). There is a dynamic mitochondrial redistribution and reorganization during oocyte maturation, which could perhaps influence mitochondrial function (72,77). Moreover, mitochondrial dysfunction and mitochondrial DNA (mtDNA) copy number of CCs might be directly related to oocyte maturity (30,78–80). For this reason, measurements of the metabolic state of CCs could be used to determine the developmental potential of the enclosed oocyte (81–84).

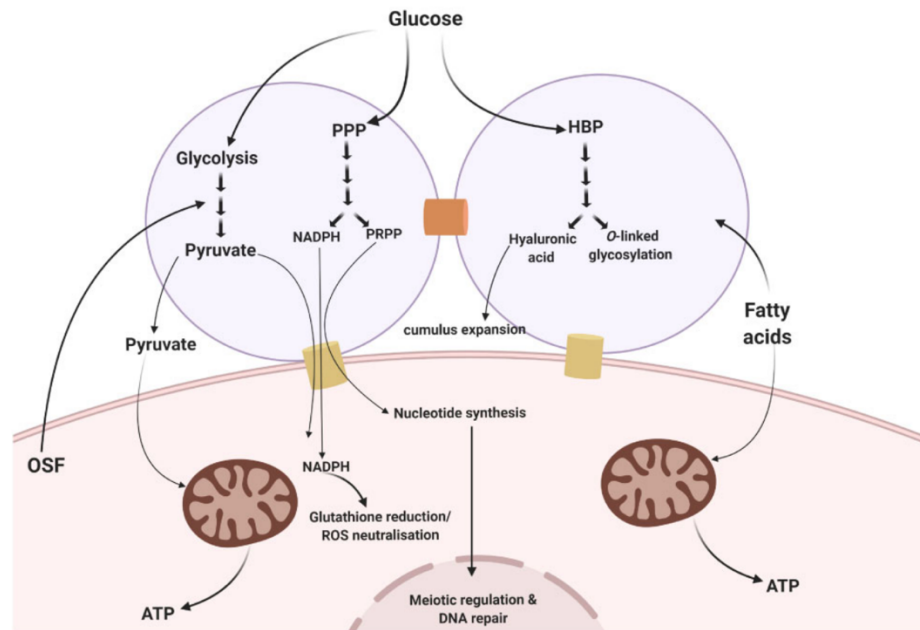


Figure 10: Cumulus cell and oocyte metabolic bidirectional crosstalk (Picture taken from Richani et al., 2021)

4.2 Preimplantation embryo dynamic metabolism

During preimplantation development, mammalian embryos exhibit characteristic metabolic variations that are essential for correct development (85–87). During the first cleavage divisions the zygote relies primarily on pyruvate for energy production (87–89). Glucose uptake and oxygen consumption increases gradually from 1 cell stage to blastocyst (90–92). Glucose plays several roles in the later stages of preimplantation development. At the 8-cell stage, the embryo undergoes a metabolic switch and glycolysis becomes the predominant pathway for ATP generation through aerobic glycolysis (87,93–95) (Figure 11). However, several recent studies have observed that glucose not only is required for energy generation but also plays signaling roles required for cell fate specification for blastocyst formation (96–100). Glucose can also be converted into lactate and facilitates embryo implantation in the uterus wall (90). The release of lactate by the TE cells creates a low pH microenvironment which is thought to help with tissue invasion, angiogenesis and modulate the immune response (90).

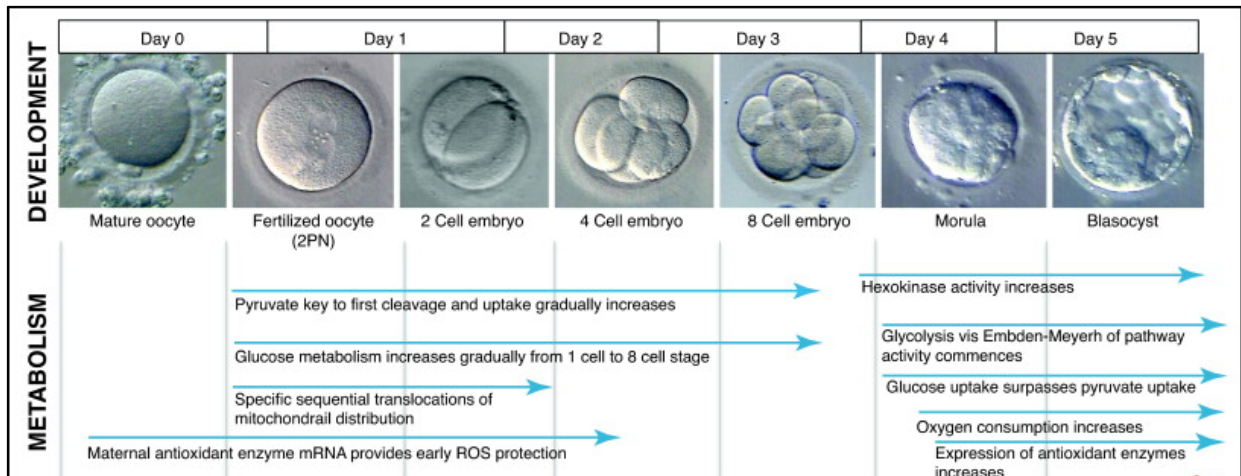


Figure 11: Metabolic changes through preimplantation embryo development (Picture taken from Chason et al. 2011).

These dynamic changes in metabolism are key to produce developmentally viable embryos (88,93,101). In addition, impaired metabolic activity has been correlated with decreased developmental potential (77,88,101,102,102). The ‘Quiet embryo hypothesis’ by Leese et al. proposes that embryos with a higher developmental capacity are characterized by a quieter metabolism rather than active (98). In line with this hypothesis, low amino acid turnover (104) and oxygen consumption (91,105) has been linked with high developmental potential.

However, glucose uptake (17) and pyruvate (106) levels are higher in embryos that develop successfully and lead to successful pregnancies.

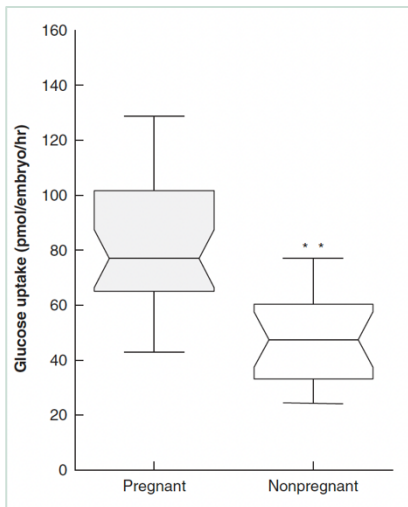


Figure 12: Glucose consumption of human embryos on day 4 after fertilization is significantly associated with outcome (Picture taken from Gardner et al 2012).

Additionally, metabolic activity of the embryo has been associated with its morphological grade (107) and time to blastocyst formation (108) and implantation potential (Figure 12)(17,93,101,109). For this reason, measuring embryo metabolism could aid in selecting high quality embryos for transfer. Several attempts have been made on this regard, but approaches based on this premise have so far not been successful (108,110). Hence, developing a non-invasive tool capable of measuring embryo metabolism could not only provide a better understanding of the metabolic underpinnings of embryo growth but also could be used to aid in embryo selection in clinical IVF.

5. Assessment of cellular metabolism

5.1 Techniques to evaluate metabolic state

Cumulus cell-oocyte metabolic interactions are essential for the acquisition of oocyte developmental competency (68,111). Hence, several studies have focused on studying the metabolic state of CCs to predict oocyte and subsequent embryo quality. In order to measure CCs metabolic state, studies have focused on the use of invasive dyes to stain subcellular structures like mitochondria (30,112) or measurements of CCs mtDNA (98,113). However, these work remains inconclusive (82,83,98,113) as some studies found that mtDNA copy number does not seem to be associated with oocyte maturity (83), while other studies observed a correlations with oocyte fate (78,79). Additionally, attempts to find gene expression biomarkers of oocyte quality in CCs are starting to develop (24,64,68). To this end, assessments to measure the metabolic state of individual CC masses could provide better insights on the metabolic crosstalk between CCs and the oocyte and potentially enable non-invasive approaches to evaluate oocyte quality and further developmental competency.

Levels of metabolites, proteins and amino acids have been linked with embryonic developmental potential and live birth rates (114,115). Methods to study oocyte and/or embryo metabolism rely on intracellular measurements using dyes (116,117) or quantification of metabolites in the spent media to determine the metabolic activity of the oocyte or embryo (16,17,93,115,118). These studies use methods like proteomic analysis using mass spectrometry, high performance liquid chromatography and microarrays. Despite the useful information that these methods provide, they are often invasive or require highly specialized skills.

For this reason, non-invasive methods to measure intracellular metabolic function of oocytes and embryos have been pursued. Some intracellular molecules

like nicotinamide adenine phosphate dinucleotide (NADPH), nicotinamide adenine dinucleotide (NADH) and flavine adenine dinucleotide (FAD+) are autofluorescent (119). These molecules are endogenous electron carriers that play important roles in several metabolic pathways, such

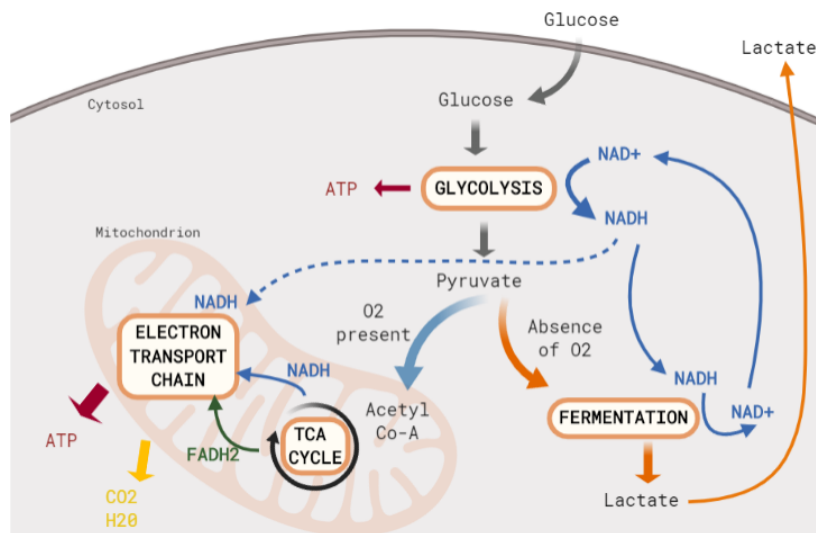


Figure 13: Schematic of some cellular metabolic pathways where NAD(P)H and FAD+ are involved. Image created with BioRender.com

as the electron transport chain, glycolysis and fermentation (120)(Figure 13). These molecules have long been used to detect cellular metabolism as NAD(P)H and FAD+ are autofluorescent, whilst NAD(P)+ FADH₂ are not (119). Hence, these coenzymes have a diagnostic potential as non-invasive biomarkers for cellular metabolic state and mitochondrial anomalies (119,121–123). Because of their natural fluorescent properties, we eliminate the potential toxicity, non-specific binding and interference with biological functions associated with exogenous dyes (119,124). NADH and NADPH fluorescence spectra is almost not distinguishable (124), therefore the fluorescence of both NADH and NADPH is often combined and called NAD(P)H. Both NAD(P)H and FAD+ two photon fluorescence spectra is quite distinct, allowing for simultaneous detection (119,125)(Figure 14). Whilst FAD+ is only located in the mitochondria (126), NAD(P)H is mainly located in the mitochondria but can also be located in cytoplasmic regions (127). Previous studies have observed strong colocalization between FAD+ autofluorescence and mitochondria (122).

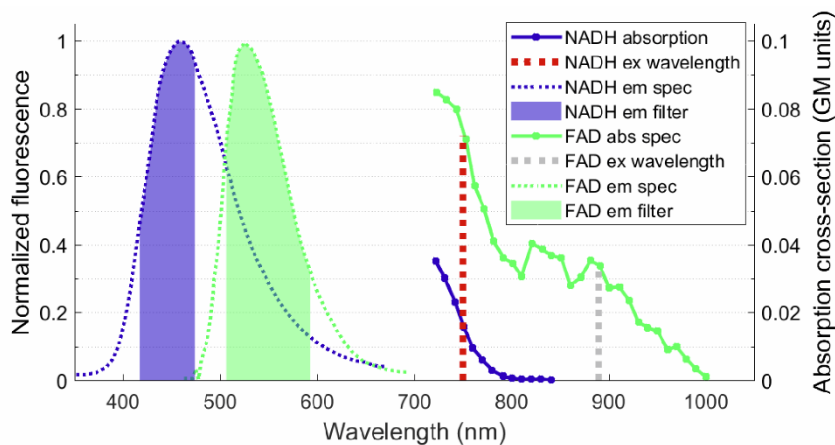


Figure 14: NAD(P)H (in blue) and FAD+ (in green) emission and two-photon excitation spectra.

5.2 Fluorescence Lifetime Imaging Microscopy

Fluorescence lifetime imaging microscopy (FLIM) of NAD(P)H and FAD+ autofluorescence can provide quantitative measurements of not only the concentration, but also the fluorescence lifetimes, and the fraction of these molecules bound to enzymes (73,124,128,129). The fluorescence intensity of a molecule correlates with its concentration (119). However, the lifetime of a molecule is independent of its concentration, and correlates with the molecular conformation and can be altered by the biological environment, such as: pH, oxygen concentration, or temperature (124,128,130). Both NAD(P)H and FAD+ have a short and long lifetime components, depending on whether these molecules are free or bound to an enzyme (131). For NAD(P)H, the short lifetime corresponds to its free state and the long lifetime to its enzyme-bound state (125,131). In contrast, for FAD+ the longer lifetime component corresponds to free FAD+ and the shorter component to protein bound FAD+ (125). NAD(P)H can be bound to many enzymes in the metabolic pathway (132) and this fluorescence lifetime

of protein-bound NADH changes depending on the enzyme it is bound to. It has been previously described in other systems that the fraction of enzyme-bound NAD(P)H is correlated with the activity of oxidative phosphorylation (132). Changes in metabolism can be measured by the lifetime of protein-bound NAD(P)H and FAD+(125,131,133).

FLIM uses two photon pulsed-laser microscopy (128,134), which is based on nonlinear excitation of molecules where two photons are then needed to excite a single molecule of NAD(P)H or FAD+. Two photon pulsed laser microscopy and TCSPC (Figure 15) offers several advantages compared to one photon microscopy: it provides high resolution, which in turn minimizes the potential photodamage that the laser can cause to the sample, and it offers great penetration depth into tissues, reducing laser scattering (135). Additionally, FLIM can measure cellular and subcellular metabolic heterogeneity with high spatiotemporal resolution (128,136).

FLIM uses time-correlated single photon counting (TCSPC) technique. With TCSPC, the sample is scanned by a focused beam of a pulsed laser. TCSPC detects single photons of the fluorescence light emitted from both NADH and FAD+. This technique records the arrival times of the photons in the detector (t_{photon}) with respect to the time of the laser pulses (t_{pulse}) as well as the position of the laser beam in the moment of detection of the photons. This process is repeated per multiple laser pulses, resulting in a three-dimensional array of data or an image that contains a fluorescence decay curve for each pixel, called FLIM curve. For our data, per each selected region of interest, we bin all photon arrival times into a separate histogram, forming a FLIM curve from the region of interest (the oocyte, embryo, or CC cluster). Fitting these curves to a two-exponential decay model produces a total of 8 parameters: fluorescence intensity, long lifetime, short lifetime, and the fraction bound to enzyme for both NAD(P)H and FAD+.

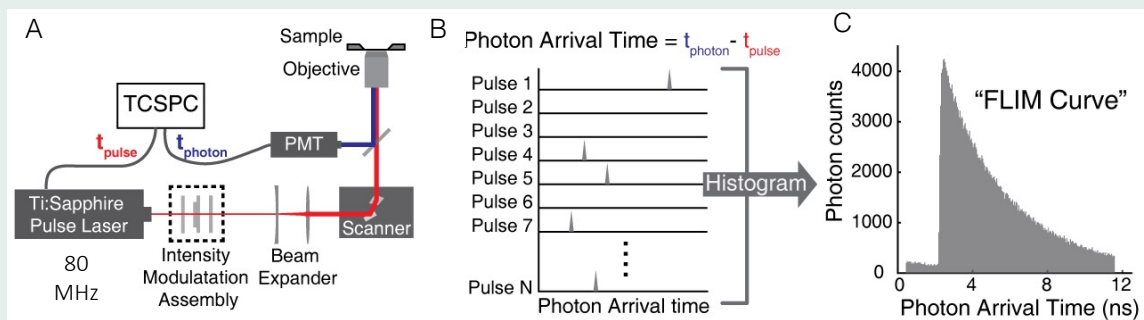


Figure 16: (A) Schematic of the components of a two-photon FLIM microscope, consisting of a 80MHz Ti-Sapphire pulsed laser, a scanning microscope and a high sensitivity TCSPC. (B) Each laser pulse (t_{pulse}) gets sent to the sample, where a photon is emitted from NAD(P)H or FAD+ at a certain time (t_{photon}). The photon arrival time gets calculated per each pixel, giving the fluorescence decay curve or FLIM curve per pixel (C) (Image taken from Becker 2005).

Thus, the fluorescence lifetimes of NAD(P)H and FAD⁺ provides a sensitive means to characterize variations in metabolic state of oocytes, CCs and embryos. Taken together, a single FLIM image provides 8 quantitative measures to non-invasively assess the metabolic state of cells. Additionally, the redox ratio can also be computed from the mean intensity of NAD(P)H divided by the mean intensity of FAD⁺. The use of non-invasive FLIM to measure both mitochondrial morphology and physiology has been widely used in other fields, like early detection of cancer cells (125) or in neurodegenerations studies. Its application in the IVF field is starting to be studied (73,129,137) but is yet to be established.

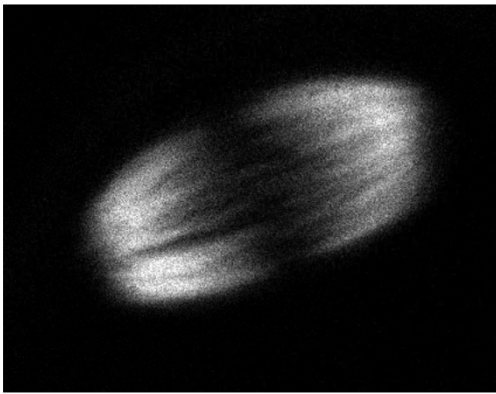



Figure 17: Non-invasive SHG imaging of a mouse spindle. (Image taken by me).

Last, another advantage of performing FLIM with two-photon microscopy, is that it enables simultaneous non-invasive imaging of spindle morphology via second harmonic generation (SHG). SHG is a nonlinear optical process in which highly polarizable, non-centrosymmetric materials emit photons with half the wavelength of incident light (135,138,139). Structures like the spindle or the zona pellucida are highly polarized and can be observed with this non-invasive technique (Figure 17).

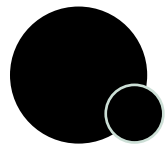
FLIM and SHG have long been used in other fields but its use in IVF to determine the metabolic state of oocytes, cumulus cells or embryos is yet to be established(129,140). This thesis aimed to determine if FLIM in combination with SHG can be used as non-invasive techniques to simultaneously measure intracellular metabolic state and spindle dynamics. And, to study a potential application of this techniques in clinical IVF, to measure the metabolic state of CCs, which could offer a better understanding of the interactions between oocytes and CCs and perhaps, aid in selecting high quality oocytes. And last, to explore a second application of FLIM to measure the metabolic state of human blastocysts, which would shed light into the application of FLIM and SHG to help in embryo selection in ART.



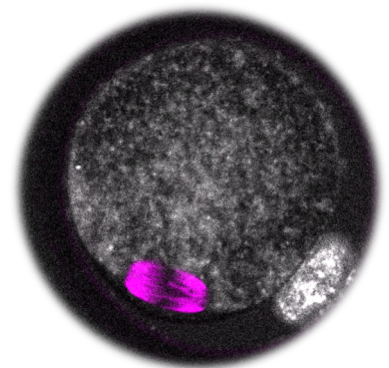
Chapter 2. Thesis Objectives

The general objective of this thesis is to gain global insights into the relation between the metabolic state of human cumulus cells, oocytes and embryos and their developmental competence. With this general objective in mind, three specific aims were set that have been worked on using FLIM and SHG.

- The first objective was to explore the use of FLIM as a non-invasive technique capable of measuring the metabolic state of cells. This thesis focused on studying the feasibility of FLIM and SHG technique to quantitatively measure the metabolic state and spindle dynamics of live mouse oocytes and embryos. And the potential safety and sensitivity of non-invasive FLIM-based imaging to measure embryo metabolism.
- The second aim was to study whether metabolic imaging via FLIM can be used to measure metabolic state of CCs in vitro. Additionally, to evaluate the sensitivity of this non-invasive metabolic imaging to investigate the associations among clinically relevant patient factors (such as age, BMI and AMH levels), and the metabolic state of the cumulus masses. And finally, to explore the extent to which quantitative measures of the metabolic state of CC clusters are associated with the maturity of the oocyte they enclose.
- The last goal was to determine the use of non-invasive FLIM to measure the metabolic state of human blastocysts of different patients. This study sought to explore the extent to which FLIM can quantitatively measure metabolic changes through human blastocyst expansion and hatching. A secondary aim was to study spatial patterns in the metabolic state within human blastocysts and their association with stage of expansion, day of development after fertilization and morphological profiles. And finally, to explore the sensitivity of this technique in detecting metabolic variations between blastocysts from the same patient and between patients.



Chapter 3. Results



6. Publication 1: *Combined non-invasive metabolic and spindle imaging as potential tools for embryo and oocyte assessment*

(DOI:10.1093/humrep/dez210)

Title: Combined noninvasive metabolic and spindle imaging as potential tools for embryo and oocyte assessment

Authors: Tim Sanchez^{1*}, Marta Venturas^{1,4}, S. Ali Aghvami², Xingbo Yang¹, Seth Fraden², Denny Sakkas^{3#}, and Dan J. Needleman^{1#}

¹Department of Molecular and Cellular Biology and School of Engineering and Applied Sciences, Harvard University, Cambridge, MA, 02138, U.S.A.

²Department of Physics, Brandeis University, Waltham, MA, 02453, USA

³Boston IVF, 130 Second Avenue, Waltham, MA, 02451, U.S.A.

⁴Departament de Biologia Cel·lular, Fisiologia i Immunologia, Universitat Autònoma de Barcelona, Cerdanyola, Spain

#The last two authors are the senior authors

Corresponding Author

* Tim Sanchez

Email: timhsanchez@gmail.com

Address: 52 Oxford St. NW building room 358, Cambridge, MA, 02138, USA.

Abstract

Study question: Is the combined use of fluorescence lifetime imaging microscopy (FLIM)-based metabolic imaging and second harmonic generation (SHG) spindle imaging a feasible and safe approach for noninvasive embryo assessment?

Summary answer: Metabolic imaging can sensitively detect meaningful metabolic changes in embryos, SHG produces high-quality images of spindles and the methods do not significantly impair embryo viability.

What is known already: Proper metabolism is essential for embryo viability. Metabolic imaging is a well-tested method for measuring metabolism of cells and tissues, but it is unclear if it is sensitive enough and safe enough for use in embryo assessment.

Study design, size, duration: This study consisted of time-course experiments and control versus treatment experiments. We monitored the metabolism of 25 mouse oocytes with a noninvasive metabolic imaging system while exposing them to oxamate (cytoplasmic lactate dehydrogenase inhibitor) and rotenone (mitochondrial oxidative phosphorylation inhibitor) in series. Mouse embryos (n =39) were measured every 2 h from the one-cell stage to blastocyst in order to characterize metabolic changes occurring during pre-implantation development. To assess the safety of FLIM illumination, n =144 illuminated embryos were implanted into n =12 mice, and n =108 nonilluminated embryos were implanted into n =9 mice.

Participants/materials, setting, methods: Experiments were performed in mouse embryos and oocytes. Samples were monitored with noninvasive, FLIM-based metabolic imaging of nicotinamide adenine dinucleotide (NADH) and flavin adenine dinucleotide (FAD) autofluorescence. Between NADH cytoplasm, NADH mitochondria and FAD mitochondria, a single metabolic measurement produces up to 12 quantitative parameters for characterizing the metabolic state of an embryo. For safety experiments,

live birth rates and pup weights (mean±SEM) were used as endpoints. For all test conditions, the level of significance was set at $P < 0.05$.

Main results and the role of chance: Measured FLIM parameters were highly sensitive to metabolic changes due to both metabolic perturbations and embryo development. For oocytes, metabolic parameter values were compared before and after exposure to oxamate and rotenone. The metabolic measurements provided a basis for complete separation of the data sets. For embryos, metabolic parameter values were compared between the first division and morula stages, morula and blastocyst and first division and blastocyst. The metabolic measurements again completely separated the data sets. Exposure of embryos to excessive illumination dosages (24 measurements) had no significant effect on live birth rate ($5.1^{\circ} \pm 0.94$ pups/mouse for illuminated group; $5.7^{\circ} \pm 1.74$ pups/mouse for control group) or pup weights ($1.88^{\circ} \pm 0.10$ g for illuminated group; $1.89^{\circ} \pm 0.11$ g for control group).

Limitations, reasons for caution: The study was performed using a mouse model, so conclusions concerning sensitivity and safety may not generalize to human embryos. A limitation of the live birth data is also that although cages were routinely monitored, we could not preclude that some runt pups may have been eaten.

Wider implications of the findings: Promising proof-of-concept results demonstrate that FLIM with SHG provide detailed biological information that may be valuable for the assessment of embryo and oocyte quality. Live birth experiments support the method's safety, arguing for further studies of the clinical utility of these techniques.

Study funding/competing interest(s): Supported by the Blavatnik Biomedical Accelerator Grant at Harvard University and by the Harvard Catalyst/The Harvard Clinical and Translational Science Center (National Institutes of Health Award UL1 TR001102), by NSF grants DMR-0820484 and PFI-TT-1827309 and by NIH grant R01HD092550-01. T.S. was supported by a National Science Foundation Postdoctoral Research Fellowship in Biology grant (1308878). S.F. and S.A. were supported by NSF MRSEC DMR-1420382. Becker and Hickl GmbH sponsored the research with the loaning of equipment for FLIM. T.S. and D.N. are cofounders and shareholders of LuminOva, Inc., and co-hold patents (US20150346100A1 and US20170039415A1) for metabolic imaging methods. D.S. is on the scientific advisory board for Cooper Surgical and has stock options with LuminOva, Inc.

Key words: metabolism / mitochondria / embryo assessment / oocyte / noninvasive / spindle / fluorescence / nicotinamide adenine dinucleotide / flavin adenine dinucleotide

Introduction

The invention of precise, noninvasive methods of assessing oocyte and embryo quality has long remained a critical goal in ART (Gardner et al., 2015; Sanchez et al., 2017). 40 years after the first IVF procedures were performed, morphological assessment remains the primary method of evaluation, despite its well-known limitations (Wong et al., 2014). Morphological features, however, have no clear connection to the underlying biochemical factors that are essential for viability, such as metabolic function (Gardner et al., 2000, 2001; Leese, 2002; Babayev and Seli, 2015) and genetic integrity (Baart et al., 2006; Vanneste et al., 2009; Niakan et al., 2012).

Innovations in recent years have offered some promise, but failed to solve the problem of low overall success rates in IVF. Time lapse imaging systems have been advanced in the hopes that embryo growth dynamics may reflect viability more accurately than single observations. Like the standard morphological assessment, though, these systems can only sample gross morphological features, and clinical trials have not demonstrated efficacy in increasing success rates (Gardner and Sakkas, 2013; Armstrong et al., 2019).

The main advance has been the development of preimplantation genetic testing for aneuploidy (PGT-A). These techniques have demonstrated some significant increase in success rates (Forman et al., 2013; Scott et al., 2013a;), mostly for older patients (Munne et al., 2017; Murphy et al., 2018). However, PGT is expensive and invasive, and concerns persist over accuracy, reproducibility between clinics, and over the role of mosaicism (Capalbo et al., 2017; Vega and Jindal, 2017). Perhaps most importantly, it conveys no information about metabolic competence. Among euploid embryos, 40% still fail (Scott et al., 2013a) due to non-genetic causes, including metabolic dysfunction.

Some studies have measured mitochondrial DNA copy number in biopsied cells in the hopes of gleaning some insight into metabolic health (Diez-Juan et al., 2015; Fragouli et al., 2016). Studies using this technique, however, have not reported consistent results, nor demonstrated predictive value (Diez-Juan et al., 2015; Treff et al., 2017; Cecchino and Garcia-Velasco, 2019). Additionally, high variation in the data remains a barrier for this technique (Treff et al., 2017).

It has long been known that embryo metabolism relates to viability (Renard et al., 1980; Van Blerkom et al., 1995; Gardner et al., 2000, 2011). Here, we investigate the potential utility of FLIM-based metabolic imaging of NADH and FAD (Becker, 2012; Heikal, 2012) with second harmonic generation (SHG)-based spindle imaging (Hsieh et al., 2008; Yu et al., 2014). This approach has several benefits. First, NADH and FAD fluorescence can serve as a basis for imaging the spatial distribution of mitochondria within cells, as NADH is highly concentrated in the mitochondria relative to the cytoplasm (Stein and Imai, 2012) and nuclei (Cinco et al., 2016), and FAD is almost entirely localized to the mitochondria (Dumollard et al., 2004). Previous studies have shown strong co-localization of FAD fluorescence with mitochondrial fluorescence in mouse oocytes using mitochondrial dyes (Dumollard et al., 2004), and other studies showed incomplete overlap between NADH fluorescence with mitochondria in other cell types (Mujat et al., 2008; Tucker et al., 2016). Abnormal mitochondrial morphology has been associated with reduced developmental competence (Nagai et al., 2006). Hence, FLIM intensity images, alone, may have the potential to assist in

oocyte/embryo screening. Fluorescence imaging of cytoplasmic NADH also contains some signal from NADPH, as their fluorescence spectra are almost identical (Ghukasyan and Heikal, 2014); however, NADH contributes the majority of the fluorescence signal in many cell types, as its concentration is typically several fold higher than that of NADPH (Klaidman et al., 1995). Therefore, for simplicity we adopt the convention of referring to this fluorescence signal as 'NADH' signal.

Beyond imaging, FLIM provides quantitative information on the local environment of NADH and FAD molecules, which is reflective of the biochemical processes they are engaged in (Ghukasyan and Heikal, 2014). FLIM not only measures the fluorescence intensity of a sample, but also the rates at which fluorophores decay from their excited state (Becker, 2012). These rates, or 'fluorescence lifetimes', are affected by the microenvironment of the fluorophores, and thus have been used to probe various intracellular processes such as protein binding via FLIM-FRET (Yoo et al., 2018), viscosity (Parker et al., 2010) and temperature (Okabe et al., 2012). Because NADH and FAD are integral to cellular respiration, their microenvironment is affected by changes in metabolic function, and these changes are reflected in their FLIM signatures (Ghukasyan and Heikal, 2014). Thus, FLIM measurements of NADH and FAD is commonly referred to as metabolic imaging. Furthermore, metabolic imaging has the potential to probe metabolic processes with subcellular resolution if cytoplasmic and mitochondrial regions are analyzed separately. NADH in the cytoplasm is involved in a variety of pathways, including glycolysis and fermentation, while NADH and FAD in mitochondria are primarily associated with the tricarboxylic acid cycle and the electron transport chain (Berg et al., 2007). In total, a single metabolic measurement can generate up to 12 quantitative metrics, providing a detailed profile of egg/embryo metabolic state.

FLIM can be performed via one-photon or two-photon excitation of fluorophores. The former typically uses pulsed photodiode lasers (Becker, 2017), and the latter typically uses mode-locked lasers, such as a Ti-sapphire (Smith, 1970), which deliver ultra-short light pulses of 100-150fs in duration. In two photon excitation, fluorophores absorb two low-energy (long wavelength) photons simultaneously. This method has several benefits, including efficiency for deep-tissue imaging, intrinsic confocal imaging, and lower phototoxicity (Potter, 1996).

The sensitivity of a metabolic assay can be investigated by probing known changes in metabolic state using chemical perturbations. Oxamate inhibits lactate dehydrogenase, which reduces NAD⁺ to NADH during the conversion of lactate into pyruvate, (Dumollard et al., 2007). Rotenone inhibits the transfer of electrons from Complex I to ubiquinone, reducing the activity of the electron transport chain (ETC) (Staniszewski et al., 2013). Embryo metabolism is known to undergo distinct shifts over the course of early development (E1-E5) (Rieger, 1992; Gardner, 1998; Chason et al., 2011), including a gradual increase in pyruvate and glucose metabolism during the cleavage stage (E1-E3) (Gardner and Leese, 1986) and the commencement of aerobic glycolysis around compaction (morula) and blastocyst formation (Gardner and Harvey, 2015). Thus, comparing developmental time points can serve as an additional standard for testing assay sensitivity to detecting known metabolic differences.

In conjunction with FLIM measurements, we also simultaneously acquire high fidelity images of meiotic spindles in oocyte and mitotic spindles via Second Harmonic Generation (SHG) (Hsieh et al., 2008; Campagnola, 2011; Yu et al., 2014). SHG is a non-linear effect, in which photons are up-

converted to a single scattered photon of exactly twice the frequency. Thus, it is commonly generated using the same kind of ultra-short pulsed light sources as two-photon fluorescence. Significant SHG signals are only produced by highly ordered, non-centrosymmetric materials. In biology, biofilament bundles such as collagen and microtubules in spindles are among the few materials that produce an SHG signal (Campagnola and Loew, 2003). This provides an endogenous source of contrast that allows for high quality, noninvasive imaging of spindles (Hsieh et al., 2008; Campagnola, 2011; Yu et al., 2014). As chromosome segregation errors are associated with spindle defects (Battaglia et al., 1996), visualizing spindle morphology could also have clinical relevance.

As these methods probe physiological factors that are known to be important for embryo viability, they could potentially serve as a basis for assessing embryo quality and identifying embryos with the highest chance of success. Furthermore, they have the potential to serve as powerful new research tools to produce new insights into early embryo biology. We have already shown that FLIM parameters exhibit strong differentiation between a mitochondria protein [caseinolytic peptidase P (Clpp)]-knockout versus wild type, and old versus young mouse oocytes (Sanchez et al., 2018). FLIM measurements of mouse embryos at the compaction stage have also been reported to correlate with blastocyst development (Ma et al., 2018).

With any noninvasive, light-based assay, an assessment of safety must be performed before any clinical application is possible, as cell illumination has the capacity to cause photo damage (Masters and So, 2008). We present evidence supporting the technique's safety for use on embryos: we implanted illuminated and non-illuminated embryos into surrogate female mice and measured both live birth rates and pup weights as indicators of possible embryo damage.

Materials and Methods

Imaging System and FLIM measurements

Fluorescence lifetime imaging microscopy (FLIM) measurements were performed on a Nikon TE300 microscope with either a Nikon 20X objective (0.75 NA) or a Nikon 40X objective (1.25 NA), with a galvanometer scanner and a TCSPC module (SPC-150, Becker and Hickl). Two photon excitation was supplied via a Ti:Sapphire pulsed laser (M-Squared Lasers) with an 80-MHz repetition rate and ~150 fs pulse width. 750nm illumination (3–60 mW) and a 447/60nm bandpass filter were used for imaging NADH fluorescence. 890nm or 845nm illumination (12– 80 mW) and a 550/88nm bandpass filter were used for imaging FAD fluorescence. Illumination intensities were calibrated by measuring power output through the objective. Fluorescence was detected in the epi direction with a hybrid detector (HPM-100–40, Becker and Hickl). SHG was detected simultaneous with FAD imaging, by a single-photon counting detector (PMC-150, Becker-Hickl), placed in the forward direction, with combined 650 short-pass and 440/20nm bandpass filters. Scans were acquired for 5–60 seconds, with either 1 or 3 separate Z-planes for metabolic measurements. A customized motorized stage (using Conex TRA12CC actuators) was used for multi-dimensional acquisition. Bright-field was performed using the same 20X and 40X objectives and an Amscope MU300 camera. Acquisitions were performed using custom Labview software.

Embryo and oocyte imaging, metabolic perturbations, and live birth experiments

Cryopreserved oocytes and 1-cell mouse embryos (EmbryoTech, Haverhill MA), from crosses between B6C3F1 females and B6D2F1 males, were thawed and transferred to pre-equilibrated dishes for either culture or perturbation experiments. Research was conducted under a protocol approved by Harvard's institution's Animal Care and Use Committee (IACUC), which has a Letter of Assurance (File No. A3593-01) from the National Institutes of Health Office of Laboratory Animal Welfare. Embryos were imaged in either custom-fabricated microwell dishes with glass coverslip bottoms, commercial plastic microwell dishes (Vitrolife Primo Vision), or commercial glass bottom dishes (MatTekP35G-0.170-14-C) in KSOM media (MR-121-D, Millipore-Sigma) in an on-stage incubator (Ibidi, 10918), at 37C, 5% CO₂ and 5% O₂. Prior to imaging, embryos were stored in a table-top commercial incubator (Panasonic MCO5MPA).

For MitoTracker experiments, embryos were incubated in advanced KSOM (Millipore-Sigma MR-101-D) with 5nM MitoTracker Red CMXRos (Thermo Fisher M7512) for 20 minutes, then transferred directly to an aKSOM droplet in a glass-bottomed dish for imaging.

For metabolic perturbation experiments, oocytes were imaged in custom glass-bottomed microwell dishes to prevent movement of oocytes due to pipetting in drugs. Oxamate and rotenone were pipetted in during acquisition to final concentrations of 10mM and 1μM, respectively.

For live birth safety experiments, illuminated and non-illuminated embryos were transported at 37oC in pre-equilibrated KSOM to the Harvard Genome Modification facility at the blastocyst stage, where they were transferred into pseudo-pregnant CD1 mice as previously described (Gardner and Sakkas, 1993). Embryos were transferred in groups of 12, with 6 embryos in each uterine horn. Pregnant mice were then monitored daily by the facility and at birth pups were counted and weighed.

Data Analyses

We used supervised machine-learning-driven segmentation software (Sonka et al., 2015) to classify pixels in intensity images into three groups: mitochondrial and cytoplasmic NADH, and mitochondrial FAD (the concentration of FAD in the cytoplasm is extremely low (Dumollard et al., 2004), so photons from that potential group were not analyzed). The classification utilized a random forest algorithm (Breiman, 2001), which considered intensity, texture, and edge properties. The algorithm was trained on representative embryo NADH and FAD intensity images, wherein the user manually draws over the regions to specify their classification (e.g. mitochondrial, cytoplasmic, background). For each embryo segment, the photon arrival time histogram was modeled as a bi-exponential model decay:

$$P(t) = A((1 - F) \exp(-t/\tau_1) + F \exp(-t/\tau_2)) + B$$

Here, A is a normalization factor, B is the background level from factors such as room light (fits typically gave B/A ~ 0.005, indicating low background levels), τ_1 is the short lifetime, τ_2 is the long lifetime, and F is the fraction of molecule with long lifetime (the fraction engaged with enzymes for NADH and unengaged for FAD). This function was convolved with a measured instrument response function to model the experimental data, and least-square fitting yielded quantitative values for these three fit parameters. An additional parameter, I, the fluorescence intensity, was calculated for each region by dividing the total number of photons detected in the region by the area of the region. Thus, between NADH cytoplasm, NADH mitochondria, and FAD mitochondria, a single metabolic

measurement produces up to 12 quantitative parameters for characterizing the metabolic state of an embryo. Alternatively, if mitochondria and cytoplasm are not segmented and analyzed separately, then 8 parameters can be measured: 4 from NADH and 4 from FAD.

To evaluate the ability of FLIM to distinguish between different metabolic states, the three FLIM parameters with the largest separation between data groups were considered together. As a test condition, a separating plane was fit between data groups using a support vector machine algorithm (Cristianini and Shawe-Taylor, 2000).

Results

Mitochondria and spindle visualization and FLIM quantification

To investigate the potential utility of metabolic and SHG imaging for revealing mammalian egg and embryo physiology, we first explored the purely morphological data these techniques provide. Standard bright field microscopy of mouse blastocysts produces a clear view of the overall morphology of the embryo but gives limited information on the cellular scale (Fig. 1A, left). In contrast, imaging NADH autofluorescence in mouse blastocysts provides a detailed view of subcellular structures, such as nuclei (Fig. 1A, center image, indicated by white arrow). Two-photon imaging provides intrinsic optical sectioning, with the 1.25 NA objective used here resulting in a theoretical lateral (XY) resolution of 230nm and an axial (Z) resolution of 536nm. We consecutively imaged Z planes 2 microns apart (Supplemental movies 1 and 2), and combining the resulting data, enabling us to create 3D reconstructions of embryo morphology (Fig. 1A, right).

Similarly, bright-field images reveal the morphology of oocytes, but do not provide information on specific subcellular structures (Fig. 1B, left), while FAD, which is almost exclusively localized to mitochondria, shows a complex mitochondrial distribution inside oocytes (Fig. 1B, second to left). The same laser illumination that excites FAD autofluorescence can also nonlinearly interact with and scatter from the sample, enabling simultaneous imaging with SHG. The meiotic spindle and the zona pellucida are the only subcellular structures in mammalian oocytes that produces SHG, with the spindle generating by far the largest signal. This provides excellent intrinsic contrast (Fig. 1B, second panel from right) for spindle imaging. The combination of FLIM imaging and SHG allows detailed visualization of the internal structure of oocytes (Fig. 1B, right). Time lapse FLIM and SHG measurements provides information on dynamics. As the 1-cell embryo proceeds to divide, the spindle assembles in the middle of the cell (Fig. 1C, 1.7h) where the nucleus previously was, then elongates and thins during cytokinesis (Fig. 1C, 2.7h). At later times the spindle midbody is clearly visible, as the 2-cell embryo's nuclei form (Fig. 1C, 5h) (Supplementary movie 3).

NADH and FAD are highly enriched in mitochondria, arguing that bright regions and puncta within the cell contain high concentrations of mitochondria. To investigate this further, we used MitoTracker to specifically label the mitochondria, and imaged one and two-cell embryos with high resolution (40X 1.25NA objective, 20s integration time). We imaged MitoTracker (4mW illumination power), then either NADH (7mW) or FAD (30mW) immediately afterward (27s delayed) and found strong colocalization between the MitoTracker signal and the bright regions of both the NADH and the FAD intensity images (Fig. 2A and 2B). Machine-learning segmentations of the mitochondria in the NADH images had a $74.0 \pm 0.65\%$ overlap with the mitochondria in the MitoTracker images.

Segmentations based on FAD images had a $77.5 \pm 3.6\%$ with mitochondria in the MitoTracker images. Thus, NADH/FAD autofluorescence imaging provides information on the localization, morphology, and dynamics of mitochondria.

Beyond mitochondrial visualization, FLIM provides a multi-parametric, quantitative characterization of metabolic state. We were able to probe metabolic processes with sub-cellular resolution by performing high resolution imaging. This allowed us to separately segment mitochondrial and cytoplasmic regions, generating distinct arrival time histograms for each segment. Performing this segmentation on NADH and FAD intensity images (Fig. 2A and 2B, right panels), and fitting resultant histograms for NADH cytoplasm, NADH mitochondrial, and FAD mitochondrial regions (Fig. 2C, left and middle panels), we obtained a total of 12 quantitative parameters (Fig. 2C, right panel). The arrival time histograms each contained $\sim 100,000$ - $200,000$ photons, allowing the parameters to be measured with high precision: the 95% confidence interval for every parameter was less than 10% of its mean.

Metabolic imaging enables in situ measurements of mitochondrial metabolism

To determine the extent to which FLIM parameters can be used to determine biologically relevant shifts in oocyte/embryo metabolism, we first investigated the impact of subjecting oocytes to the metabolic inhibitors, oxamate and rotenone. To obtain good spatial and temporal resolution, we performed these experiments in custom-fabricated, glass-bottomed microwell dishes with only one z-plane, 3mW NADH, 12.5mW FAD, 60s integration time, and a 40X objective.

Exposing oocytes to oxamate, a lactate dehydrogenase inhibitor, resulted in a readily visible decrease in cytosolic NADH intensity (Fig. 3A). Subsequent addition of rotenone caused a pronounced increase in NADH intensity and a decrease in FAD intensity (hence an increase in the redox ratio, NADH/FAD) in mitochondria. SHG images (Fig. 3B, overlaid in magenta) revealed that oxamate did not disrupt the meiotic spindle, but exposure to rotenone caused it to disappear (Supplementary movie 4).

Averaging data from the 25 oocytes (Fig. 3C) revealed a significant change after oxamate exposure in six FLIM parameters: NADH intensity decreased by $33 \pm 2\%$ ($p = 1.7e-9$); NADH fraction engaged decreased by $7 \pm 2\%$ ($p = 1.5e-6$); NADH τ_1 decreased by $35 \pm 2\%$ ($p = 1.4e-16$); FAD fraction engaged decreased by $4.9 \pm 0.6\%$ ($p = 1.8e-11$); FAD τ_1 increased by $29 \pm 7\%$ ($p = 1.7e-6$); FAD τ_2 increased by $6 \pm 2\%$ ($p = 3e-4$). Oxamate is known to change cytosolic metabolic activity, and we detected highly significant changes in our measured FLIM parameters after exposure to the chemical. Thus, the results support our hypothesis that FLIM parameters can measure metabolic state and distinguish different states.

Subsequent exposure of oocytes to rotenone, an inhibitor of the electron transport chain, also caused a significant, but distinct set of parameter changes: NADH intensity increased by $32 \pm 3\%$ ($p = 4e-6$); NADH fraction engaged decreased by $14 \pm 1.4\%$ ($p = 9e-20$); NADH τ_1 increased by $19 \pm 4\%$ ($p = 1.6e-6$); NADH τ_2 increased by $14 \pm 2\%$ ($p = 3e-14$); FAD intensity decreased by $19 \pm 2\%$ ($p = 7e-8$); FAD fraction engaged decreased by $4.7 \pm 0.6\%$ ($p = 7e-11$). Rotenone is known to change mitochondrial metabolic activity, and we detected highly significant changes in our measured FLIM

parameters after exposure to the chemical. Thus, the results support our hypothesis that FLIM parameters can measure metabolic state and distinguish different states.

To further characterize the ability of metabolic imaging to distinguish between different metabolic states, we compared discrete time points by plotting the three metabolic parameters with the highest degree of separation on a 3D plot (Fig. 3D-F). Support vector machine planes were fit to the data as a test condition, and this comparison was performed for no perturbation vs oxamate (Fig. 3D), oxamate vs oxamate + rotenone (Fig. 3E), and no perturbation vs oxamate + rotenone (Fig. 3F). In all cases, the data sets were perfectly separated by FLIM.

These oxamate and rotenone experiments indicate that metabolic imaging can be used to readily resolve changes in metabolism induced by poisons. We next sought to determine if metabolic imaging is sensitive enough to also measure the changes in embryo metabolism that take place during pre-implantation development. For these experiments, we used multi-well plastic dishes with five embryos per well. Metabolic images were taken at 3 different Z planes every two hours, over the course of seventy hours, using 30mW NADH, 50mW FAD, and 60s integration time for each plane. Individual embryos were tracked from the 1-cell stage to blastocyst (Fig. 4A, Supplementary movie 5). To obtain strong signal, photons from all three planes were binned into one histogram for each time point. We calculated metabolic parameters for each embryo, which underwent highly significant changes over the course of pre-implantation embryo development (Fig. 4B). Plotting data from 39 different embryos shows that changes over development were highly stereotyped (Fig. 4C). To further investigate the repeatability of these measurements, we split the data into two batches (with $n = 20$ and $n = 19$ embryos) from separately acquired time courses. The metabolic parameters from two batches were highly similar (Supplementary Fig. 1), arguing that these measurements are robust and repeatable.

Metabolic parameters changed monotonically between the period shortly after the first division ($t=0$ in Fig. 4B and C) and compaction (44h), and different monotonic changes were observed between compaction and expanded blastocyst. Comparing the 1-cell embryo to morula revealed highly significant changes in four FLIM parameters (each with $p < 10^{-6}$): NADH intensity, NADH τ_1 , FAD intensity, and FAD τ_1 . Comparing morula to blastocyst revealed highly significant changes in four FLIM parameters (each with $P < 0.002$): NADH intensity, NADH fraction bound, NADH τ_1 , and FAD intensity. These observations reflect the known changes in metabolism which occur over the course of embryo development. Using just three of the measured FLIM parameters, it is possible to completely separate one cell embryos from morula (Figure 4D), morula from blastocyst (Fig. 4E), and one cell embryos from blastocyst (Fig. 4F). Thus, metabolic imaging is sensitive enough to measure natural changes in embryo metabolism.

Live birth safety study

The ability of metabolic imaging and SHG to visualize mitochondria and spindles, and the obtained quantitative information on embryo metabolism, suggests that these techniques may be helpful in clinical embryology. These techniques are noninvasive in that they do not require exposing the embryos to any reagents; however, illumination light can damage embryos. Thus, we sought to determine if the illumination required for high signal-to-noise metabolic measurements damaged

embryos. We exposed experimental groups of embryos to repeated acquisitions, every 2 hours for 48 hours, taking metabolic measurements with settings identical to those used in Fig. 4 (30mW NADH, 50mW FAD, 60s integration time, 3 z-planes). Control groups of embryos were incubated in the same dishes as the experimental groups, but not exposed to any illumination. For the experimental group, n=144 illuminated embryos were implanted into n=12 mice; and for the control group, n=108 non-illuminated embryos were implanted into n=9 mice. Numbers of pups per mouse and individual pup weights were later measured when the mice gave birth.

There was no significant difference in either birth rate or pup weight between the illuminated and control groups (Fig. 5). For the birth rate measurement, the high labor cost per data point (pups/mouse) limited the feasibility of obtaining a very high sample size. As such, it was only possible to power this study to detect a 50% decrease in birth rate with an alpha of 0.05 and beta of 0.8. For pup weight, however, the sample size was much larger, such that the study was powered to detect a 7% decrease in weight. We observed an average experimental pup weight that differed by less than 1% from the control group.

Discussion

Here we have explored the utility of FLIM and SHG for imaging mammalian oocytes and embryos. These techniques allow noninvasive measurements of the location and morphology of mitochondria, nuclei, and spindles. We also demonstrated that FLIM of NADH and FAD is robust and sensitive enough to detect metabolic changes in individual embryos associated with metabolic poisons and the natural changes that occur during embryo development. We found that this imaging does not significantly impair live births in mice. These results argue that FLIM and SHG can be used to noninvasively obtain relevant biological information on oocytes and embryos, and thus are highly promising tools for ART.

Measuring Metabolism of Oocytes and Embryos with FLIM

Proper metabolism is crucial for embryo development, and metabolic fluxes of glycolysis and oxidative phosphorylation, determined by nutrient uptake and oxygen consumption, have been found to correlate with embryo quality (Gardner and Leese, 1987; Gardner et al., 2011; Gardner and Wale, 2013). However, previous non-targeted assessments of embryo metabolism have not been clinically useful, likely because of their complexity and lack of sensitivity (Hardarson et al., 2012; Vergouw et al., 2012). Metabolic imaging via two-photon FLIM of NADH and FAD is a highly promising alternative approach for measuring embryo metabolism for ART because: it can provide detailed metabolic information on both the cytoplasm, related to glycolysis, and mitochondria, related to oxidative phosphorylation; it is highly quantitative and robust; it is noninvasive, and does not require the use of any foreign stains or specialized media. Here, we have also shown that metabolic imaging with FLIM can be used to characterize the changes in metabolism that occur during preimplantation embryo development. The observed large shifts in metabolism at the morula stage are consistent with expectations from previous studies (Houghton et al., 1996; Chason et al., 2011), but these measurements also yielded unexpected results that should be further investigated. For example, blastocysts engage in aerobic glycolysis (Gardner and Harvey, 2015), which would naively be

expected to result in increases of NADH concentration (e.g. as in cancer cells (Yu and Heikal, 2009)). However, we observe an approximately 50% decrease in NADH intensity with blastocyst formation, suggesting further study is needed to understand this metabolic transition. This could be due to the oxidation of cytosolic NADH during the conversion of pyruvate to lactate, which occurs as the blastocyst prepares to implant (Gardner, 2015). In addition to enabling new, fundamental insights, improved metabolic measures may also allow better refinement of embryo culture media.

Imaging Spindles with SHG

A microscopy system for two-photon FLIM can also be used to simultaneously acquire SHG images, without the need for additional acquisition time or photo-exposure. SHG can produce high-quality images of meiotic and mitotic spindles (Campagnola and Loew, 2003; Hsieh et al., 2008; Campagnola, 2011; Yu et al., 2014) (Fig. 1B and C). Previous work has investigated the use of polarized light microscopy for imaging the spindle, and it has been reported that there are associations between meiotic spindle morphology and oocyte quality (Battaglia et al., 1996; Zeng et al., 2007; Tomari et al., 2011, 2018; Korkmaz et al., 2015; García-Oro et al., 2017; Guo et al., 2017). Thus, SHG imaging of meiotic spindles might also provide useful information for selecting high-quality oocytes. It will be interesting for future work to determine if imaging mitotic spindles in early embryos can provide additional information to aid in identifying aneuploid embryos.

Safety

It is paramount to investigate the safety of new technologies before attempts are made to apply them clinically. While metabolic imaging with FLIM does not entail exposing oocytes and embryos to foreign material, there is the potential concern that that illumination could cause harm. Excess light dosage from conventional microscopy is detrimental (Masters and So, 2008), but such effects can be minimized or eliminated by controlling light exposure, as performed in time lapse imaging systems (Nakahara et al., 2010). Similarly, the repeated laser pulses blastocysts conventionally receive during trophectoderm biopsy procedures do not appear to reduce embryo viability (Scott et al., 2013b), although when performed in excess they may lead to damage (Bradley et al., 2017). We thus investigated the safety of illumination during FLIM imaging of embryos and found that time lapse exposure of 1 measurement every 2 hours for 48 hours did not significantly impact live birth rates or pup weights. Previous work also demonstrated that this level of illumination did not cause a measurable difference in intracellular reactive oxygen species and blastocyst formation rates (Pedro et al., 2018). It is likely that in a clinical setting far fewer measurements of metabolism would be sufficient to aid in selection, perhaps at only 1-3 time points.

Strengths and limitations

Because these experiments were performed in mouse, conclusions around the sensitivity and safety of these new methods may not generalize to human. Inbred mice used here are genetically homogenous, and the level of variation between human patients is not yet known. Performing these studies in human, where tracking individual embryos is possible, is the only way to measure the direct correspondence between FLIM measurements and birth outcome. True evaluation of this imaging system as an IVF tool will require clinical studies, including measurements on discarded embryos to obtain baseline data, expanded safety assessment, observational studies, and clinical

trials to demonstrate efficacy for predicting live birth. A limitation of the live birth data is also that although cages were routinely monitored, early morning and during the day, we could not preclude that some runt pups may have been eaten.

Conclusion

Our results indicate that metabolic imaging is a highly sensitive assay for measuring changes in embryo metabolic function, which is known to be essential for viability. Taken together with simultaneous spindle imaging via SHG, we believe these proof-of-concept data and initial safety studies are encouraging indications that noninvasive metabolic imaging may be helpful for clinical embryo and oocyte assessment.

Acknowledgments

The authors would like to thank Becker Hickl GmbH for contributing a single-photon counting detector and time-correlated single photon counting (TCSPC) electronics to this research. We would also like to thank the Harvard Genome Modification Facility for performing the mouse transfer experiments.

Authors' Roles

Tim Sanchez – contributed to conception and design, acquisition, analysis, and interpretation of experiments and was involved in drafting and completion of the article. He has approved the final version.

Marta Venturas – contributed to the design, acquisition, analysis, and interpretation of the experiments. She was involved in completion of the article and has approved the final version.

Ali Aghvami – Co-designed and manufactured the custom glass-bottomed microwell dishes. He was involved in completion of the article and has approved the final version.

Xingbo Yang – Performed the segmentation analysis of the MitoTracker and NADH/FAD data. He was involved in completion of the article and approved the final version.

Seth Fraden – Was involved in the completion of the article and approved the final version.

Denny Sakkas – contributed to conception and design of experiments and to the interpretation of the data, and he was involved in drafting and completion of the article. He has approved the final version.

Dan Needleman – contributed to conception, design, and interpretation of experiments, and he was involved in drafting and completion of the article. He has approved the final version.

Funding Statement

Supported by the Blavatnik Biomedical Accelerator Grant at Harvard University, and by the Harvard Catalyst | The Harvard Clinical and Translational Science Center (National Institutes of Health Award UL1 TR001102), by NSF grants DMR-0820484 and PFI-TT-1827309, and NIH grant R01HD092550-01. T.S. was supported by a National Science Foundation Postdoctoral Research Fellowship in Biology grant (1308878). S.F. and A.A. were supported by NSF MRSEC DMR-1420382. Becker and Hickl GmbH sponsored research with the loaning of equipment for FLIM.

Conflict of Interest

T.S. is cofounder and a shareholder and officer of LuminOva, Inc. and co-holds patent US20150346100A1 pending for metabolic imaging methods for assessment of oocytes and embryos and patent US20170039415A1 issued for nonlinear imaging systems and methods for assisted reproductive technologies. D.N. is cofounder and a shareholder and officer of LuminOva and co-holds patent US20150346100A1 pending for metabolic imaging methods for assessment of oocytes and embryos and patent US20170039415A1 issued for nonlinear imaging systems and methods for assisted reproductive technologies. D.S. is on the scientific advisory board for Cooper Surgical and has stock options with LuminOva.

References

- Armstrong S, Bhide P, Jordan V, Pacey A, Marjoribanks J, Farquhar C. Time-lapse systems for embryo incubation and assessment in assisted reproduction. *Cochrane Database Syst Rev* [Internet] 2019; John Wiley & Sons, Ltd Available from: <http://doi.wiley.com/10.1002/14651858.CD011320.pub4>.
- Baart EB, Martini E, Berg I van den, Macklon NS, Galjaard RJH, Fauser BCJM, Opstal D Van. Preimplantation genetic screening reveals a high incidence of aneuploidy and mosaicism in embryos from young women undergoing IVF. *Hum Reprod* 2006;21:223–233.
- Babayev E, Seli E. Oocyte mitochondrial function and reproduction. *Curr Opin Obstet Gynecol* [Internet] 2015;27:175–181.
- Battaglia DE, Goodwin P, Klein NA, Soules MR. Influence of maternal age on meiotic spindle assembly in oocytes from naturally cycling women. *Hum Reprod* [Internet] 1996;11:2217–2222.
- Becker W. Fluorescence lifetime imaging – techniques and applications. *J Microsc* [Internet] 2012;247:119–136.
- Becker W. *The bh TCSPC Handbook*. 2017; Becker & Hickl GmbH: Berlin, Germany.
- Berg J, Tymoczko J, Stryer L. *Biochemistry*. *Biochemistry* 2007;
- Blerkom J Van, Davis PW, Lee J. ATP content of human oocytes and developmental potential and outcome after in-vitro fertilization and embryo transfer. *Hum Reprod* [Internet] 1995;10:415–424.
- Bradley CK, Livingstone M, Traversa M V., McArthur SJ. Impact of multiple blastocyst biopsy and vitrification-warming procedures on pregnancy outcomes. *Fertil Steril* [Internet] 2017;108:999–1006. Elsevier Inc.
- Breiman L. Random forests. *Mach Learn* 2001;45:1–32.
- Campagnola P. Second harmonic generation imaging microscopy: applications to diseases diagnostics. *Anal Chem* [Internet] 2011;83:3224–3231.
- Campagnola PJ, Loew LM. Second-harmonic imaging microscopy for visualizing biomolecular arrays in cells, tissues and organisms. *Nat Biotechnol* [Internet] 2003;21:1356–1360.
- Capalbo A, Ubaldi FM, Rienzi L, Scott R, Treff N. Detecting mosaicism in trophectoderm biopsies: Current challenges and future possibilities. *Hum Reprod* 2017;32:492–498.
- Cecchino GN, Garcia-Velasco JA. Mitochondrial DNA copy number as a predictor of embryo viability. *Fertil Steril* [Internet] 2019;111:205–211. Elsevier Inc.
- Chason RJ, Csokmay J, Segars JH, DeCherney AH, Armant DR. Environmental and epigenetic effects upon preimplantation embryo metabolism and development. *Trends Endocrinol Metab* [Internet] 2011;22:412–420. Elsevier Ltd.
- Cinco R, Digman MA, Gratton E, Luderer U. Spatial Characterization of Bioenergetics and Metabolism of Primordial to Preovulatory Follicles in Whole Ex Vivo Murine Ovary. *Biol Reprod* [Internet] 2016;95:biolreprod.116.142141.
- Cristianini N, Shawe-Taylor J. *An Introduction to Support Vector Machines: And Other Kernel-based Learning Methods*. 2000; Cambridge University Press: New York, NY, USA.
- Diez-Juan A, Rubio C, Marin C, Martinez S, Al-Asmar N, Riboldi M, Diaz-Gimeno P, Valbuena D, Simon C. Mitochondrial DNA content as a viability score in human euploid embryos: less is better. *Fertil Steril* 2015;11:373–378.
- Dumollard R, Marangos P, Fitzharris G, Swann K, Duchon M, Carroll J. Sperm-triggered $[Ca^{2+}]$ oscillations and Ca^{2+} homeostasis in the mouse egg have an absolute requirement for mitochondrial ATP production. *Development* 2004;131:3057–3067.
- Dumollard R, Ward Z, Carroll J, Duchon MR. Regulation of redox metabolism in the mouse oocyte and embryo. *Development* [Internet] 2007;134:455–465.
- Forman EJ, Hong KH, Ferry KM, Tao X, Taylor D, Levy B, Treff NR, Scott RT. In vitro fertilization with single euploid blastocyst transfer: A randomized controlled trial. *Fertil Steril* [Internet] 2013;100:100–107.e1. Elsevier Inc.

- Fragouli E, Spath K, Alfarawati S, Kaper F, Craig A, Michel CE, Kokocinski F, Cohen J, Munne S, Wells D. Altered Levels of Mitochondrial DNA Are Associated with Female Age, Aneuploidy, and Provide an Independent Measure of Embryonic Implantation Potential. *Obstet Gynecol Surv* 2016;71:28–29.
- García-Oro S, Rey MI, Rodríguez M, Durán Á, Devesa R, Valverde D. Predictive value of spindle retardance in embryo implantation rate. *J Assist Reprod Genet* 2017;34:617–625. *Journal of Assisted Reproduction and Genetics*.
- Gardner DK. Changes in requirements and utilization of nutrients during mammalian preimplantation embryo development and their significance in embryo culture. *Theriogenology* 1998;49:, p. 83–102.
- Gardner DK. Lactate production by the mammalian blastocyst: Manipulating the microenvironment for uterine implantation and invasion? *BioEssays* 2015;37:364–371.
- Gardner DK, Harvey AJ. Blastocyst metabolism. *Reprod Fertil Dev* 2015;27:638–654.
- Gardner DK, Lane M, Stevens J, Schoolcraft WB. Noninvasive assessment of human embryo nutrient consumption as a measure of developmental potential. *Fertil Steril* 2001;76:1175–1180.
- Gardner DK, Leese HJ. Non-invasive measurement of nutrient uptake by single cultured pre-implantation mouse embryos. *Hum Reprod* 1986;1:25–27.
- Gardner DK, Leese HJ. Assessment of embryo viability prior to transfer by the noninvasive measurement of glucose uptake. *J Exp Zool* 1987;242:103–105.
- Gardner DK, Meseguer M, Rubio C, Treff NR. Diagnosis of human preimplantation embryo viability. *Hum Reprod Update* 2015;21:727–747.
- Gardner DK, Pool TB, Lane M. Embryo nutrition and energy metabolism and its relationship to embryo growth, differentiation, and viability. *Semin Reprod Med* 2000;18:205–218.
- Gardner DK, Sakkas D. Mouse embryo cleavage, metabolism and viability: Role of medium composition. *Hum Reprod* 1993;8:288–295.
- Gardner DK, Sakkas D. Human Gametes and Preimplantation Embryos [Internet]. In Gardner DK, Sakkas D, Seli E, Wells D, editors. 2013; Springer New York: New York, NY Available from: <http://link.springer.com/10.1007/978-1-4614-6651-2>.
- Gardner DK, Wale PL. Analysis of metabolism to select viable human embryos for transfer. *Fertil Steril* [Internet] 2013;99:1062–1072. Elsevier Inc.
- Gardner DK, Wale PL, Collins R, Lane M. Glucose consumption of single post-compaction human embryos is predictive of embryo sex and live birth outcome. *Hum Reprod* 2011;26:1981–1986.
- Ghukasyan V V., Heikal AA. Natural Biomarkers for Cellular Metabolism: Biology, Techniques, and Applications [Internet]. 2014; CRC Press Available from: <https://www.crcpress.com/Natural-Biomarkers-for-Cellular-Metabolism-Biology-Techniques-and-Applications/Ghukasyan-Heikal/9781466509986>.
- Guo Y, Liu W, Wang Y, Pan J, Liang S, Ruan J, Teng X. Polarization microscopy imaging for the identification of unfertilized oocytes after short-term insemination. *Fertil Steril* [Internet] 2017;108:78–83. Elsevier Inc.
- Hardarson T, Ahlström A, Rogberg L, Botros L, Hillensjö T, Westlander G, Sakkas D, Wikland M. Non-invasive metabolomic profiling of Day 2 and 5 embryo culture medium: A prospective randomized trial. *Hum Reprod* 2012;27:89–96.
- Heikal A. A Multiparametric Imaging of Cellular Coenzymes for Monitoring Metabolic and Mitochondrial Activities. *Rev Fluoresc* 2010 [Internet] 2012;2010:223–243.
- Houghton FD, Thompson JG, Kennedy CJ, Leese HJ. Oxygen Consumption and Energy Metabolism of the Early Mouse Embryo. *Mol Reprod Dev* 1996;44:476–485.
- Hsieh C-S, Chen S-U, Lee Y-W, Yang Y-S, Sun C-K. Higher harmonic generation microscopy of in vitro cultured mammal oocytes and embryos. *Opt Express* [Internet] 2008;16:11574–11588.
- Klaidman LK, Leung AC, Adams JD. High-Performance Liquid Chromatography Analysis of Oxidized and Reduced Pyridine Dinucleotides in Specific Brain Regions. *Anal Biochem* [Internet] 1995;228:312–317.
- Korkmaz C, Tekin YB, Sakinci M, Ercan CM. Effects of maternal ageing on ICSI outcomes and embryo development in relation to oocytes morphological characteristics of birefringent structures. *Zygote* 2015;23:550–555.
- Leese HJ. Quiet please, do not disturb: A hypothesis of embryo metabolism and viability. *BioEssays* 2002;24:845–849.
- Ma N, Mochel NR de, Pham PDA, Yoo TY, Ken WY, Cho MAD. Label-free assessment of preimplantation embryo quality by the Fluorescence Lifetime Imaging Microscopy (FLIM)-phasor approach. *bioRxiv* [Internet] 2018; Available from: <https://doi.org/10.1101/286682>.
- Masters BR, So P. Handbook of biomedical nonlinear optical microscopy [Internet]. *J Biomed Opt* [Internet] 2008;14:. Oxford University Press.
- Mujat C, Greiner C, Baldwin A, Levitt JM, Tian F, Stucenski LA, Hunter M, Kim YL, Backman V, Feld M, et al. Endogenous optical biomarkers of normal and human papillomavirus immortalized epithelial cells. *Int J Cancer* 2008;122:363–371.
- Munne S, Kaplan B, Frattarelli JL, Gysler M, Child TJ, Nakhuda G, Shamma FN, Silverberg K, Kalista T, Oliver K, et al. Global multicenter randomized controlled trial comparing single embryo transfer with embryo selected by preimplantation genetic screening using next-generation sequencing versus morphologic assessment. *Fertil Steril* [Internet] 2017;108:e19.

- Murphy LA, Seidler EA, Vaughan DA, Resetkova N, Penzias AS, Toth TL, Thornton KL, Sakkas D. To test or not to test? A framework for counselling patients on preimplantation genetic testing for aneuploidy (PGT-A). *Hum Reprod* [Internet] 2018;1–8 Available from: <https://academic.oup.com/humrep/advance-article/doi/10.1093/humrep/dey346/5219186>.
- Nagai S, Mabuchi T, Hirata S, Shoda T, Kasai T, Yokota S, Shitara H, Yonekawa H, Hoshi K. Correlation of abnormal mitochondrial distribution in mouse oocytes with reduced developmental competence. *Tohoku J Exp Med* 2006;210:137–144.
- Nakahara T, Iwase A, Goto M, Harata T, Suzuki M, Ienaga M, Kobayashi H, Takikawa S, Manabe S, Kikkawa F, et al. Evaluation of the safety of time-lapse observations for human embryos. *J Assist Reprod Genet* [Internet] 2010;27:93–96.
- Niakan KK, Han J, Pedersen RA, Simon C, Pera RAR. Human pre-implantation embryo development. *Development* [Internet] 2012;139:829–841.
- Okabe K, Inada N, Gota C, Harada Y, Funatsu T, Uchiyama S. Intracellular temperature mapping with a fluorescent polymeric thermometer and fluorescence lifetime imaging microscopy. *Nat Commun* [Internet] 2012;3:705–709. Nature Publishing Group.
- Parker WC, Chakraborty N, Vrikkis R, Elliott G, Smith S, Moyer PJ. High-resolution intracellular viscosity measurement using time-dependent fluorescence anisotropy. *Opt Express* [Internet] 2010;18:16607–16617.
- Pedro MV, Sanchez T, Seidler EA, Sakkas D, Needleman D. Safety of fluorescence lifetime imaging microscopy (FLIM) as a non-invasive assessment of embryo metabolism. *Eur Soc Hum Reprod Embryol* [Internet] 2018; p. P-193 Available from: <https://www.eshre.eu/Books/ESHRE2018/Programme2018/files/basic-html/page337.html>.
- Potter SM. Vital imaging: Two photons are better than one. *Curr Biol* 1996;6:1595–1598.
- Renard J, Philippon A, Menezo Y. In-vitro uptake of glucose by bovine blastocysts. *J Reprod ...* 1980;58:161–164.
- Rieger D. Relationships between energy metabolism and development of early mammalian embryos. *Theriogenology* 1992;37:75–93.
- Sanchez T, Seidler EA, Gardner DK, Needleman D, Sakkas D. Will noninvasive methods surpass invasive for assessing gametes and embryos? *Fertil Steril* [Internet] 2017;108:730–737. Elsevier Inc.
- Sanchez T, Wang T, Venturas Pedro M, Zhang M, Esencan E, Sakkas D, Needleman D, Seli E. Metabolic imaging with the use of fluorescence lifetime imaging microscopy (FLIM) accurately detects mitochondrial dysfunction in mouse oocytes. *Fertil Steril* [Internet] 2018;110:1387–1397. Elsevier Inc.
- Scott RT, Upham KM, Forman EJ, Hong KH, Scott KL, Taylor D, Tao X, Treff NR. Blastocyst biopsy with comprehensive chromosome screening and fresh embryo transfer significantly increases in vitro fertilization implantation and delivery rates: A randomized controlled trial. *Fertil Steril* [Internet] 2013a;100:697–703. Elsevier Inc.
- Scott RT, Upham KM, Forman EJ, Zhao T, Treff NR. Cleavage-stage biopsy significantly impairs human embryonic implantation potential while blastocyst biopsy does not: A randomized and paired clinical trial. *Fertil Steril* [Internet] 2013b;100:624–630. Elsevier Inc.
- Smith PW. Mode-locking of lasers. *Proc IEEE* 1970;58:1342–1355.
- Sonka M, Hlavac V, Boyle R. *Image Processing, Analysis, and Machine Vision*. 2015; Cengage Learning.
- Staniszewski K, Audi SH, Sepehr R, Jacobs ER, Ranji M. Surface fluorescence studies of tissue mitochondrial redox state in isolated perfused rat lungs. *Ann Biomed Eng* [Internet] 2013;41:827–836.
- Stein LR, Imai SI. The dynamic regulation of NAD metabolism in mitochondria. *Trends Endocrinol Metab* 2012;23:420–428.
- Tomari H, Honjo K, Kunitake K, Aramaki N, Kuhara S, Hidaka N, Nishimura K, Nagata Y, Horiuchi T. Meiotic spindle size is a strong indicator of human oocyte quality. *Reprod Med Biol* 2018;17:268–274.
- Tomari H, Honjou K, Nagata Y, Horiuchi T. Relationship between meiotic spindle characteristics in human oocytes and the timing of the first zygotic cleavage after intracytoplasmic sperm injection. *J Assist Reprod Genet* 2011;28:1099–1104.
- Treff NR, Zhan Y, Tao X, Olcha M, Han M, Rajchel J, Morrison L, Morin SJ, Scott RT. Levels of trophectoderm mitochondrial DNA do not predict the reproductive potential of sibling embryos. *Hum Reprod* 2017;32:954–962.
- Tucker KR, Cavolo SL, Levitan ES. Elevated mitochondria-coupled NAD(P)H in endoplasmic reticulum of dopamine neurons. *Mol Biol Cell* [Internet] 2016;27:3214–3220.
- Vanneste E, Voet T, Caignec C Le, Ampe M, Konings P, Melotte C, Debrock S, Amyere M, Vikkula M, Schuit F, et al. Chromosome instability is common in human cleavage-stage embryos. *Nat Med* 2009;15:577–583.
- Vega M, Jindal S. Mosaicism: throwing the baby out with the bath water? *J Assist Reprod Genet* [Internet] 2017;34:11–13. *Journal of Assisted Reproduction and Genetics*.
- Vergouw CG, Kieslinger DC, Kosteljik EH, Botros LL, Schats R, Hompes PG, Sakkas D, Lambalk CB. Day 3 embryo selection by metabolomic profiling of culture medium with near-infrared spectroscopy as an adjunct to morphology: A randomized controlled trial. *Hum Reprod* 2012;27:2304–2311.
- Wong KM, Repping S, Mastenbroek S. Limitations of embryo selection methods. *Semin Reprod Med* 2014;32:127–133.
- Yoo TY, Choi JM, Conway W, Yu CH, Pappu R V., Needleman DJ. Measuring NDC80 binding reveals the molecular basis of tension-dependent kinetochore-microtubule attachments. *Elife* 2018;7:1–34.
- Yu CH, Langowitz N, Wu HY, Farhadifar R, Bragues J, Yoo TY, Needleman D. Measuring microtubule polarity in spindles with second-harmonic generation. *Biophys J* [Internet] 2014;106:1578–1587. Elsevier.

- Yu Q, Heikal A a. Two-photon autofluorescence dynamics imaging reveals sensitivity of intracellular NADH concentration and conformation to cell physiology at the single-cell level. *J Photochem Photobiol B* [Internet] 2009;95:46–57. Elsevier B.V.
- Zeng H, Ren Z, Yeung WSB, Shu Y, Xu Y, Zhuang G, Liang X-Y. Low mitochondrial DNA and ATP contents contribute to the absence of birefringent spindle imaged with PolScope in in vitro matured human oocytes. *Hum Reprod* [Internet] 2007;22:1681–1686.

Figures and Tables

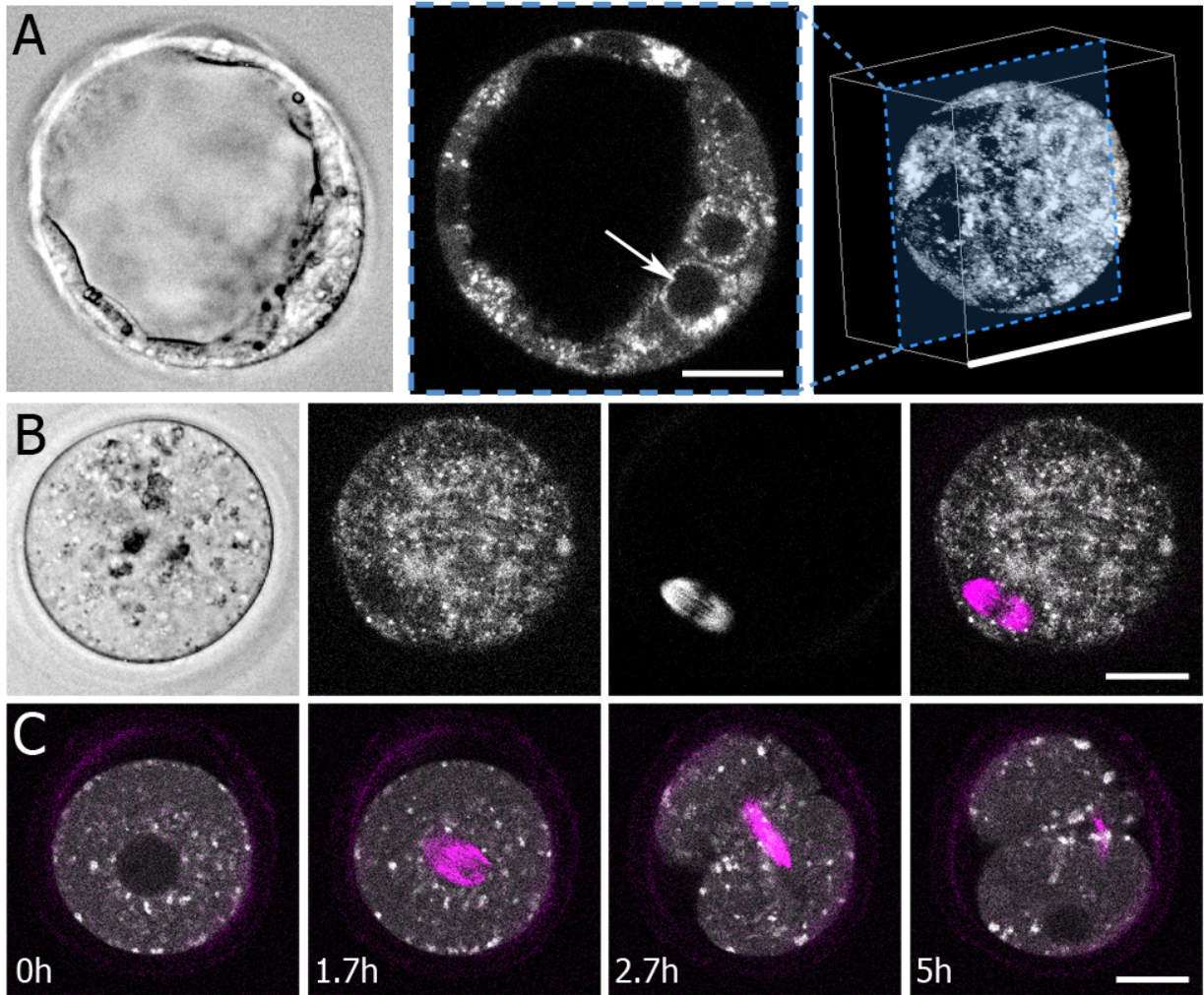


Figure 1: Morphological features imaged with FLIM and SHG imaging. A) Left: a standard bright-field image of a blastocyst shows gross morphological features. Middle: FLIM measurements of NADH generate intensity images that visualize subcellular structures, including nuclei (white arrow, 25µm scale bar). Right: 3D reconstruction from multiple focal planes. (100µm scale bar). B) Left: Bright-field image of an oocyte. Second to left: an FAD FLIM image of the same oocyte. Second to right: an SHG image of the same oocyte, which clearly shows the oocyte's spindle. Right: Overlay image of SHG (magenta) and FAD (grey scale) (25µm scale bar). C) Time lapse FLIM (NADH) and spindle measurements capture key embryo dynamics, such as cell division. (25µm scale bar).

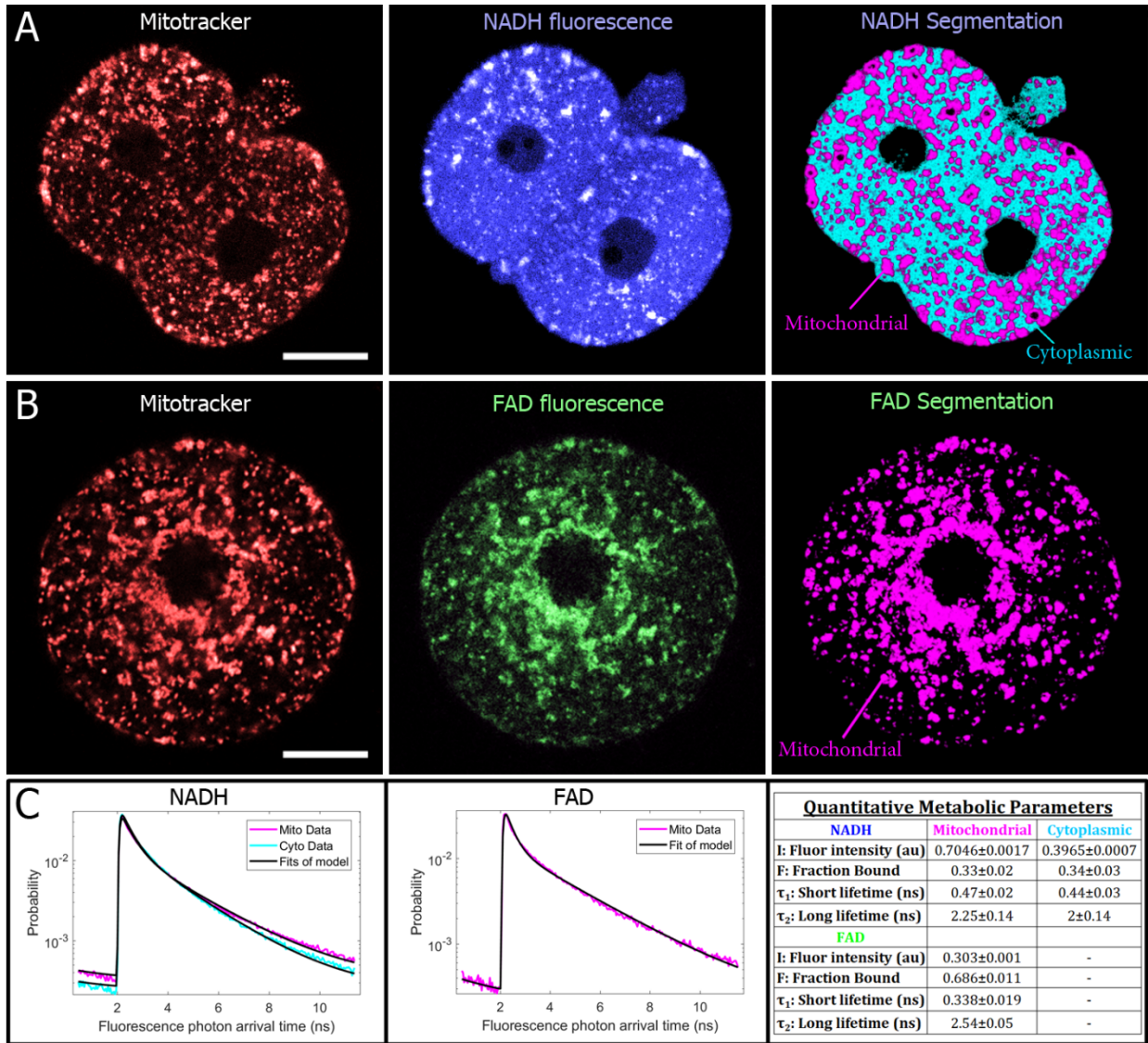


Figure 2: (A) MitoTracker images (left) of a two-cell embryo shows co-localization with brighter regions of NADH (center) (25 μ m scale bars). A machine-learning based algorithm performed on autofluorescence images successfully segments mitochondria and cytoplasm (right). (B) MitoTracker and FAD autofluorescence images of a one-cell embryo also show co-localization. For FAD images, only mitochondrial regions were segmented. C) For each region, all photon arrival times were binned into a separate histogram, which were normalized to produce a probability distribution, which represents the probability of being in an excited state after excitation. Fitting these curves to a two-exponential decay model produces a total of 12 parameters for characterizing the metabolic state of an embryo or oocyte (right).

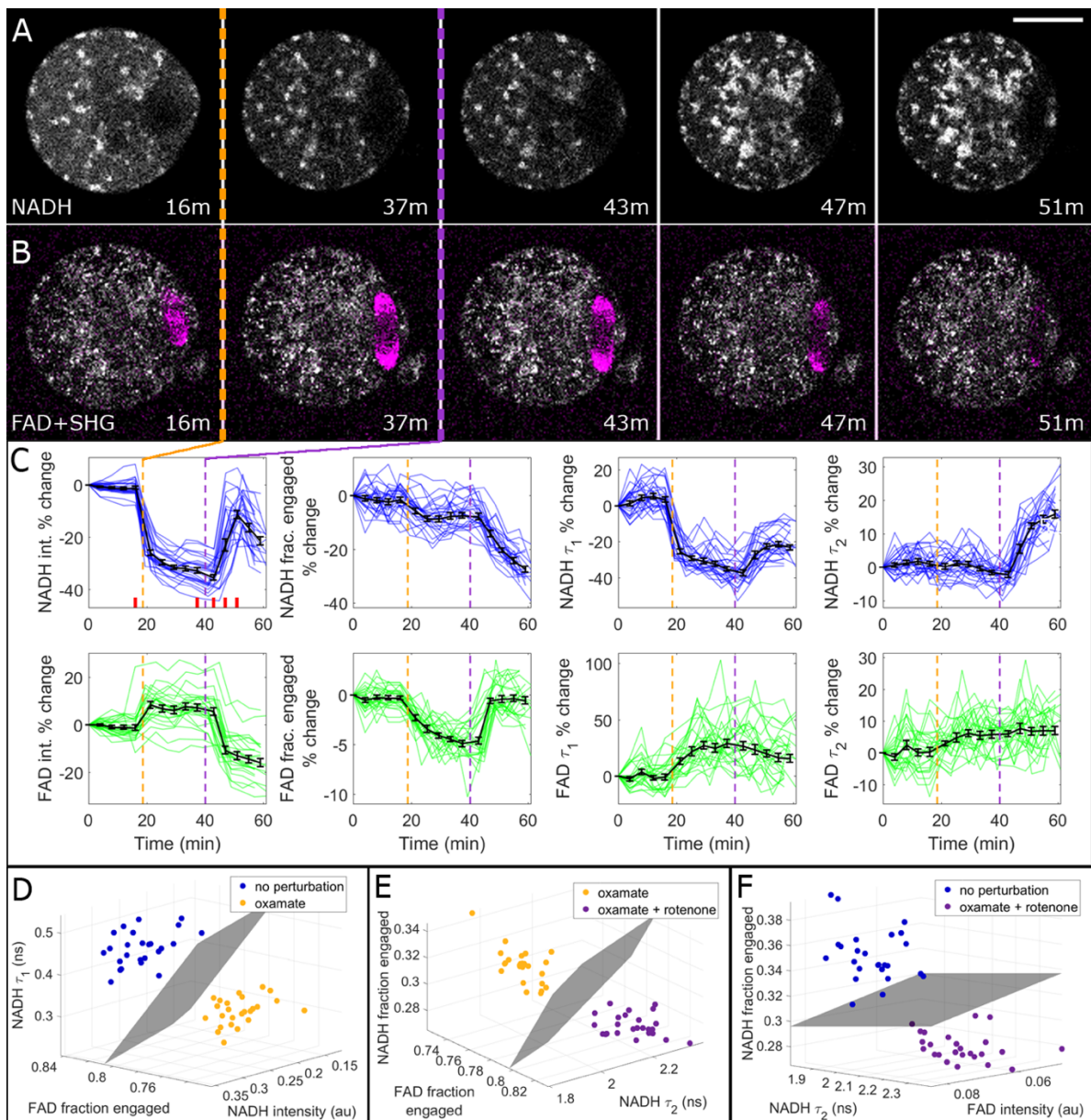


Figure 3: Oocytes were exposed to 10mM oxamate, and then to 1 μ M rotenone. A) Oxamate exposure (indicated with a dashed orange line) caused a visible drop in cytosolic NADH FLIM intensity, whereas rotenone exposure (purple line) caused an increase in mitochondrial NADH intensity. Bar is 30 μ m. B) For the same oocyte, oxamate slightly increased FAD intensity, while rotenone decreased it. Simultaneous SHG imaging, overlaid in magenta, revealed that spindles were not disrupted by oxamate, but were disintegrated by rotenone. C) Percentage-change time courses for all 8 metabolic parameters. Colored traces represent individual oocyte trajectories (n=25), and average curves are shown in black with standard error bars. Vertical dashed lines indicate oxamate (orange) and rotenone (purple) exposures. Red bars in the NADH intensity panel correspond to the time stamps of the images shown in (A) and (B). D) FLIM parameters were compared before and after oxamate exposure, and the three FLIM parameters with the largest separation were plotted on 3D plots, yielding perfect separation. This comparison was also performed for (E) oxamate vs oxamate + rotenone, and (F) no perturbation vs oxamate + rotenone.

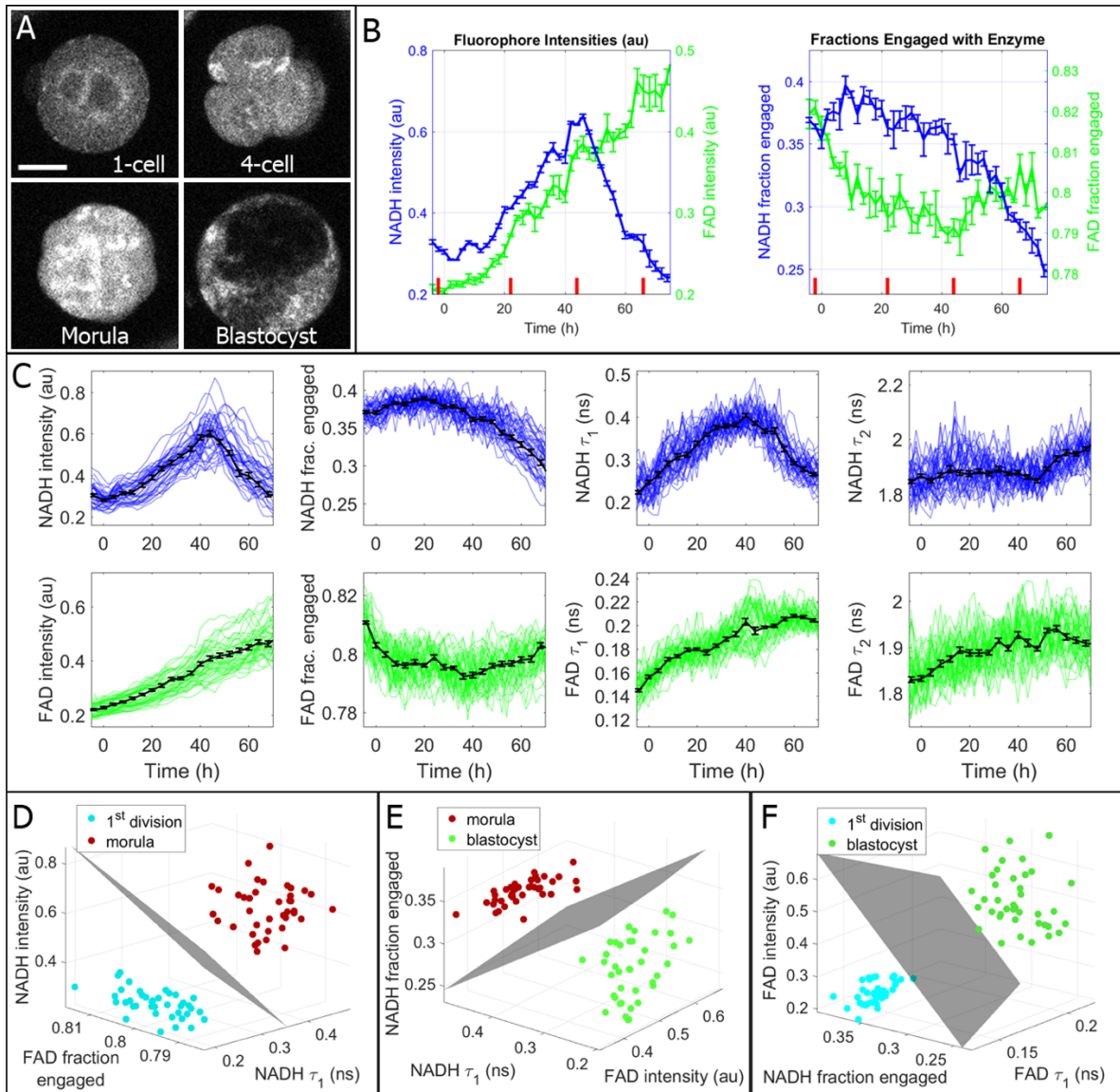


Figure 4: High time-resolution measurements of metabolic state during embryo development. A) Embryos were imaged together in 9-microwell dishes and individually tracked and analyzed to generate time plots for all FLIM parameters. Bar is 30 μ m. B) Time plots for NADH and FAD intensities and fractions engaged for the individual embryo shown in (A). Distinct changes are evident in multiple parameters, especially around the onset of blastocyst formation (\sim 44h after the 1st division, which is represented here as t=0h). Corresponding time points for the four images are displayed with red dashes on the plots. C) The observed trends were robust and reproducible among all healthy embryos. These plots display individual embryo trajectories as thin colored lines (n=39), which were synchronized by 1st division. Averaged metabolic curves from all 39 embryos are displayed as thick black lines with standard error bars. D) FLIM parameters were compared between the 1st division and morula stages, and the three FLIM parameters with the largest separation were plotted as 3D plots, yielding perfect separation. This comparison was also performed for (E) compaction vs expanded blastocyst and (F) 1st division vs expanded blastocyst.

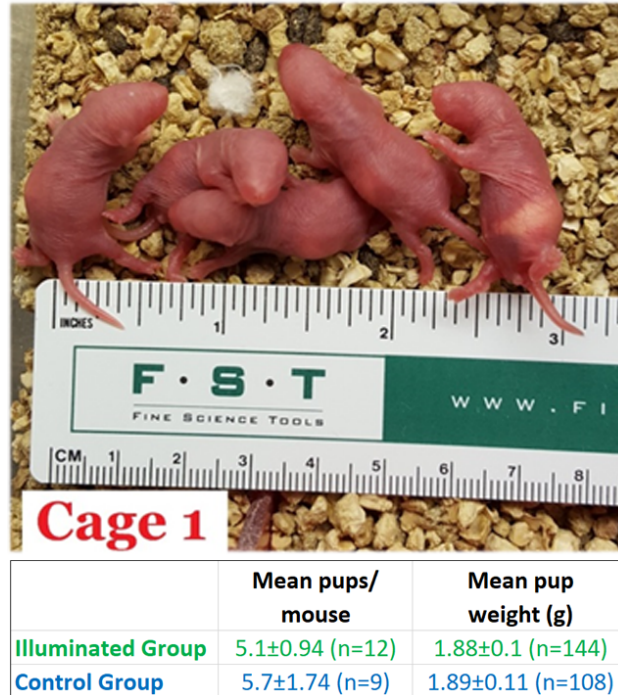
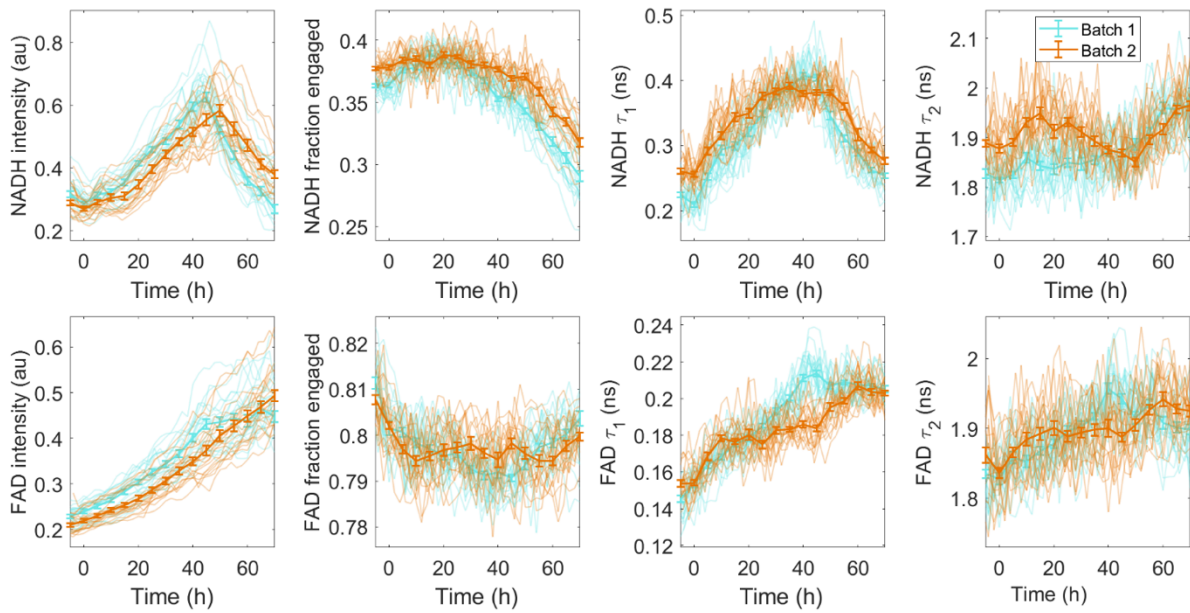
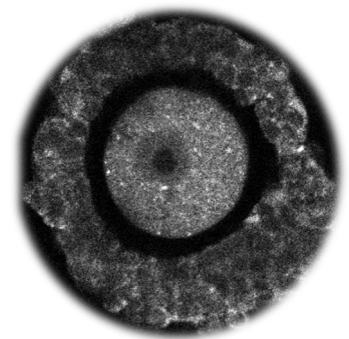


Figure 5: Live birth safety study. To evaluate the safety of FLIM illumination on embryos, we implanted illuminated and non-illuminated embryos into pseudo-pregnant mice, later measuring birth rates and pup weights as metrics for possible damage. Sample numbers indicate number of mice and number of pups, respectively. No significant differences were observed.

Supplementary Figures



Supplementary Figure 3: Metabolic trajectories from two separate time lapse acquisitions, with $n=20$ embryos in Batch 1, and $n=19$ in Batch 2. Embryo parameter distributions exhibited similar absolute parameter values, as well as parameter trends over development. Both batches were pooled together for the averages displayed in Fig. 4.



7. Publication 2: *Metabolic imaging of human cumulus cells reveals associations among metabolic profiles of cumulus cells, patient clinical factors and oocyte maturity*

(DOI:10.1016/j.fertnstert.2021.07.1204)

Title: Metabolic imaging of human cumulus cells reveals associations among metabolic profiles of cumulus cells, patient clinical factors and oocyte maturity

Marta Venturas, M.Sc.^{1,2}, Xingbo Yang, Ph.D.¹, Kishlay Kumar Ph.D.³, Dagan Wells Ph.D.^{3,4}, Catherine Racowsky, Ph.D.^{5,6}, and Daniel J. Needleman, Ph.D.^{1,7}

¹ Molecular and Cellular Biology and School of Engineering and Applied Sciences, Harvard University, Cambridge, Massachusetts, U.S.A.

² Department de Biologia Cel·lular, Fisiologia i Immunologia, Universitat Autònoma de Barcelona, Cerdanyola, Spain

³ Nuffield Department of Women's and Reproductive Health, John Radcliffe Hospital, Oxford University, Oxford, U.K.

⁴ Juno Genetics, Oxford Science Park, Oxford, U.K.

⁵ Brigham & Women's Hospital and Harvard Medical School, Boston, Massachusetts, U.S.A.

⁶ Department of Obstetrics and Gynecology and Reproductive Medicine, Hospital Foch, Suresnes, France

⁷ Center for Computational Biology, Flatiron Institute, New York, United States

Running title: Metabolic Imaging of human cumulus cells

Corresponding author: Marta Venturas

Phone: +1(857)-829-7645

Email: marta_venturas@fas.harvard.edu.

Address: Molecular and Cellular Biology and School of Engineering and Applied Sciences, Harvard University, Cambridge, Massachusetts, 02138, U.S.A.

Capsule: Metabolic imaging using fluorescence lifetime imaging microscopy (FLIM) sensitively detects variations in metabolic state of human cumulus cells. These variations are associated with maturity of the enclosed oocyte and patient clinical factors.

Abstract

Objective: To study whether fluorescence lifetime imaging microscopy (FLIM) detects differences in metabolic state among cumulus samples and if this metabolic state is associated with patient age, BMI and/or AMH, and maturity of the oocyte.

Design: Prospective observational study.

Setting: Academic laboratory.

Patients/Animals: Cumulus cell (CC) clusters from cumulus-oocyte complexes were collected after oocyte retrieval and vitrified.

Interventions: CC metabolism was assessed using FLIM to measure autofluorescence of NAD(P)H and FAD+, two coenzymes essential for cellular respiration and glycolysis. Patient age, BMI, and AMH, and the maturity of corresponding oocytes were recorded.

Main Outcome measure(s): Quantitative information from FLIM was obtained regarding: 1) metabolite concentrations from fluorescence intensity; and 2) metabolite enzyme engagement from fluorescence

lifetimes. Associations were investigated between each FLIM parameter and oocyte maturity, patient age, BMI and AMH. Variance between CC clusters within and between patients.

Results: Of 619 CC clusters from 193 patients, 90 were associated with immature oocytes, 505 with metaphase II oocytes. FLIM enabled quantitative measurements of metabolic state of CC clusters. These parameters were significantly correlated with patient age and AMH, independently, but not BMI. CC NAD(P)H FLIM parameters and Redox Ratio were significantly associated with maturity of the enclosed oocyte.

Conclusions: FLIM detects variations in metabolic state of CC, showing a greater variance among clusters from each patient than between patients. FLIM can detect CC metabolic associations with patient age and AMH and detects variations between mature and immature oocytes, suggesting the potential utility of this technique to help identify superior oocytes.

Keywords: Metabolism, cumulus cells, cumulus-oocyte complexes, human oocytes, fluorescence lifetime imaging microscopy, maturity.

Introduction

Extensive evidence supports the role of bidirectional crosstalk between the oocyte and its surrounding cumulus mass for successful oocyte development (1,2). Oocyte growth is dependent on the metabolic cooperation between the oocyte and its cumulus cells (CCs), which is facilitated by the exchange of molecules through gap junctions and paracrine signals (3,4). This interaction is bidirectional: CCs provide growth factors, lipids and metabolites for oocyte maturation and development (5,6,9); oocyte secreted factors enable CCs differentiation and mucification (7,8).

Oocyte developmental potential depends on oocyte quality (9), which in turn, is reflected in nuclear and cytoplasmic maturity, both of which are essential for successful fertilization and embryo development (10). In addition, CCs help maintain the oocyte in meiotic arrest at prophase I (1). This communication is essential for the resumption of meiosis in response to the luteinizing hormone surge (11). Conversely, the meiotic status can influence the metabolism not only of the oocyte, but also of the surrounding cumulus mass. Pyruvate consumption by cumulus oocyte complexes (COCs) has been positively associated with oocyte nuclear maturation (7,12). Moreover, mitochondrial dysfunction and mitochondrial DNA (mtDNA) copy number of CCs might be directly related to oocyte maturity (13–15).

Because of the intimate interactions between the oocyte and its surrounding CC mass, measurements of the metabolic state of CCs provide a promising means to determine the developmental competence of the associated oocyte (16–19). Since cumulus masses are routinely removed for intracytoplasmic sperm injection (ICSI), and are frequently trimmed before conventional insemination, these otherwise discarded cells have the potential for use in a non-invasive assay of oocyte developmental competence (20–25). However, reliable biomarkers in CCs have yet to be identified (23).

A number of recent studies have focused on measurements of mtDNA in CCs, the results of which have been inconclusive (17,18,26). Some studies found that mtDNA copy number does not seem to be associated with oocyte maturity or fertilization (18), while other studies observed a correlation with oocyte fate (14,15). Additional studies have used mitochondrial dyes (13,27) to study mitochondrial activity in CCs. Establishing quantitative tools to measure the metabolic state of single cumulus complexes could be helpful for developing an improved understanding of the metabolic relationship between CCs and the enclosed oocyte and might enable non-invasive approaches to evaluate oocyte maturity and overall quality.

Nicotinamide adenine dinucleotide (NADH), Nicotinamide adenine phosphate dinucleotide (NADPH) and flavine adenine dinucleotide (FAD⁺), are central metabolic coenzymes that are naturally fluorescent (28). These molecules are electron carriers that have essential roles in metabolic pathways, such as the electron transport chain and glycolysis, hence they are ideal biomarkers of cellular metabolic state (29,30). The fluorescence spectra NADH and NADPH are almost indistinguishable (31), therefore the combined fluorescence of NADH and NADPH is often referred to as the NAD(P)H signal. Fluorescence lifetime imaging microscopy (FLIM) of NAD(P)H and FAD⁺ provides a means to measure the fluorescence intensity and fluorescence lifetime of these molecules. The fluorescence intensity is related to the concentrations of the coenzymes, while the

fluorescence lifetime depends on the local environment of the coenzyme, varying drastically if they are bound to an enzyme or free (32).

In the present study, we used metabolic imaging via FLIM to measure metabolic state of CCs in vitro. We evaluated the sensitivity of this non-invasive metabolic imaging to investigate the associations among clinically relevant patient factors (such as age, BMI and anti-müllerian hormone (AMH) levels), and the metabolic state of the cumulus masses. And finally, we explored the extent to which quantitative measures of the metabolic state of CC clusters are associated with the maturity of the oocyte they enclose.

Material and Methods

Study design

Cumulus cell clusters were donated for research under consent by patients undergoing ART treatments after institutional review board (IRB) approval of the study protocol by Partners Healthcare IRB (Partners IRB # 2014P000874).

After collection, vitrification and subsequent thawing, the metabolic state of each CC cluster was assessed using metabolic imaging by FLIM. Patient age, BMI and AMH within 6 months of treatment, Follicle-stimulating hormone (FSH) and luteinizing hormone (LH) levels, the number of oocytes retrieved, and the percentage of mature oocytes (number mature oocytes / total of oocytes retrieved) were recorded. The meiotic status of each oocyte was retrospectively tied to its corresponding CC cluster.

Sample preparation

COCs were retrieved, using standard clinical protocols following ovarian stimulation and ovulatory trigger, isolated and set up in individual drops of 25 μ l of culture medium (Global[®] total, Life Global Group, Cooper Surgical; Guilford, CT) overlaid with oil (Vitrolife Ovoil) and incubated for 1-4h. CC masses of each oocyte were trimmed, and trimmed CCs were rinsed and vitrified following the Irvine vitrification protocol (90133-SO - Vit Kit-Freeze, FUJIFILM Irvine Scientific, USA). Each CC mass was then thawed, following the Irvine thawing protocol (90137-SO - Vit Kit-Thaw, FUJIFILM Irvine Scientific, USA), and their hyaluronan matrix was disaggregated following exposure to hyaluronidase (80 IU/mL of Hyaluronidase, FUJIFILM Irvine Scientific, USA). The disaggregated CCs were centrifuged and the pellet, which consisted of a cluster of CCs, was collected. The cluster was then placed in 5 μ L droplets of culture media covered with oil in a glass bottom dish (MatTek P35G-0.170-14-C, USA) designed for imaging. CC clusters were imaged in an on-stage incubation system (Ibidi GmbH, Martinsried, Germany) to maintain culture environment conditions of 37°C and 5% CO₂, 5% O₂, balanced with N₂.

Staining protocols

For TMRM (tetramethylrhodamine, methyl ester) experiments, CC clusters were incubated with 5nM of TMRM (Thermo Fisher, USA) for 10 minutes. For DNA staining experiments, CCs were stained with 1:400 of Syto 9 (Thermo Fisher, USA) for 60 minutes. The samples were then washed 3 times through

culture media (Global® total, Life Global Group, Cooper Surgical; Guilford, CT) and transferred to a glass bottom dish for imaging.

Metabolic Imaging using Fluorescence Lifetime Imaging Microscopy (FLIM)

FLIM measurements were performed on a Nikon Eclipse Ti microscope using two-photon excitation from a Ti:Sapphire pulsed laser (Mai-Tai, Spectral-Physics) with a 80MHz repetition rate and 70fs pulse width, a Galvano scanner (DCS-120, Becker and Hickl, Germany), TCSPC module (SPC-150, Becker and Hickl, Germany) and a hybrid single photon counting detector (HPM-100-40, Becker and Hickl, Germany). The wavelength of excitation was set to 750nm for NAD(P)H and 890nm for FAD+, with powers measured at the objective of 3mW for NAD(P)H and 16.8mW for FAD+. Optical bandpass filters were positioned in a filter wheel in front of the detector – 460/50 nm for NAD(P)H and 550/88nm for FAD+ and a 650nm short pass filter (Chroma technologies) was mounted on the detector. Imaging was performed with a 40X Nikon objective with 1.25 numerical aperture (NA) (CFI Apo 40 × WI, NA 1.25, Nikon). Each NAD(P)H and FAD+ FLIM image was acquired with 60 seconds of integration time. Objective piezo stage (P-725, Physik Instruments) and motorized stage (ProScan II, Prior Scientific) were used to perform multi-dimensional acquisition. Ten images were acquired per cumulus cluster varying x, y, and z axis. All the electronics were controlled by SPCM software (Becker and Hickl, Germany) and custom LabVIEW software.

Data Analysis

Data was analyzed using customized MATLAB (version R2019b, MathWorks, USA) code. NAD(P)H and FAD+ FLIM intensity images were subject to an intensity-based threshold to classify pixels as being in cells or background. For each cell segment, the photon arrival time histogram was modeled as a bi-exponential decay:

$$P(t) = A[(1 - F) * e^{-t/\tau_1} + F * e^{-t/\tau_2}] + B \quad (1)$$

Where, A is a normalization factor, B is the background, τ_1 is the short lifetime, τ_2 is the long lifetime and F is the fraction of molecule with long lifetime (fraction engaged with enzymes for NAD(P)H and unengaged for FAD+). This function was convolved with a measured instrument response function, and a least square fit was used to determine the parameters. The fluorescence intensity was calculated for each cumulus cell cluster as the number of photons divided by the area of the cluster. Thus, a single FLIM measurement produced 9 parameters, 4 for NAD(P)H and 4 for FAD+ and 1 Redox Ratio (NAD(P)H fluorescence intensity / FAD+ fluorescence intensity) to characterize the metabolic state of CC clusters.

Statistical Analysis

All statistical tests were performed using Stata Statistical Software (version 16.0, LLC Stata Corp, Texas, USA) and R Studio (Version 1.3.959, R Foundation for Statistical Computing, Vienna, Austria). Our data was structured hierarchically, 1- 10 images for each cluster (i) and 1- 4 clusters (j) per patient (k). We thus used multilevel models, on the standardized FLIM parameters ($\frac{x - \text{mean}(x)}{\text{sd}}$), to analyze this structured data. Data points that lay either 40% above or below the mean were considered outliers and removed from the analysis. We incorporated additional predictors (age, BMI, AMH levels, and oocyte maturity) for certain analysis, resulting in the multilevel model:

$$\text{FLIMparam}_{ijk} = \beta_0 + \beta_1 * \text{Patient Factor} + c_{0,k} + b_{0,jk} + e_{ijk}$$

where β_0 corresponds to the intercept; β_1 is the slope; Patient Factor is age, BMI, AMH levels, or oocyte maturity (if considered); $c_{0,k}$ is the patient level random error; $b_{0,jk}$ is the cluster level random error; e_{ijk} is the image level random error (33). This modelling encodes information on the variance associated with each level: patient, CC clusters within patients and images within CC cluster. To correct for multiple comparisons, we used Benjamini – Hochberg's false discovery rate (FDR), at a q value of 0.05. FDR p-values of <0.05 were considered significant.

Results

NAD(P)H autofluorescence of CCs predominantly originates from mitochondria

We first sought to explore the subcellular localization of NAD(P)H and FAD+ autofluorescence. After centrifuging the dissociated CCs from a cluster, the resulting pellet was moved to an onstage incubation system and imaged for NAD(P)H and FAD+ autofluorescence (Figure 1A and B, respectively) with FLIM. Each acquired image was 220 μm by 220 μm , which contains tens to hundreds of CCs (Figure 1A and B, left panels), but represented only a small region of an entire CC pellet. To quantitatively analyse the CC metabolic state in the imaged region, we used an intensity-based threshold to create masks (Figure 1A and B, left panels). We grouped all photons from each of the masked regions to create histograms of the fluorescence decay of NAD(P)H (Figure 1C, upper, blue) and FAD+ (Figure 1C, lower, green). We then fit these histograms using two-exponential decay models (equation 1) (Figure 1C, black lines), thereby obtaining a total of 6 parameters: short and long lifetimes, and the fraction of engaged molecules, for both NAD(P)H and FAD+. In addition, we computed the NAD(P)H intensity, FAD+ intensity, and the Redox Ratio, providing a total of 9 quantitative metabolic parameters per each cluster.

While FAD+ is highly enriched in mitochondria (29), NADH and NADPH participate in different pathways in mitochondria, the nucleus, and the cytoplasm (31,32). To better understand the source of the NAD(P)H signal in CCs, we compared NAD(P)H images to images with dyes for either mitochondria or DNA. We first stained a cumulus mass with TMRM, a dye known to localize to active mitochondria (Figure 1C). We segmented the mitochondria from the TMRM images using a machine-learning based segmentation software (Illastik, version 1.0,(35)), and, by comparing the overlap of the segmented TMRM and NAD(P)H images, determined that $73 \pm 5\%$ of NAD(P)H photons come from mitochondria. We next stained the cumulus mass with Syto 9, a DNA dye (Figure 1E) and by comparing the overlap with NAD(P)H signal, we found that $16 \pm 1\%$ of the NAD(P)H photons come from the nucleus. Hence, the remaining photons come from the cytoplasm. Thus, while the acquired NAD(P)H signal has contributions from all compartments, the majority of the signal comes from mitochondria.

CC processing for FLIM analyses

We next explored the extent to which variations in sample preparation procedures impacted the results of FLIM measurements of CC clusters. CCs that were imaged fresh gave indistinguishable FLIM parameters as compared to CCs that were first vitrified and then thawed (Figure S1). Since vitrified samples are more convenient to work with than fresh samples, we opted to vitrify CCs in subsequent experiments. We next tested the impact of hyaluronidase on FLIM parameters of CCs. CCs that were not exposed to hyaluronidase, and thus maintained their hyaluronan matrix, gave indistinguishable fraction engaged and lifetimes (Figure S2) compared to those that were dispersed with hyaluronidase. However, CCs not exposed to hyaluronidase did give significantly different intensities and Redox Ratio, which was likely caused by difficulties in successfully segmenting these far less dense cells. Thus, we proceeded to use vitrified CCs exposed to hyaluronidase in subsequent experiments.

We then explored how the location of the CCs within a cumulus cluster impacted the results of FLIM measurements. FLIM parameters of CCs that were trimmed from closer to the oocytes did not show significant differences from those of CCs that were trimmed further from the oocyte (Figure S3). Since the further the CCs are trimmed from the oocyte, the less likely any risk of damage will be introduced to the oocyte, we trimmed CCs further away from the oocytes for all subsequent sample collections. Taken together, these experiments led us to use CCs trimmed further away from the oocyte, which were vitrified and then exposed to hyaluronidase before imaging.

Metabolic variance between CCs clusters exceeds variance between patients and between images

A total of 619 CC samples were collected from 193 patients, 90 of which were associated with immature oocytes, 58 at the germinal vesicle (GV) stage and 32 at metaphase I (n=32), 505 were associated with mature oocytes, and 24 were associated with either degenerated or abnormal oocytes. We acquired 8-10 non-overlapping FLIM images at different locations throughout each CC pellet (Figure 2A). We used a multilevel model (33,36) to analyze this hierarchically organized data, and decomposed the variance in the FLIM parameters into three levels: variance associated with differences between patients, variance associated with differences between CC clusters from the same patient, and variance associated with differences between individual images from the same CC cluster. For all FLIM parameters, the variance associated with differences between CC clusters from one patient was substantially larger than the variance associated with differences between individual images, or the variance associated with differences among patients (Figure 2B). The large variance in FLIM parameters associated with CC clusters indicates that different clusters from the same patient have significantly different metabolic states. The small variance in FLIM parameters associated with differences between individual images suggests a relative homogeneity of metabolic state within a CC cluster and demonstrates the high robustness and reproducibility of these measurements. Despite being small, the variance in FLIM parameters associated with differences between patients indicates that patient specific factors impact the metabolism of their CCs.

CC metabolic parameters are associated with maternal clinical factors

We next explored the extent to which maternal age, AMH levels and BMI independently account for the variance in FLIM parameters associated with differences between patients. These factors varied greatly across the 193 patients we studied: maternal age ranged from 23.5 to 45 years, with a mean of 36.7 years (58.0% of the patients were less and 42.0% more than 38 years); AMH levels ranged from 0.1 to 12 ng/mL, with a mean of 2.9 ng/mL; BMI ranged from 17.8 to 49.5 kg/m², with a mean of 26.7 kg/m². 49.8% of the patients had a BMI lower than 24.9, 38.8% had a BMI between 25 and 29.9, and 11.4% had a BMI greater than 30. Plotting FLIM parameters versus maternal age and AMH levels revealed apparent associations (Figure 3A, 3B, respectively). Incorporating these patient factors into the multilevel model allowed us to determine that maternal age was significantly correlated with NAD(P)H irradiance, fraction engaged and long lifetime, and FAD+ fraction engaged and short lifetime; while AMH levels were significantly correlated with NAD(P)H irradiance, fraction engaged, and both short and long lifetime, and FAD+ irradiance and short lifetime (Figure 3D). The correlations with maternal age remained after controlling for AMH levels, and correlations with AMH levels remained after controlling for maternal age. In contrast, we found no significant correlations between any FLIM parameters and maternal BMI (Figure 3C, 3D) nor when stratifying the BMI by the three groups. However, the percentage of variance in CC FLIM measurements between patients was not entirely explained by maternal age and AMH levels, suggesting that other patient specific factors impact the metabolic state of their CC clusters (Figure 3D). We also found that levels of both FSH and LH administered were significantly correlated with FLIM parameters (FDR $p < 0.05$). These associations were dependent on both maternal age and AMH levels. Further studies are planned to study these interactions.

CC FLIM parameters are associated with the maturity of the enclosed oocyte

We next sought to determine if the metabolic state of CC clusters was correlated with the maturity of the oocyte with which they were associated. The percentage of mature oocytes (of total oocytes retrieved) from a patient was not associated with maternal age ($p = 0.20$), or BMI ($p = 1.0$), or AMH ($p = 0.74$), or the total number of oocytes retrieved from that patient ($p = 0.69$) (Figure 3A and B). Comparison of CC FLIM parameters from mature oocytes with those from immature oocytes revealed several interesting contrasts: NAD(P)H irradiance (FDR $p = 0.02$), NAD(P)H fraction engaged (FDR $p < 1 \times 10^{-5}$), NAD(P)H long lifetime (FDR $p < 1 \times 10^{-5}$) and Redox Ratio (FDR $p = 0.02$) were significantly different between mature and immature oocytes (Figure 4 C, D and E). These significant differences were upheld after controlling for maternal age and AMH levels. Plotting these three FLIM parameters for each CC cluster on a three-dimensional graph revealed that while the distributions were significantly different between CCs from mature and immature oocytes, there was also substantial overlap between these two populations (Figure 4E, blue, immature; yellow, mature; grey, support vector machine generated hyperplane that best separates the two populations).

Discussion

Cumulus cells and oocyte metabolic interconnections are essential for cumulus mass expansion, oocyte maturation and development (25). Mitochondrial dysfunction in CCs affects oocyte growth and quality (37). The effects of CC metabolic state on the corresponding oocyte have attracted much attention in recent years. In view of the importance of CC mitochondrial function for successful oocyte developmental competence (14), CC metabolic state may act as a biological marker of oocyte quality.

In this study, we used FLIM of NAD(P)H and FAD+ to quantitatively determine the metabolic state of CCs. Analysis of 8-10 FLIM images acquired throughout each of 619 CC clusters from 193 patients, revealed that for all FLIM parameters, the variance associated with differences between CCs of different oocytes was larger than the variance associated with differences between patients and between individual images obtained from the same cluster. Additionally, we observed that CC metabolic parameters are associated with maternal clinical factors that are known to be key determinants of oocyte quality. Lastly, we found significant differences in NAD(P)H FLIM parameters and the Redox Ratio between CC clusters from mature and immature oocytes.

By analyzing our hierarchically organized data using multilevel modelling (33,36) we obtained the variances in the FLIM parameters within the three levels: variance associated with differences between patients, variance associated with differences between CC clusters from the same patient, and variance associated with differences between individual images from the same cluster. We found a large variance in all FLIM metabolic parameters between CC clusters, indicating that CCs associated with individual oocytes from the same patient have significantly different metabolic states.

The fact that there are measurable differences between CCs associated with individual oocytes highlight the potential use of this approach to determine oocyte specific characteristics. Additionally, the small variance in FLIM parameters associated with the differences between images of the same CC cluster, indicates the high reproducibility of these measurements. However, this variance was not null, which might either be due to minor errors in the FLIM measurements or a true heterogeneity of metabolic state within a CC cluster. The latter is unlikely as our validation studies showed only minor deviations in FLIM measurements among samples from the same cumulus clusters. The variance in FLIM parameters associated with differences between patients indicates that patient specific factors impact the metabolism of their CCs. Patient specific effects on CC mtDNA measures have been previously reported (18).

Patient factors such as age, BMI and measures of ovarian reserve, such as AMH, have long been associated with oocyte quality (38,39). Here, we found significant associations of CC metabolic state, as measured by FLIM of NAD(P)H and FAD+, and maternal age. The influence of maternal ageing on CC metabolism has been demonstrated in several studies (21,40–42). Both proteomic and genomic analyses of CCs in woman with advanced age differ from those of younger women (40,41). CCs from older woman have been shown to contain higher number of damaged mitochondria and mtDNA alterations (42,43). In addition, we observed a significant association between CC FLIM parameters and AMH levels, even after controlling for maternal age. This observation is consistent with previous results that found a correlation between CC mitochondrial membrane potential and measures of ovarian reserve (13). The levels of gonadotropins administered were significantly

correlated with several FLIM parameters and these associations depend on both maternal age and AMH levels. Future studies are required to further study these interactions.

Our results did not indicate an association between CC metabolic state and maternal BMI. This contrasts with a study by Gorshinova et al., where they observed a reduction in active mitochondria with increasing maternal BMI in a group of 13 patients (27). However, only a small portion of the patient level variance in FLIM parameters can be explained by age and AMH levels. This argues that CC metabolic state is also influenced by other patient specific factors. Perhaps either the presence of metabolic diseases, genetic predisposition, diet, or smoking can influence the intracellular metabolic state of CC and their enclosed oocytes. Future studies will disentangle the nature of those additional factors. It has been demonstrated that in mitochondria of mouse oocytes, a simultaneous increase in NAD(P)H intensity and fraction engaged correspond to an increase in metabolic flux through the electron transport chain (44). If the same held for human CCs, this would imply that mitochondrial metabolic fluxes in CCs increase with patient age and decreases with ovarian reserve. However, this conclusion must be treated with caution because of the extensive metabolic differences between CCs and oocytes. Additional experiments will be necessary to definitively determine the biological basis of the trends in FLIM parameters in CCs we observed in this study.

Cumulus cell-oocyte crosstalk is a key determinant for acquisition of oocyte developmental competence and CC maturation (4,7,11,12). Oocyte quality depends on successful nuclear and cytoplasmic maturation (9,10) as well as maternal clinical factors (38,39). The results of our study indicate that the fraction of mature oocytes at retrieval did not correlate with any patient clinical characteristic such as age, BMI or AMH levels, or even the number of oocytes retrieved. However, variations in FLIM metabolic parameters were observed between those CC clusters associated with mature oocytes and those associated with oocytes that were immature. CC and oocyte metabolic communication is essential not only for the resumption of meiosis (1,11), but also for acquisition of developmental competence (7,12). Interestingly, we found that CCs from mature oocytes showed a higher NAD(P)H fraction Bound, NAD(P)H long lifetime and Redox Ratio (NAD(P)H intensity: FAD+ intensity) than cumulus masses from immature oocytes. These findings are in line with previous studies demonstrating a low mitochondrial membrane potential in CCs from immature oocytes compared to those from matured oocytes (13), as well as those demonstrating differences in mtDNA copy number(14,15). We therefore conclude that FLIM imaging can detect metabolic variations of cumulus masses from immature oocytes compared to mature oocytes. However, we also observed large variations in FLIM parameters across CC clusters from mature oocytes and large variations in FLIM parameters across CCs from immature oocytes. These findings highlight the difficulty in developing a prediction model to assess oocyte maturity.

Conclusions

In summary, metabolic imaging via FLIM of human CCs is a promising approach for detecting variations of metabolic state of these cells. FLIM sensitively detects variations in CC metabolism and shows a greater variance in FLIM parameters among oocytes than between patients. CC metabolic parameters are associated with clinically relevant factors such as age and AMH levels, but not with BMI. Moreover, metabolic imaging detects significant differences between CC metabolic state of

immature oocytes and those that matured. A greater understanding of the metabolic underpinnings of human cumulus-oocyte interactions could offer new opportunities for improving fertility interventions, in particular in vitro maturation protocols.

Acknowledgements

Authors thank Becker and Hickl for contributing a single-photon-counting detector and TCSPC electronics to this research. Authors would also like to acknowledge Brian Leahy for useful advice, as well as all members of the embryology team at Brigham and Women's Hospital for their assistance in the collection of the cumulus samples for this research. Images Created with BioRender.com

Funding

NIH RO1HD092559-03

References

1. Eppig JJ. Intercommunication between mammalian oocytes and companion somatic cells. *Bioessays* 1991;13(11):569–74.
2. Albertini DF, Combelles CM, Benecchi E, Carabatsos MJ. Cellular basis for paracrine regulation of ovarian follicle development. *Reproduction* 2001;121(5):647–53.
3. Anderson E, Albertini DF. Gap junctions between the oocyte and companion follicle cells in the mammalian ovary. *J Cell Biol* 1976;71(2):680–6.
4. Eppig JJ. Oocyte control of ovarian follicular development and function in mammals. *Reproduction* 2001;122(6):829–38.
5. Seli E, Babayev E, Collins SC, Nemeth G, Horvath TL. Minireview: Metabolism of Female Reproduction: Regulatory Mechanisms and Clinical Implications. *Mol Endocrinol* 2014;28(6):790–804.
6. Dumesic DA, Meldrum DR, Katz-Jaffe MG, Krisher RL, Schoolcraft WB. Oocyte environment: follicular fluid and cumulus cells are critical for oocyte health. *Fertility and Sterility* 2015;103(2):303–16.
7. Sutton ML, Cetica PD, Beconi MT, Kind KL, Gilchrist RB, Thompson JG. Influence of oocyte-secreted factors and culture duration on the metabolic activity of bovine cumulus cell complexes. *Reproduction* 2003;126(1):27–34.
8. Gilchrist RB, Lane M, Thompson JG. Oocyte-secreted factors: regulators of cumulus cell function and oocyte quality. *Hum Reprod Update* 2008;14(2):159–77.
9. Keefe D, Kumar M, Kalmbach K. Oocyte competency is the key to embryo potential. *Fertil Steril* 2015;103(2):317–22.
10. Watson AJ. Oocyte cytoplasmic maturation: a key mediator of oocyte and embryo developmental competence. *J Anim Sci* 2007;85(13 Suppl):E1–3.
11. Funsho Fagbohun C, Downs SM. Metabolic Coupling and Ligand-Stimulated Meiotic Maturation in the Mouse Oocyte-Cumulus Cell Complex1. *Biology of Reproduction* 1991;45(6):851–9.
12. Downs SM, Humpherson PG, Leese HJ. Pyruvate utilization by mouse oocytes is influenced by meiotic status and the cumulus oophorus. *Mol Reprod Dev* 2002;62(1):113–23.
13. Anderson SH, Glassner MJ, Melnikov A, Friedman G, Orynbayeva Z. Respirometric reserve capacity of cumulus cell mitochondria correlates with oocyte maturity. *J Assist Reprod Genet* 2018;35(10):1821–30.
14. Boucrot L, Bris C, Seegers V, Goudenège D, Desquret-Dumas V, Domin-Bernhard M, et al. Deep sequencing shows that oocytes are not prone to accumulate mtDNA heteroplasmic mutations during ovarian ageing. *Hum Reprod* 2017;32(10):2101–9.
15. Lan Y, Zhang S, Gong F, Lu C, Lin G, Hu L. The mitochondrial DNA copy number of cumulus granulosa cells may be related to the maturity of oocyte cytoplasm. *Hum Reprod* 2020;35(5):1120–9.
16. Fontana J, Martínková S, Petr J, Žalmanová T, Trnka J. Metabolic cooperation in the ovarian follicle. *Physiol Res* 2020;69(1):33–48.
17. Ogino M, Tsubamoto H, Sakata K, Oohama N, Hayakawa H, Kojima T, et al. Mitochondrial DNA copy number in cumulus cells is a strong predictor of obtaining good-quality embryos after IVF. *J Assist Reprod Genet* 2016;33(3):367–71.
18. Desquret-Dumas V, Clément A, Seegers V, Boucrot L, Ferré-L'Hotellier V, Bouet PE, et al. The mitochondrial DNA content of cumulus granulosa cells is linked to embryo quality. *Hum Reprod* 2017;32(3):607–14.
19. Cinco R, Digman MA, Gratton E, Luderer U. Spatial Characterization of Bioenergetics and Metabolism of Primordial to Preovulatory Follicles in Whole Ex Vivo Murine Ovary. *Biol Reprod* [Internet] 2016 [cited 2021 Mar 23];95(6). Available from: <https://www.ncbi.nlm.nih.gov/pmc/articles/PMC5315427/>

20. Assou S, Haouzi D, Mahmoud K, Aouacheria A, Guillemin Y, Pantesco V, et al. A non-invasive test for assessing embryo potential by gene expression profiles of human cumulus cells: a proof of concept study. *Molecular Human Reproduction* 2008;14(12):711–9.
21. Boucret L, Chao de la Barca JM, Morinière C, Desquret V, Ferré-L'Hôtelier V, Descamps P, et al. Relationship between diminished ovarian reserve and mitochondrial biogenesis in cumulus cells. *Hum Reprod* 2015;30(7):1653–64.
22. Gebhardt KM, Feil DK, Dunning KR, Lane M, Russell DL. Human cumulus cell gene expression as a biomarker of pregnancy outcome after single embryo transfer. *Fertility and Sterility* 2011;96(1):47-52.e2.
23. Huang Z, Wells D. The human oocyte and cumulus cells relationship: new insights from the cumulus cell transcriptome. *Mol Hum Reprod* 2010;16(10):715–25.
24. McKenzie LJ, Pangas SA, Carson SA, Kovanci E, Cisneros P, Buster JE, et al. Human cumulus granulosa cell gene expression: a predictor of fertilization and embryo selection in women undergoing IVF. *Hum Reprod* 2004;19(12):2869–74.
25. Uyar A, Torrealday S, Seli E. Cumulus and granulosa cell markers of oocyte and embryo quality. *Fertility and Sterility* 2013;99(4):979–97.
26. Taugourdeau A, Desquret-Dumas V, Hamel JF, Chupin S, Boucret L, Ferré-L'Hotellier V, et al. The mitochondrial DNA content of cumulus cells may help predict embryo implantation. *J Assist Reprod Genet* 2019;36(2):223–8.
27. Gorshinova VK, Tsvirkun DV, Sukhanova IA, Tarasova NV, Volodina MA, Marey MV, et al. Cumulus cell mitochondrial activity in relation to body mass index in women undergoing assisted reproductive therapy. *BBA Clin* 2017;7:141–6.
28. Heikal AA. Intracellular coenzymes as natural biomarkers for metabolic activities and mitochondrial anomalies. *Biomark Med* 2010;4(2):241–63.
29. Dumollard R, Marangos P, Fitzharris G, Swann K, Duchon M, Carroll J. Sperm-triggered [Ca²⁺] oscillations and Ca²⁺ homeostasis in the mouse egg have an absolute requirement for mitochondrial ATP production. *Development* 2004;131(13):3057–67.
30. Klaidman LK, Leung AC, Adams JD. High-performance liquid chromatography analysis of oxidized and reduced pyridine dinucleotides in specific brain regions. *Anal Biochem* 1995;228(2):312–7.
31. Ghukasyan VV, Heikal AA. *Natural Biomarkers for Cellular Metabolism: Biology, Techniques, and Applications*. CRC Press; 2014.
32. Becker W. Fluorescence lifetime imaging--techniques and applications. *J Microsc* 2012;247(2):119–36.
33. Snijders TAB, Bosker RJ. *Multilevel Analysis: An Introduction to Basic and Advanced Multilevel Modeling*. SAGE; 2011.
34. Stein LR, Imai S. The dynamic regulation of NAD metabolism in mitochondria. *Trends Endocrinol Metab* 2012;23(9):420–8.
35. Berg S, Kutra D, Kroeger T, Straehle CN, Kausler BX, Haubold C, et al. ilastik: interactive machine learning for (bio)image analysis. *Nat Methods* 2019;16(12):1226–32.
36. Lorah J. Effect size measures for multilevel models: definition, interpretation, and TIMSS example. *Large-scale Assessments in Education* 2018;6(1):8.
37. Dumesic DA, Guedikian AA, Madrigal VK, Phan JD, Hill DL, Alvarez JP, et al. Cumulus Cell Mitochondrial Resistance to Stress In Vitro Predicts Oocyte Development During Assisted Reproduction. *J Clin Endocrinol Metab* 2016;101(5):2235–45.
38. Cimadomo D, Fabozzi G, Vaiarelli A, Ubaldi N, Ubaldi FM, Rienzi L. Impact of Maternal Age on Oocyte and Embryo Competence. *Front Endocrinol (Lausanne)* [Internet] 2018 [cited 2021 Mar 26];9. Available from: <https://www.ncbi.nlm.nih.gov/pmc/articles/PMC6033961/>
39. Zhang J-J, Liu X, Chen L, Zhang S, Zhang X, Hao C, et al. Advanced maternal age alters expression of maternal effect genes that are essential for human oocyte quality. *Aging (Albany NY)* 2020;12(4):3950–61.
40. May-Panloup P, Boucret L, Chao de la Barca J-M, Desquret-Dumas V, Ferré-L'Hotellier V, Morinière C, et al. Ovarian ageing: the role of mitochondria in oocytes and follicles. *Human Reproduction Update* 2016;22(6):725–43.
41. McReynolds S, Dzieciatkowska M, McCallie BR, Mitchell SD, Stevens J, Hansen K, et al. Impact of maternal aging on the molecular signature of human cumulus cells. *Fertil Steril* 2012;98(6):1574-1580.e5.
42. Tatone C, Carbone MC, Falone S, Aimola P, Giardinelli A, Caserta D, et al. Age-dependent changes in the expression of superoxide dismutases and catalase are associated with ultrastructural modifications in human granulosa cells. *Mol Hum Reprod* 2006;12(11):655–60.
43. Seifer DB, DeJesus V, Hubbard K. Mitochondrial deletions in luteinized granulosa cells as a function of age in women undergoing in vitro fertilization. *Fertility and Sterility* 2002;78(5):1046–8.
44. Yang X, Needleman DJ. Coarse-grained model of mitochondrial metabolism enables subcellular flux inference from fluorescence lifetime imaging of NADH [Internet]. *Biophysics*; 2020 [cited 2021 Apr 13]. Available from: <http://biorxiv.org/lookup/doi/10.1101/2020.11.20.392225>

Figures and Tables

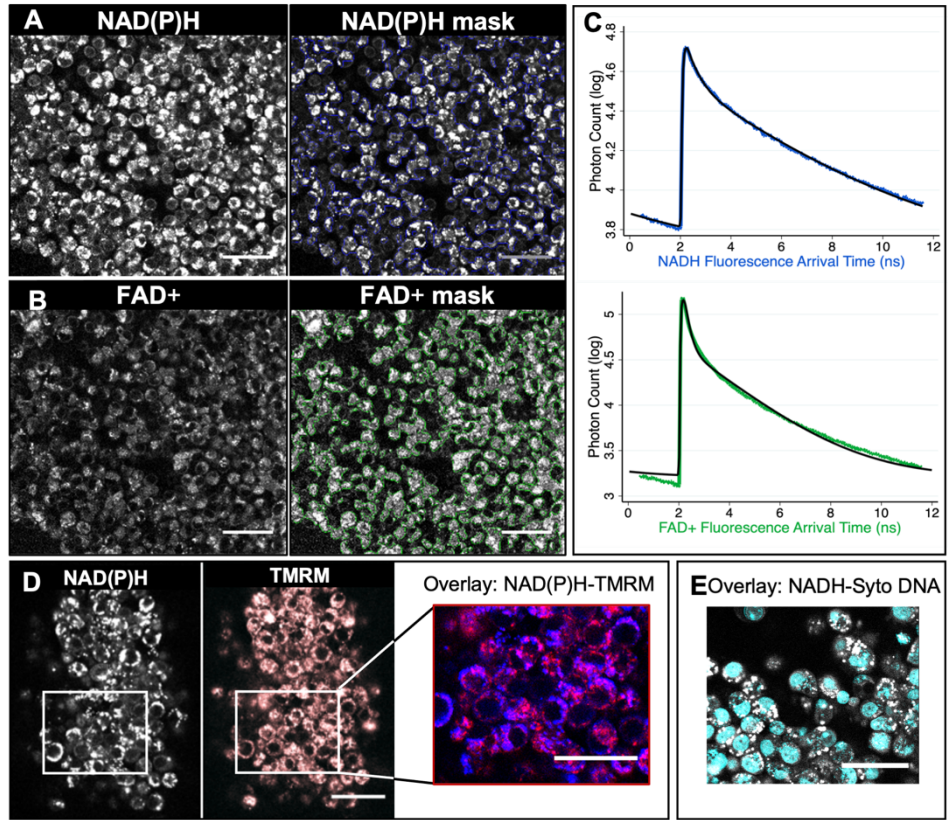
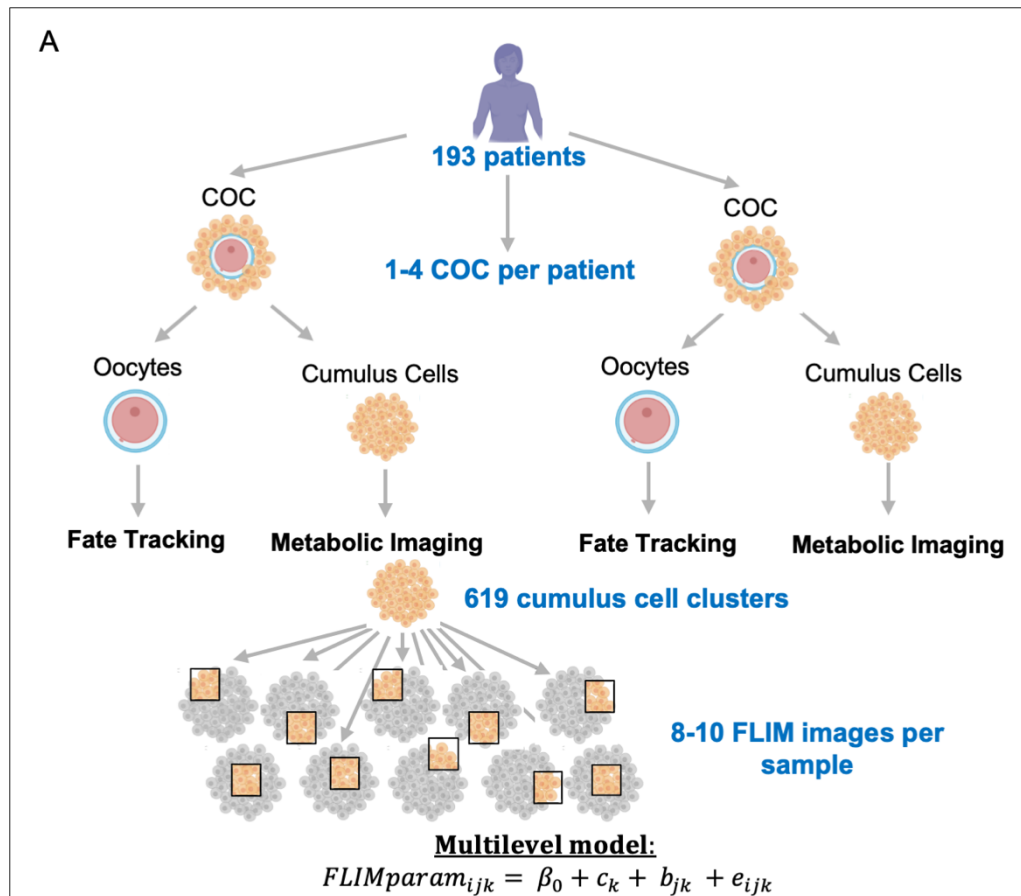


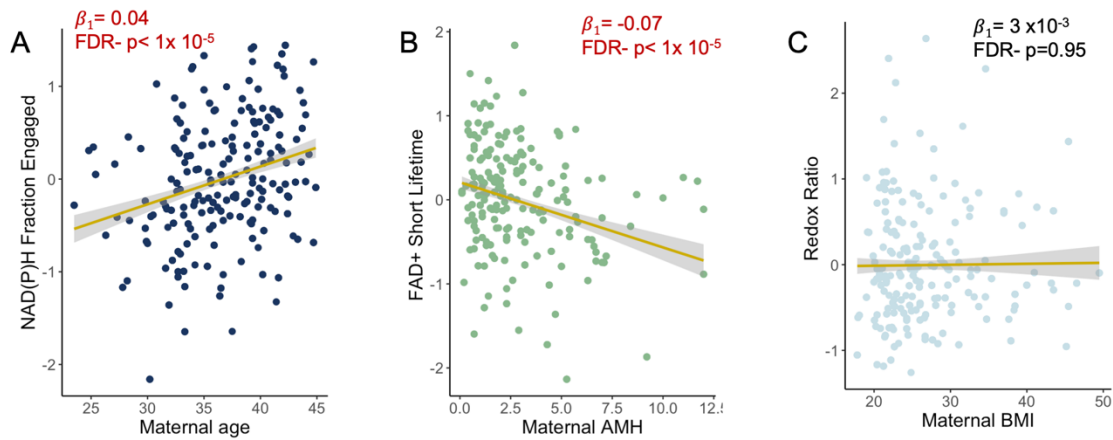
Figure 1. Fluorescence Lifetime Imaging Microscopy (FLIM) imaging of cumulus cells. (A) FLIM imaging of the autofluorescence of NAD(P)H (A) of a cumulus cell mass, and FAD+(B). An intensity-based thresholding algorithm was used to create masks of CCs to integrate the fluorescence signal of NAD(P)H or FAD+ (right panels). All photon arrival times from that mask were combined to create a fluorescence decay curve for each fluorophore (NAD(P)H in blue, C top and FAD+ in green, C bottom). These curves were fit to two-exponential models (C, black curves). This approach provides 9 quantitative parameters for characterizing the metabolic state of CCs: fluorescence intensity, long and short lifetime and the fraction engaged to enzyme for molecules NAD(P)H and FAD+ and the Redox Ratio. (D) NAD(P)H autofluorescence (left) image showings a co-localization with mitochondria dye TMRM image (in red, overlay in purple). (E) Overlay image of NAD(P)H autofluorescence in grey and DNA dye Syto in Cyan. Scale bars, 40 μm.



B

Level	NAD(P)H irradiance	NAD(P)H Fraction Engaged	NAD(P)H Long Lifetime	NAD(P)H Short Lifetime	FAD+ irradiance	FAD+ Fraction Engaged	FAD+ Long Lifetime	FAD+ Short Lifetime	Redox Ratio
$Var(c_k)$	0.30	0.23	0.27	0.18	0.29	0.15	0.47	0.19	0.21
$Var(b_{jk})$	0.59	0.67	0.63	0.72	0.55	0.74	0.83	0.69	0.84
$Var(e_{ijk})$	0.10	0.13	0.19	0.30	0.07	0.15	0.13	0.15	0.08

Figure 2. Metabolic variance between patients, between cumulus clusters and between images. (A) Diagram of the experimental design of this study. 1-4 COCs were collected per patient. CC masses were trimmed from the COCs and imaged using metabolic imaging. The fate of the corresponding oocyte was monitored. 8-10 FLIM metabolic images at different locations throughout the cluster were taken for each cumulus cluster. A multilevel model was applied to analyze this structured data. (B) The multilevel model encodes information on the variance of each FLIM parameter between patients, between CC clusters from the same patient, and between images from the same CC cluster. Numbers in the table correspond to the variance of each FLIM parameter associated with each level: patients, CC clusters and images.



$$D \quad FLIMparam_{ijk} = \beta_0 + \beta_1 * Patient\ Factor + c_k + b_{jk} + e_{ijk}$$

Patient Factor	NAD(P)H irradiance	NAD(P)H Fraction Engaged	NAD(P)H Long Lifetime	NAD(P)H Short Lifetime	FAD+ irradiance	FAD+ Fraction Engaged	FAD+ Long Lifetime	FAD+ Short Lifetime	Redox Ratio
Age	$\beta_1 = 0.03$ FDR- $p=5 \times 10^{-3}$	$\beta_1 = 0.04$ FDR- $p < 1 \times 10^{-5}$	$\beta_1 = 0.04$ FDR- $p < 1 \times 10^{-5}$	$\beta_1 = 0.01$ FDR- $p=0.26$	$\beta_1 = 0.02$ FDR- $p=0.08$	$\beta_1 = -0.29$ FDR- $p=0.05$	$\beta_1 = 0.02$ FDR- $p=0.15$	$\beta_1 = 0.05$ FDR- $p < 1 \times 10^{-5}$	$\beta_1 = 0.02$ FDR- $p=0.15$
AMH	$\beta_1 = -0.05$ FDR- $p=0.02$	$\beta_1 = -0.08$ FDR- $p < 1 \times 10^{-5}$	$\beta_1 = -0.09$ FDR- $p < 1 \times 10^{-5}$	$\beta_1 = -0.04$ FDR- $p=0.03$	$\beta_1 = -0.05$ FDR- $p=3 \times 10^{-3}$	$\beta_1 = 0.03$ FDR- $p=0.27$	$\beta_1 = 1 \times 10^{-4}$ FDR- $p=1.0$	$\beta_1 = -0.07$ FDR- $p < 1 \times 10^{-5}$	$\beta_1 = -0.02$ FDR- $p=0.48$
BMI	$\beta_1 = -4 \times 10^{-3}$ FDR- $p=0.95$	$\beta_1 = 4 \times 10^{-4}$ FDR- $p=0.95$	$\beta_1 = -9 \times 10^{-4}$ FDR- $p=0.95$	$\beta_1 = 6 \times 10^{-3}$ FDR- $p=0.95$	$\beta_1 = -6 \times 10^{-3}$ FDR- $p=0.95$	$\beta_1 = 2 \times 10^{-3}$ FDR- $p=0.95$	$\beta_1 = 4 \times 10^{-3}$ FDR- $p=0.95$	$\beta_1 = -7 \times 10^{-3}$ FDR- $p=0.95$	$\beta_1 = 1 \times 10^{-3}$ FDR- $p=0.95$
% Patient Variance explained by age and AMH	9%	20%	20%	2%	3%	11%	0%	33%	0.1%

Figure 3. CC FLIM metabolic parameters are associated with patient clinically relevant factors. Normalized NAD(P)H fraction engaged is significantly associated with maternal age (A), FAD+ short lifetime is significantly associated with maternal AMH levels (B) and Redox Ratio is not significantly associated with maternal BMI (C). Each dot corresponds to the mean of each patient. (D) A multilevel model was used to determine the significance (i.e., p values) extent of correlation (i.e., β_1 -coefficients) of CC FLIM parameters with maternal age, BMI and AMH levels. Numbers in red are statically significant after correcting for multiple comparisons using Benjamini – Hochberg’s false discovery rate (FDR p values<0.05). The last row shows the percentage of the CC FLIM parameters variance between patients that is explained by both age and AMH levels.

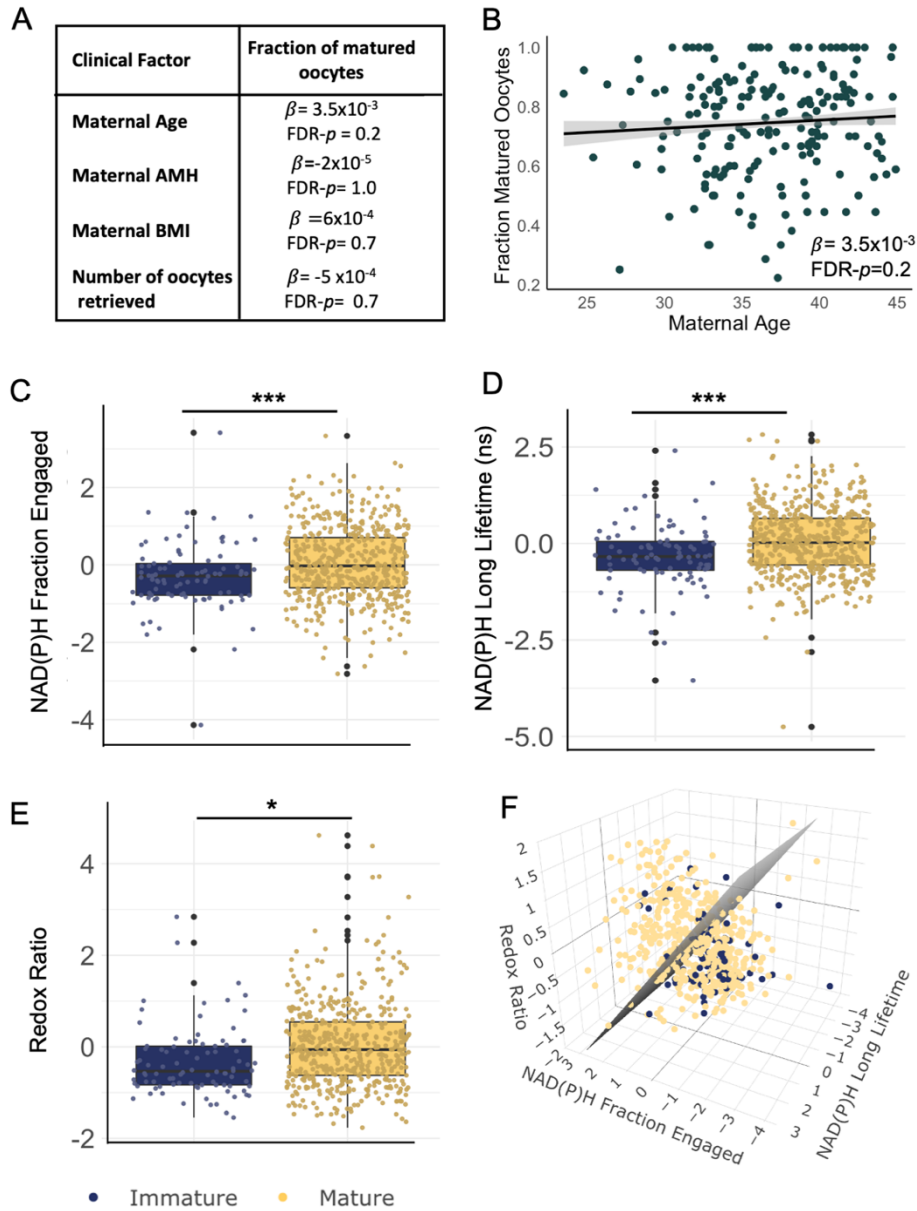


Figure 4. CC FLIM metabolic parameters are associated with the maturity of the enclosed oocyte. (A) β -coefficients and FDR- p values of the linear regression of maternal age, BMI, AMH levels, and number of oocytes retrieved, with the fraction of matured oocytes (number of matured oocytes / total of oocytes retrieved). There are no significant associations between these patient clinical factors and the fraction of matured oocytes. (B) Fraction of matured oocytes plotted vs maternal age indicates no significant association. However, significant differences were found in CC normalized NAD(P)H irradiance, NAD(P)H fraction bound (C), NAD(P)H long lifetime (D) and Redox Ratio (E) between CCs of immature ($n=90$, in blue) or mature oocytes ($n=505$, in yellow). (F) 3D plot of these three FLIM parameters for each CC cluster. In grey, support vector machine was applied to draw a hyperplane that best separates both groups. * signifies FDR- $p < 0.05$, *** signifies FDR- $p < 0.001$.

Supplementary Information

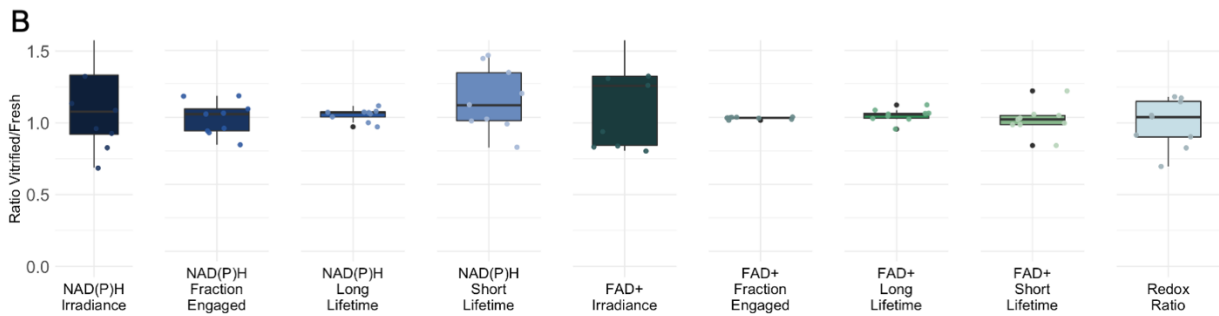
The CCs clusters were trimmed from their COCs and vitrified for further analysis. We performed preliminary studies on the effect of vitrification on the metabolic state of CCs. Cumulus masses (n=9) were divided into two clusters, one portion was vitrified. Each cumulus cluster was then thawed, following Irvine thawing protocol, and imaged using FLIM, while the other portion was imaged fresh. The ratio between CCs metabolic parameters of the portion that was vitrified versus the portion that was fresh was computed. A t-test indicated that these ratios were not significantly different from 1 (FDR $p > 0.05$, Supplementary figure 1A).

We also studied the effect of the use of hyaluronidase enzyme on the metabolic state of CCs. Cumulus masses (n=9) were divided into two, one portion was imaged without exposure to hyaluronidase, and the other portion was treated with hyaluronidase enzyme solution to dissolve the hyaluronan matrix. The CCs were then centrifuged, and the pellet was imaged using FLIM. The ratio between CCs FLIM parameters of the portion exposed with hyaluronidase versus the fresh was computed. A t-test indicated that the ratios of the fraction engaged, and the lifetime ratios were not significantly different from 1, while the NAD(P)H irradiance, FAD+ irradiance and the Redox Ratio were significantly different (supplementary figure 2B).

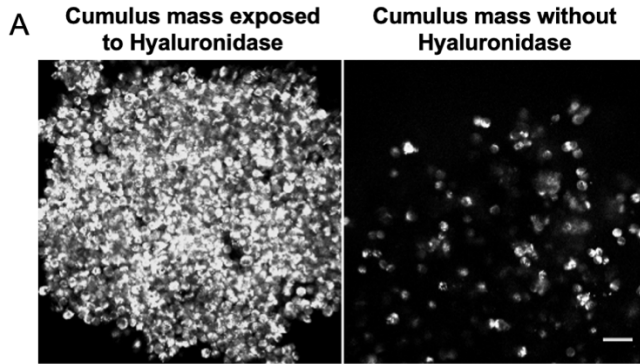
Finally, we studied the effect of CCs location through the cumulus cluster on the metabolic state. Cumulus masses (n=7) trimmed further from the oocyte were compared with cumulus masses from the same oocytes trimmed closer to the oocyte. The ratio between CCs FLIM parameters further from the oocytes versus closer to the oocyte was computed. A t-test indicated that these ratios were not significantly different from 1 (FDR $p > 0.05$, Supplementary figure 3A).

Supplementary Figures

A	NAD(P)H irradiance (photons/area)	NAD(P)H Fraction Engaged	NAD(P)H Long Lifetime (ns)	NAD(P)H Short Lifetime (ns)	FAD+ irradiance (photons/area)	FAD+ Fraction Engaged	FAD+ Long Lifetime (ns)	FAD+ Short Lifetime (ns)	Redox Ratio
Mean cumulus mass fresh	0.50	0.31	2.93	0.14	0.42	0.83	2.15	0.15	1.34
Mean cumulus mass vitrified	0.61	0.31	2.98	0.16	0.52	0.83	2.18	0.15	1.3
FDR p-values	0.51	0.90	0.51	0.44	0.44	0.44	0.63	0.84	0.90

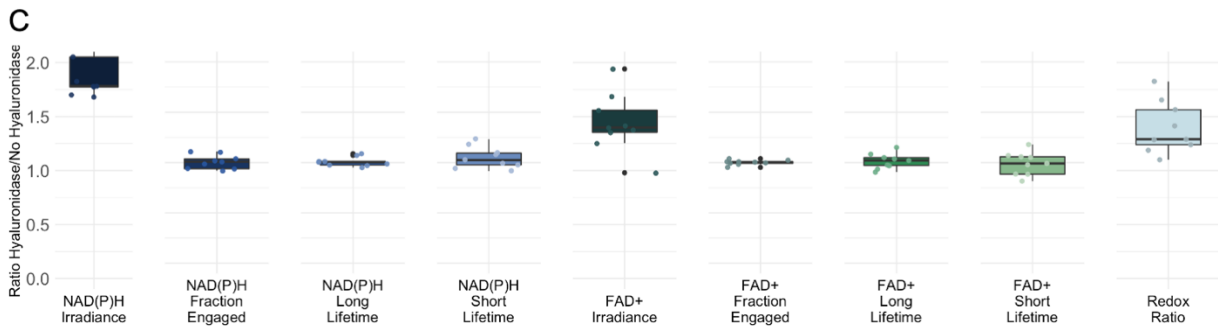


Supplementary Figure 1. CCs that were imaged fresh show no significant differences in FLIM parameter from CCs that were first vitrified and then thawed (A) Mean FLIM measurements of both fresh and vitrified cumulus clusters (n=9), the FDR p-value of the t-test performed in the ratio between fresh/ vitrified compared to 1. (B) Box plots showing the ratios of each FLIM measurement.



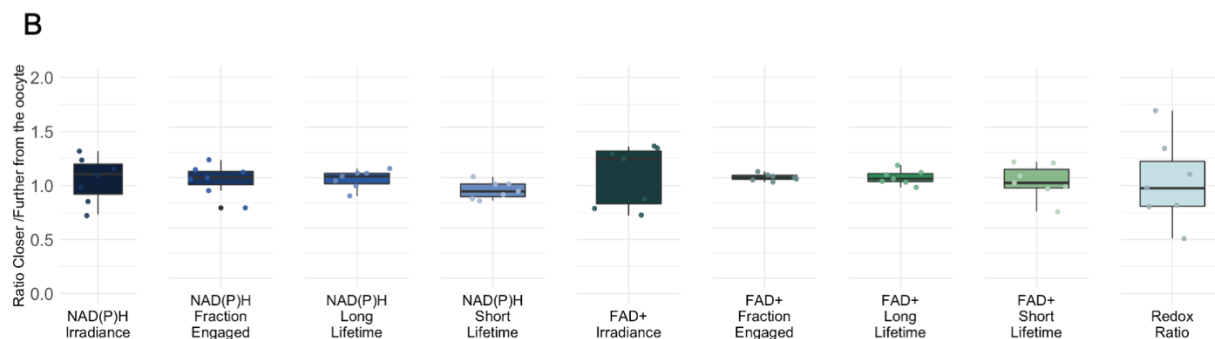
B

	NAD(P)H irradiance (photons/area)	NAD(P)H Fraction Engaged	NAD(P)H Long Lifetime (ns)	NAD(P)H Short Lifetime (ns)	FAD+ irradiance (photons/area)	FAD+ Fraction Engaged	FAD+ Long Lifetime (ns)	FAD+ Short Lifetime (ns)	Redox Ratio
Mean cumulus mass without Hyaluronidase	2.20	0.41	3.46	0.28	0.74	0.84	2.0	0.14	3.05
Mean cumulus mass exposed to Hyaluronidase	4.27	0.41	3.49	0.30	1.05	0.85	2.01	0.13	4.22
FDR p-values	9x10⁻⁴	0.92	0.92	0.47	3x10⁻³	0.93	0.92	0.92	3x10⁻³

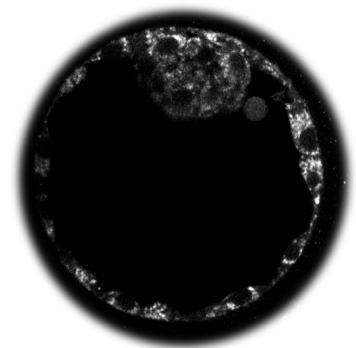


Supplementary Figure 2. CCs that were not exposed to hyaluronidase show significant differences in intensities and redox ratio from those exposed to hyaluronidase (A, left) NAD(P)H autofluorescent intensity image of CCs exposed to hyaluronidase enzyme to dissolve its matrix and (A, right) CCs not exposed with hyaluronidase. (B) Mean of FLIM measurements of CCs exposed and not exposed to hyaluronidase (n=9), the p-values obtained from the comparison of the ratio between CCs not exposed to hyaluronidase / CCs exposed with hyaluronidase enzyme to 1 and FDR p-values. (C) Box plots showing these ratios of each FLIM measurement.

A	NAD(P)H irradiance (photons/area)	NAD(P)H Fraction Engaged	NAD(P)H Long Lifetime (ns)	NAD(P)H Short Lifetime (ns)	FAD+ irradiance (photons/area)	FAD+ Fraction Engaged	FAD+ Long Lifetime (ns)	FAD+ Short Lifetime (ns)	Redox Ratio
Mean cumulus mass closer to the oocyte	4.41	0.38	3.44	0.29	1.12	0.86	2.0	0.13	4.00
Mean cumulus mass further from the oocyte	4.14	0.40	3.37	0.25	1.06	0.85	2.0	0.13	4.01
FDR p-values	0.94	0.94	0.94	0.08	0.94	0.94	0.94	0.94	0.94



Supplementary Figure 3. CCs closed to the oocyte show no significant differences in FLIM parameters from CCs that were located further from the oocyte (A) Mean FLIM parameter values of both the CCs closer to the oocytes and those further from the oocytes ($n=7$), the p-value after a t-test performed in the ratio between CCs further from the oocytes / CCs closer to the oocytes compared to 1 and FDR p-values. (C) Box plots showing these ratios of each FLIM measurement.



8. Publication 3: *Metabolic state of human blastocysts measured by fluorescence lifetime imaging microscopy*

(DOI:10.1093/humrep/deab283)

Title: Metabolic state of human blastocysts measured by fluorescence lifetime imaging microscopy

Authors: Marta Venturas.^{1,2*}, Jaimin S. Shah.^{3,4}, Xingbo Yang.¹, Tim H Sanchez, William Conway.^{1,5}, Denny Sakkas^{4#} and Dan J. Needleman.,^{1,5,6#}

¹Molecular and Cellular Biology and School of Engineering and Applied Sciences, Harvard University, Cambridge, MA, U.S.A.

²Departament de Biologia Cel·lular, Fisiologia i Immunologia, Universitat Autònoma de Barcelona, Cerdanyola, Spain

³Beth Israel Deaconess Medical Center/ Harvard Medical School, Boston, MA, U.S.A.

⁴Boston IVF, Waltham, MA, U.S.A.

⁵Physics Department, Harvard University, Cambridge, MA, U.S.A.

⁶Center for Computational Biology, Flatiron Institute, New York, United States

#The last two authors are the senior authors

Corresponding Author

* Marta Venturas.

Email: martaventu22@gmail.com

Address: 52 Oxford St. NW building room 358, Cambridge, MA, 02138, USA.

Abstract

Study question: Can non-invasive metabolic imaging via fluorescence lifetime imaging microscopy (FLIM) detect variations in metabolic profiles between discarded human blastocysts?

Summary answer: FLIM revealed extensive variations in the metabolic state of discarded human blastocysts associated with blastocyst development over 36h, the day after fertilization and blastocyst developmental stage, as well as metabolic heterogeneity within individual blastocysts.

What is known already: Mammalian embryos undergo large changes in metabolism over the course of preimplantation development. Embryo metabolism has long been linked to embryo viability, suggesting its potential utility in Assisted Reproductive Technologies (ART) to aid in selecting high quality embryos. However, the metabolism of human embryos remains poorly characterized due to a lack of non-invasive methods to measure their metabolic state.

Study design, size, duration: We conducted a prospective observational study. We used 215 morphologically normal human embryos from 137 patients that were discarded and donated for research under an approved institutional review board protocol. These embryos were imaged using metabolic imaging via Fluorescence Lifetime Imaging Microscopy (FLIM) to measure the autofluorescence of two central coenzymes, NAD(P)H and FAD⁺, which are essential for cellular respiration and glycolysis.

Participants/materials, setting, methods: Here we used non-invasive FLIM to measure the metabolic state of human blastocysts. We first studied spatial patterns in the metabolic state within human blastocysts and the association of the metabolic state of the whole blastocysts with stage of expansion, day of development since fertilization and morphology. We explored the sensitivity of this technique in detecting metabolic variations between blastocysts from the same patient and between patients. Next, we explored whether FLIM can quantitatively measure metabolic changes through human blastocyst expansion and

hatching via time-lapse imaging. For all test conditions, the level of significance was set at $p < 0.05$ after correction for multiple comparisons using Benjamini - Hochberg's false discovery rate (FDR).

Main results and the role of chance: We found that FLIM is sensitive enough to detect significant metabolic differences between blastocysts. We found that metabolic variations between blastocyst are partially explained by both the time since fertilization and their developmental expansion stage ($p < 0.05$), but not their morphological grade. Substantial metabolic variations between blastocysts from the same patients remain, even after controlling for these factors. We also observe significant metabolic heterogeneity within individual blastocysts, including between the inner cell mass and the trophectoderm, and between the portions of hatching blastocysts within and without the zona pellucida ($p < 0.05$). And finally, we observed that the metabolic state of human blastocysts continuously varies over time.

Limitations, reasons for caution: Although we observed significant variations in metabolic parameters, our data is taken from human blastocysts that were discarded and donated for research and we do not know their clinical outcome. Moreover, the embryos used in this study are a mixture of aneuploid, euploid, and embryos of unknown ploidy.

Wider implications of the findings: This work reveals novel aspects of the metabolism of human blastocysts and suggests that FLIM is a promising approach to assess embryo viability through non-invasive, quantitative measurements of their metabolism. These results further demonstrate that FLIM can provide biologically relevant information that may be valuable for the assessment of embryo quality.

Study funding/competing interest(s): Funding/Support: Supported by the Blavatnik Biomedical Accelerator Grant at Harvard University. Becker and Hickl GmbH and Boston Electronics sponsored research with the loaning of equipment for FLIM.

Trial registration number: n/a

Keywords: metabolism / human blastocysts / embryo assessment / noninvasive / fluorescence lifetime imaging microscopy / embryo development

Introduction

Mammalian preimplantation embryos undergo dynamic metabolic changes necessary to support distinctive developmental events (Gardner et al., 2001; Leese, 2012, 2015). Early stages of preimplantation embryo development rely primarily on pyruvate for energy generation (Leese, 2015; Harvey, 2019). It was previously thought that once the embryo reached the 8-cell stage, the embryo underwent a metabolic switch and glycolysis became the predominant pathway for ATP production (Gardner et al., 2011; Gardner and Harvey, 2015; Leese, 2015). However, a number of studies have shown that glucose does not only contribute to energy production in mouse embryos, but instead plays crucial signaling roles required for blastocyst formation and cell fate specification (Chi et al., 2020; Saha et al., 2020; Zhu and Zernicka-Goetz, 2020). Glucose is also partially converted to lactate, which is thought to facilitate different aspects of implantation, including tissue invasion, angiogenesis and modulation of the immune response (Gardner, 2015). In parallel, oxygen consumption increases at the blastocysts stage (Houghton et al., 1996; Trimarchi et al., 2000; Gardner, 2015). Proper metabolic function is essential for producing developmentally viable eggs and embryos (Van Blerkom et al., 1995; Gardner et al., 2011; Harvey, 2019), and impaired metabolic activity has been correlated with decreased developmental potential in mouse (Wakefield et al., 2011; Harvey, 2019) and human embryos (Van Blerkom et al., 1995; Wilding et al., 2001; Harvey, 2019). Embryos with the highest developmental potential were found to have low amino acid turnover (Brison et al., 2004) and low rates of oxygen consumption (Houghton et al., 1996; Lopes et al., 2010). These observations led to the 'Quiet embryo hypothesis' by Leese et al. which proposes that embryos with a higher developmental capacity are characterized by a quieter metabolism rather than an active one (Leese, 2002), which is suggested to be linked with cellular or molecular damage (Baumann et al., 2007; Leese, 2012). However, in apparent contradiction with this hypothesis, some studies indicate that pyruvate (Turner et al., 1994) and glucose uptake (Gardner and Leese, 1987) levels are higher in embryos that develop successfully.

Blastomeres in preimplantation embryos are genetically, morphologically, and metabolically heterogeneous. Metabolic heterogeneity between blastomeres is thought to be associated with either cell lineage specification (Chi et al., 2020) or cellular stress (Brison et al., 2004) as high levels of heterogeneity have been linked with developmental arrest (Sutton-McDowall et al., 2017). Cellular stress may be associated with increased DNA damage (Sturmey et al., 2008) which could be either a cause or a consequence of cell metabolic (dys)function. At the blastocyst stage, clear cellular differentiation already exists, with the apical trophectoderm (TE) and inner cell mass (ICM), which give rise to the placenta and fetus, respectively. Studies in mouse (Hewitson and Leese, 1993; Van Blerkom et al., 1995; Houghton, 2006; Van Blerkom, 2011; Gardner and Harvey, 2015) and human embryos (Gardner and Harvey, 2015), have found differences in mitochondrial physiology and activity between cells in the TE and ICM.

Developing tools to select the best embryo to transfer has been a long term focus in IVF (Gardner et al., 2000; Seli et al., 2007; Urbanski et al., 2008). Improved embryo selection would decrease the number of transfers a patient must undergo, which would in turn, reduce its economical and emotional cost (Gardner and Leese, 1987; Gerris et al., 2004). Current selection methods primarily rely on embryo morphology assessments (Schoolcraft et al., 1999). Blastocyst morphology grading

is typically based on the expansion stage, the consistency of both the ICM and TE, and the time to blastocyst formation since fertilization (Schoolcraft et al., 1999). Despite its widespread use, embryo morphological assessments have limited predictive power, and the further disadvantage that they are unable to provide a direct measure of the physiology of the embryo (Wong et al., 2014). Alternative embryo selection approaches include: invasive preimplantation genetic testing for aneuploidy (PGT-A), which is increasingly being used (Penzias et al., 2018; Munné et al., 2019; Patrizio et al., 2019); time-lapse imaging (Coticchio et al., 2018), which provides detailed information on developmental dynamics; and, more recently, artificial intelligence (Tran et al., 2019). Additionally, several studies in mouse and human embryos showed a clear association between metabolic function and implantation potential (Gardner and Leese, 1987; Van Blerkom et al., 1995; Gardner et al., 2011; Ahlström et al., 2013). Embryo morphology (Tejera et al., 2012) and time to blastocyst formation (Jones et al., 2001) have also been found to be linked with embryo metabolism. This suggests that measures of metabolism might provide a means to select high quality embryos for transfer, but approaches based on this premise have so far not been successful (Jones et al., 2001; Thompson et al., 2016).

Many approaches to study embryo metabolism hinge on either intracellular measurements (Alm et al., 2005; Al-Zubaidi et al., 2019) or quantification of metabolites in the spent media to detect the metabolic activity of the whole embryo (Gardner and Leese, 1987; Conaghan et al., 1993; Urbanski et al., 2008; Vergouw et al., 2008; Gardner et al., 2011). These methods are often either invasive or require highly specialized skills to perform. Recently, non-invasive methods to measure intracellular metabolic activity of oocytes and embryos have also been pursued. Several endogenous molecules like nicotinamide adenine phosphate dinucleotide (NADPH), nicotinamide adenine dinucleotide (NADH) and flavine adenine dinucleotide (FAD⁺) are autofluorescent (Heikal, 2010). These molecules are electron carriers that play key roles in metabolic pathways, which makes them ideal candidates for characterizing cellular metabolism (Klaidman et al., 1995; Dumollard et al., 2004). The fluorescence spectra of NADH and NADPH are almost indistinguishable (Ghukasyan and Heikal, 2014), therefore the combined fluorescence of NADH and NADPH is often referred to as the NAD(P)H signal. NAD(P)H (Dumollard et al., 2007, 2009) and FAD⁺ (Sutton-McDowall et al., 2017; Santos Monteiro et al., 2021) autofluorescence intensity can be used to measure switches in the metabolic state of cells throughout development.

Additional information on NAD(P)H and FAD⁺ can be obtained using fluorescence lifetime imaging microscopy (FLIM) (Becker, 2012). FLIM not only provides information on fluorescence intensity, but also gives information on the fluorescence lifetime, i.e. the time the fluorophores remain in their excited state. The fluorescence lifetimes of NAD(P)H and FAD⁺ depend on their microenvironment, including their engagement with enzymes, and thus provides a sensitive means to characterize variations in metabolic state (Ghukasyan and Heikal, 2014). FLIM enables non-invasive, quantitative measurements of the metabolic state of mouse embryos (Sanchez et al., 2018, 2019; Ma et al., 2019), but its application to human preimplantation embryos has yet to be established (Cinco et al., 2016). FLIM can be performed with two-photon fluorescence microscopy (Becker, 2005, 2012), which allows intrinsic sectioning and deep imaging (Mertz, 2019). Another advantage of performing FLIM with two-photon microscopy, is that it enables simultaneous non-invasive imaging of spindle morphology via second harmonic generation (SHG). SHG is a non-

linear phenomenon that occurs when light scatters from highly ordered structures that lack inversion symmetry, like the spindle (Hsieh et al., 2008; Yu et al., 2014; Mertz, 2019; Sanchez et al., 2019). The use of non-invasive FLIM in combination with SHG has been previously described in mouse embryos (Sanchez et al., 2019). However, its utility for studying preimplantation human embryos has not been demonstrated. A key question is: is this technique sensitive enough to measure the metabolic differences that occur within and between human embryos? Non-invasive techniques to simultaneously measure the cellular metabolic state and spindle dynamics of human embryos can offer a better understanding of basic embryo biology and may assist in improving embryo screening in a clinical setting.

In the present study, we used non-invasive FLIM to measure the metabolic state of human blastocysts. First, we studied spatial patterns in the metabolic state within human blastocysts and the association of embryo metabolic state with the stage of expansion, day of development since fertilization and morphology. Second, we show that this technique is sensitive enough to resolve the metabolic variations between blastocysts from the same patient and between patients. Last, we explored the extent to which time-lapse FLIM imaging can quantitatively measure metabolic changes through human blastocyst expansion and hatching.

Materials and Methods

Sample preparation

Human blastocysts were discarded and donated for research under determinations by the Beth Israel Deaconess Medical Center and New England institutional review boards (New England IRB WO 1-6450-1). Two hundred and fifteen vitrified human blastocysts from 137 patients, with a mean \pm standard deviation age of 35.4 ± 4.7 years, BMI of 25.9 ± 5.2 kg/m², and mean AMH of 3.55 ± 2.9 ng/mL were analyzed in this experiment. These embryos were thawed according to the manufacturer's recommendations (90137-SO - Vit Kit-Thaw, FUJIFILM Irvine Scientific, USA) and cultured for two hours in individual drops of 50 μ l of Continuous Single Culture Complete (CSC) media with human serum albumin media (HSA) (FUJIFILM Irvine Scientific, USA) overlain with mineral oil in an incubator at 37C, 7% CO₂ and 6% O₂. Patient clinical characteristics such as age, BMI and AMH hormone levels were provided in a de-identified database. Blastocyst's morphological grade (Schoolcraft et al., 1999) were evaluated at the time of imaging by a senior embryologist. An ICM and TE grade A, B, or C was assigned for each blastocyst. Stage of development (early, expanded, hatching or hatched blastocyst) and day since fertilization (day 5 or 6) was also monitored for each embryo.

For the blastocyst development time-lapse imaging experiment, 17 human blastocysts from 17 different patients were analyzed. Blastocyst's morphological grade was assessed before and after the 36 hours time-lapse experiment.

Imaging Protocols

Discarded blastocysts were transferred and imaged in a custom glass-bottomed microwell dish with 80 μ L of media overlain with mineral oil, in an on-stage incubation system (Ibidi GmbH, Martinsried, Germany) to maintain environmental culture conditions of 37C, 7% CO₂ and 6% O₂.

For the single time-point blastocyst experiment, FLIM images were taken once 2 hours after thawing at three Z-planes 7 μm apart, using 12mW for NAD(P)H and 20mW for FAD⁺ and 60 seconds of integration time for each plane.

For the blastocyst development time-lapse experiment, we compared the results from two different protocols. Two hours after thawing embryos: 1) for 10 human blastocysts, metabolic measurements were taken every two hours over the course of 36 h (at three Z-planes 7 μm apart) using the same parameters as explained above for each plane; 2) for 7 human blastocyst, one metabolic measurement was taken (at three Z planes 7 μm apart), and the embryos were incubated on the microscope without further exposure to illumination for 36 hours. For all 17 blastocysts, a final metabolic image was taken after 36h on the microscope.

Staining protocols

For MitoTraker experiments, five blastocysts were incubated with 5nM MitoTraker Red CMXRos (M7512, Thermo Fisher, USA) for 20 minutes. For DNA staining experiments, five embryos were stained with 1 $\mu\text{g}/\text{mL}$ of Hoechst (Thermo Fisher, USA) for 20 minutes. The samples were then washed three times in CSC + HSA and transferred to a glass bottom dish for imaging.

Fluorescence Lifetime Imaging Microscopy (FLIM)

FLIM measurements were performed on a Nikon TE300 (Nikon, Japan) microscope using two-photon excitation from a Ti:Sapphire pulsed laser (M-squared Lasers, UK) with a 80MHz repetition rate and 150 fs pulse width, a galvanometric scanner, time correlated single photon counting (TCSPC) module (SPC-150, Becker and Hickl, Germany) and a hybrid single photon counting detector (HPM-100-40, Becker and Hickl, Germany). Imaging was performed with a 20X Nikon objective with 0.75 numerical aperture (CFI Apo 20X, NA 0.75, Nikon). The wavelengths of NAD(P)H and FAD⁺ excitation were set to 750nm and 890nm, respectively. The power output was measured through the objective in the sample plane with a handheld power meter (Thorlabs, USA). The corresponding powers measured at the sample plane used were 12mW for NAD(P)H and 20mW for FAD⁺. Optical bandpass filters were positioned in a filter wheel in front of the detector – 447 \pm 30 nm bandwidth for NAD(P)H (BrightLine, Semrock, USA) and 550 \pm 44 nm bandwidth for FAD⁺ (Chroma technologies) with an additional 650nm short pass filter mounted on the detector (Chroma technologies). SHG was detected simultaneous with FAD imaging by a single-photon counting detector (PMC-150, Becker-Hickl GmbH, Germany) in the forward direction, with 650 short-pass and 440 \pm 10 nm bandwidth bandpass filters (BrightLine, Semrock, USA). Each NAD(P)H and FAD⁺ image was acquired with 60 seconds of integration time. A customized motorized stage (using CONEX TRA12CC actuators, Newport, USA) was used to perform multi-dimensional acquisitions. We acquired three FLIM images varying Z axis per each human blastocyst. All the electronics were controlled by SPCM software (Becker and Hickl, Germany) and custom LabVIEW software.

Data Analysis

Data was analyzed using a custom code written in MATLAB version R2019b (MathWorks, USA). Samples were incorporated to the analysis according to the information available. NAD(P)H and FAD⁺ images were trained using a supervised machine learning segmentation software (Illastik, version 1.0 (Berg et al., 2019)) to classify pixels in intensity images into either NAD(P)H or FAD⁺

signal from the cells or the background. The algorithm was trained using 40 random NAD(P)H and FAD+ intensity images. For each cell segment, the photon arrival time histogram was modeled as a bi-exponential decay:

$$P(t) = A[(1 - F) * e^{(-t/\tau_1)} + F * e^{(-t/\tau_2)}] + B$$

Where, A is a normalization factor, B is the background, τ_1 is the short lifetime, τ_2 is the long lifetime and F is the fraction of molecule with long lifetime (fraction engaged with enzymes for NAD(P)H and unengaged for FAD+). This function was convolved with a measured instrument response function to model the experimental data, and the least square fitting yielded quantitative values for these fit parameters. The fluorescence intensity was calculated for each embryo dividing the number of photons by the area of the embryo. An additional parameter, the redox ratio (NAD(P)H fluorescence intensity/FAD+ fluorescence intensity) was also calculated per image. Together, a single FLIM measurement produced 9 parameters, 4 for NAD(P)H and 4 for FAD+ and redox ratio, to quantitatively characterize the metabolic state of human blastocysts.

The average photon arrival time of NAD(P)H and FAD+ was computed for each pixel within the embryo by averaging over the directly measured photon arrival time of all photons coming from NAD(P)H and FAD+ within a single pixel. Since the single pixel average is noisy due to limited photon counts per pixel, we smoothed the data by averaging each pixel over its neighboring pixels weighted by a gaussian kernel with a 20 pixel standard deviation. We only averaged over pixels within the embryo and exclude pixels of the background and the cavity of the embryo. As a statistical control, we randomized the photon arrival times in each pixel by drawing a random photon arrival time from a gaussian distribution with a mean of the average photon arrive time and a variance equal to that of the photon arrival time distribution of the blastocyst. This procedure produces a randomized photon arrival time image of the blastocyst with the exact same geometry. We repeated the average photon arrival time calculation described above for this “control image” to test if there was any artifact associated with the averaging procedure. The control image consistently produced a homogeneous average photon arrival time, suggesting the heterogeneity observed in the blastocyst is of a biological origin rather than statistical artifact.

Statistical Analysis

All statistical tests were performed using Stata Statistical Software version 16.0 (LLC Stata Corp, Texas, USA) and R Studio Version 1.3.959 (R Foundation for Statistical Computing, Vienna, Austria). Our data was structured hierarchically, three images per embryo (i) and 1 – 7 embryos (j) per patient (k). Therefore, we used multilevel models with restricted maximum likelihood estimates (Snijders and Bosker, 2011) to analyze this structured data. We incorporated the corresponding predictors (embryo morphology, day, expansion stage or patient age, BMI and AMH) for each analysis, using the multilevel model:

$$FLIMparam_{ijk} = \beta_0 + \beta_1 * embryo\ characteristics + c_{0,k} + b_{0,jk} + e_{ijk}$$

Where β_0 corresponds to the intercept; β_1 to the slope; *embryo characteristics* to the day, stage or morphological grading of the embryos; $c_{0,k}$ is the patient level random error; $b_{0,jk}$ is the embryo level random error; e_{ijk} is the image random error (Snijders and Bosker, 2011). This modelling encodes

information on the variance associated with each level: patient, embryos within patients and images within an embryo. One tailed Z-test was performed to determine whether these variances were significantly different than zero. The described experiments were performed by two different operators. Controlling for the operator in the multilevel model did not impact the results.

Additionally, paired t-test were performed to detect metabolic variations between the ICM and the TE of each embryo. For all comparisons of ratios, one sample t-test was performed to determine whether these ratios were significantly different than one. Furthermore, we calculated the percentage change of all metabolic parameters between each expansion stage compared to the early blastocyst stage and pairwise comparisons were performed to analyze their significance. All p-values were corrected for multiple comparisons using Benjamini - Hochberg's false discovery rate (FDR), at a q value of 0.05. FDR p-values of <0.05 were considered statistically significant.

We used a support vector machine algorithm (SVM)(Cristianini and Shawe-Taylor, 1999) to fit a hyperplane that best separates day 5 and day 6 embryos. All the data was randomly divided into two sets, a training set (70%) and a test set (30%). We performed SVM on the training set, and then we tested the accuracy of this model using the test set.

Furthermore, to understand the conditional dependencies between embryo day, expansion stage and the metabolic parameters, we constructed probabilistic graphical models(Neapolitan, 2009; Pearl, 2016) using standardized embryo metabolic parameters ($\frac{x-\text{mean}(x)}{\text{sd}}$), embryo day and stage. A directed arrow was drawn from variable a (embryo day) to variable b (embryo stage) if the probability distribution of a depends on b, and can be written as $P(a, b) = P(a)P(b|a)$. These conditional dependencies can be represented by a directed acyclic graph (DAG). We then computed the percentage of variance explained by both embryo day and stage for each level ($\frac{\text{Variance Patient Level}}{\text{Total Variance}}$ %), which can represent the effect size of the model(Lorah, 2018).

Finally, we calculated the percentage change of all metabolic parameters between embryos at day 5 and day 6 and between timepoint 0 hours and 24 hours after time-lapse imaging. T-test with FDR correction were performed to analyze their significance.

Results

Two-photon microscopy of endogenous autofluorescence and second harmonic generation imaging enable visualization of subcellular structures in preimplantation human embryos

Preimplantation human embryos are often visualized using bright-field microscopy in IVF clinics, which is sufficient for blastocyst morphological grading but provides limited cellular and subcellular information (Figure 1A). We first investigated what additional morphological information can be provided by two-photon microscopy of endogenous NAD(P)H and FAD+. Two-photon microscopy enables deep tissue imaging with optical sectioning(Mertz, 2019), allowing us to perform three dimensional (3D) reconstruction of blastocysts by combing multiple Z plane images of NAD(P)H autofluorescence (Figure 1B). Cell nuclei appear as dark ovals in these 3D reconstructions (Figure 1B, arrow), as confirmed by comparison to 3D reconstruction of human embryos stained for DNA with Hoechst (Figure 1C). As FAD+ is significantly more enriched in mitochondria than NAD(P)H in

many systems(Klaidman et al., 1995; Dumollard et al., 2004), we sought to determine the extent to which two-photon microscopy of FAD⁺ can provide information on mitochondrial localization in human preimplantation embryos. We stained five human blastocysts from 5 different patients with MitoTraker Red CMXRos, a dye that specifically labels mitochondria, and simultaneously imaged MitoTraker and FAD⁺ autofluorescence (Figure 1D). We used machine-learning based software (Ilastik, version 1.0(Berg et al., 2019)) to segment bright intracellular regions in both the MitoTraker and FAD⁺ images and found an overlap of photons between regions of 89±8%. Hence, the overwhelming majority of the FAD⁺ signal in human blastocyst is associated with mitochondria, and thus FAD⁺ imaging provides information on mitochondrial localization. The same laser illumination used for two-photon microscopy can be simultaneously employed for SHG, which we combined with FAD⁺ imaging, as previously described(Sanchez et al., 2019). Using both autofluorescence and SHG imaging, it was possible to observe spindles in mitotic cells in all human blastocysts, along with the subsequent cell divisions (Figure 1E, S11 and Movies SM1 and SM2). Thus, two-photon microscopy of NAD(P)H and FAD⁺, combined with SHG imaging, provides a non-invasive means to image cellular and subcellular structures in human blastocysts, including mitochondria, nuclei and spindles.

To quantify the metabolic state of human blastocysts, we used an intensity-based machine learning algorithm (see methods) to segment both the NAD(P)H (Figure 1G, upper) and the FAD⁺ signal (Figure 1G, lower). We then grouped all photons from the segmented regions to obtain histograms of NAD(P)H (Figure 1H, upper) and FAD⁺ (Figure 1H, lower) photon arrival times, which we fit using two-exponential decay models (Figure 1H, black lines). This provided nine metabolic FLIM related parameters at each point in time: fluorescence intensity, short and long lifetimes, and the fraction of molecules engaged with enzymes for both NAD(P)H and FAD⁺, as well as the redox ratio (NAD(P)H intensity/ FAD⁺ intensity).

Spatial variation in human blastocysts metabolic parameters

We next imaged a total of 215 human blastocysts from 137 patients that were discarded and donated for research. FLIM data was taken at a single time point for each blastocyst, acquired two hours after thawing.

We first used this data to investigate the spatial variation in metabolic parameters within human blastocysts. In the segmented the images we calculated the average photon arrival time (see methods) and visualized the spatial distribution of average photon arrival times for NAD(P)H (Figure 2A) and FAD⁺ (Figure 2B), which appeared to indicate different metabolic signatures in the ICM and TE. These spatial patterns disappear after randomizing the photon arrival times for each pixel in the segmented region (SI 2), indicating that the observed spatial patterns are real and not an artifact of the averaging procedure or the geometry of the blastocyst (Methods). To further investigate the difference in metabolism between the ICM and TE, we manually segmented them and grouped photons from each region to determine their FLIM parameters (n=187 from 125 patients). All metabolic parameters displayed significant differences between ICM and TE as measured by a paired t-test with post-hoc correction using Benjamini - Hochberg's false discovery rate (FDR), (FDR p<0.0001). We were concerned that the different number of photons acquired from the two regions might artificially contribute to the measured difference in FLIM parameters. We therefore repeated

the analysis, but by randomly selecting the same number of photons from the ICM and the TE. All the significant differences were upheld (FDR $p < 0.0005$), indicating that the measured difference in FLIM parameters is robust to the number of photons acquired. The observed differences in FLIM parameters between ICM and TE argues that cells in these regions are in different metabolic states (Figure 2C). To further investigate this on the single embryo level, we calculated the ratio of each FLIM parameter between the ICM and TE of every embryo. While the average of each ratio across embryos was significantly different from 1 (FDR $p < 0.0001$), there was substantial embryo-to-embryo variability (Figure 2D).

We next explored if the embryo-to-embryo differences in FLIM of TE and ICM was related to the known large variations in TE and ICM morphology in human blastocysts. A senior embryologist graded the ICM and TE morphology of each embryo at the time of imaging using the standard grading system described by Schoolcraft et al. (Schoolcraft et al., 1999). Briefly, an ICM with many, compacted cells are considered to be grade A, if it has several cells and they are loosely grouped, it is grade B, whereas if it contains very few cells, it is considered grade C. For the TE, a score A is assigned if the blastocyst has many cells that form a cohesive epithelium, if it has fewer cells, then it is graded as B, and if the TE has very few, large cells it is given a grade of C. These embryos then were divided into five categories: 16 embryos from 12 patients with grade AA, 32 from 32 patients with grade AB, 12 from 12 patients with BA, 55 from 48 patients with BB and 98 from 79 patients were categorized as other (any with C). The first and second letter corresponds to the ICM and TE grade, respectively. None of the FLIM parameters showed significant differences between morphological groups (FDR $p > 0.05$) (Figure 2F). Thus, the embryo-to-embryo differences in FLIM of TE and ICM is not associated with variations in TE and ICM morphology.

Temporal variations of human blastocysts metabolic state

Blastocyst stage: To further study the metabolic shifts observed during blastocyst development, we explored the relationship between FLIM parameters, averaged over the entire embryo at a single timepoint, and embryo stage. A senior embryologist assigned each human discarded blastocyst to one of four stages (Figure 3A): early blastocysts ($n=25$ embryos from 25 patients), expanded blastocyst ($n=56$ from 45 patients), hatching blastocyst ($n=101$ from 74 patients), and fully hatched blastocyst ($n=31$ from 29 patients). We computed the percentage relative to early blastocyst for each FLIM parameter and stage. FAD+ fraction engaged, FAD+ long lifetime, FAD+ short lifetime, and redox ratio all exhibited significant variations (FDR $p < 0.001$), with the largest occurring for hatching and fully hatched blastocysts (Figure 3B). We next investigated the potential existence of subtle changes in FLIM parameters during blastocysts expansion by testing for correlations between the diameter of early and expanding blastocysts with FLIM parameters. There were no significant correlations between these metabolic profiles and the diameter of the blastocysts (FDR $p > 0.05$). Thus, the largest changes in FLIM parameters are associated with the process of blastocyst hatching.

To better understand the metabolic variations associated with hatching, we examined the differences in FLIM parameters between the portions of TE inside the zona pellucida compared to those outside. We analysed 36 hatching blastocysts from our cohort that had a substantial area both inside and outside the zona pellucida (Figure 3C). We computed the ratio of FLIM parameters

between the TE portion of the blastocyst inside and outside the zona pellucida. NAD(P)H intensity (FDR $p < 0.02$), fraction engaged (FDR $p < 0.02$), NAD(P)H long (FDR $p < 0.03$) and short lifetime (FDR $p < 0.03$), FAD+ fraction engaged (FDR $p = 0.03$), FAD+ short lifetime (FDR $p = 0.04$), and the redox ratio (FDR $p = 0.02$), all exhibit significant differences between the TE portion of the blastocyst inside and outside the zona pellucida (Figure 3D).

Day of development since fertilization: The discarded human blastocysts we studied were vitrified at different periods of time after fertilization, the majority either on day 5 ($n = 98$ embryos from 71 patients) or on day 6 ($n = 111$ from 77 patients). We used multilevel models to compare FLIM parameters of day 5 and day 6 blastocysts. We found significant variations in NAD(P)H intensity (FDR $p = 0.002$), FAD+ intensity (FDR $p = 0.01$), FAD+ fraction engaged, FAD+ long and short lifetime, and redox ratio (FDR $p < 0.0002$). The separation was so strong that a support vector machine generated hyperplane based on just three FLIM parameters gave predictions of whether an embryo was day 5 or day 6 with an accuracy of 77% (Figure 3E).

Embryos develop to later stages over time, so, it would be possible that differences in FLIM parameters between day 5 and day 6 embryos might be due to embryos being at different developmental stages on these days. To investigate this, we explored the conditional dependencies between the day of embryo development since fertilization, stage of expansion and the FLIM parameters that were significantly associated with both of those (FAD+ fraction engaged, FAD+ long lifetime, FAD+ short lifetime and redox ratio). We began by investigating FAD+ short lifetime. Subdividing the embryos into two different stage categories (early/expanded or hatching/hatched) on both day 5 and day 6 demonstrates that day and stage both impact FAD+ short lifetime (Figure 4F). Upon conditioning on stage of expansion, the partial correlation between day of embryo development and FAD+ short lifetime, (day, FAD+ short lifetime | stage), is 0.53 ($p < 0.0001$). Upon condition on day of embryo development, the partial correlation between embryo stage of expansion and FAD+ short lifetime, (stage, FAD+ short lifetime | day), is 0.39 ($p < 0.0001$). Thus, expansion stage and day of embryo development are both associated with FAD+ short lifetime. Furthermore, day of embryo development and expansion stage are correlated with a coefficient of 0.46 ($p < 0.00001$), after conditioning on FLIM parameters. These conditional dependencies can be represented by a directed acyclic graph (DAG), which shows that day of embryo development, expansion stage and FAD+ short lifetime all depend on each other (Figure 3G). Similar results held for the other FLIM parameters (SI 3).

Metabolic variance between human blastocysts, between patients and between images

Embryo day of development and expansion stage are two factors which lead to differences in metabolism between different human preimplantation embryos. There are presumably other factors that also contributed to these differences. Some of these factors may cause differences in metabolism between embryos from different patients, whereas other factors may cause differences in metabolism between different embryos from the same patient. Indeed, plotting FLIM measurements from different embryos from the same patient often leads to a clear separation between embryos (Figure 4A). In contrast, plotting FLIM parameters from embryos from different patients often produces substantial overlap (Figure 4B). Thus, factors that produce differences in metabolism between embryos from different patients appear to be more subtle than the factors that

produce variations between embryos from one patient. To more systematically quantify these effects, we used multilevel models (Snijders and Bosker, 2011; Lorah, 2018) to determine the residual variance in FLIM parameters explained by three levels: the differences between patients, between embryos from the same patient, and between images taken at different Z positions of the same embryo (Figure 4C). The residual variances of FLIM parameters for each level were significantly different than 0 (FDR $p > 0.05$), except for the variance of NADH Long Lifetime and FAD+ fraction engaged between patients. For the fluorescence lifetimes, the fractions engaged, and the redox ratio, the variance associated with differences between patients and between different Z positions were smaller than the variances associated with differences between embryos from the same patient.

We next investigated factors that might lead to the differences in FLIM parameters associated with these different levels (Figure 4D). Over 70% of the variance in NAD(P)H intensity and over 50% of the variance in FAD+ intensity between different Z positions of the same embryo can be explained by a combination of imaging depth and the proportion of photons coming from the ICM vs TE. Surprisingly, we found no association between FLIM parameters of blastocysts and maternal age at oocyte retrieval, patient body mass index (BMI), or levels of anti-Mullerian hormone (FDR $p > 0.05$), all of which are known to be associated with successful IVF outcome (Schoolcraft et al., 1999; Moragianni et al., 2012; Cimadomo et al., 2018). Differences in FLIM parameters between patients were largely explained by differences in day of embryo development and expansion stage: after controlling for these two factors, NAD(P)H fraction engaged was the only FLIM parameter with statistically significant variance at the patient level. In contrast, there was still substantial variance in FLIM parameters between embryos from the same patient, even after controlling for day of embryo development, expansion stage, imaging depth, and the proportion of photons coming from the ICM vs TE. Thus, there are metabolic differences between embryos from the same patient which cannot be accounted for by these factors, and FLIM is sensitive enough to detect these metabolic differences.

Metabolic variations during human blastocyst expansion and hatching

The single time point FLIM measurements described above entail minimal exposure of the embryos to laser illumination and can be rapidly acquired, allowing us to obtain data on a large number of blastocysts. However, these measurements only provide information on the metabolic state of each blastocyst at one single instance in time. We next investigated the evolution of individual human blastocysts by performing continual time-lapse FLIM imaging.

To study the dynamic changes in metabolism during the expansion and hatching of preimplantation embryos, we performed time-lapse imaging of NAD(P)H (Figure 5A), FAD+ (Figure 5B, grey) and SHG (Figure 5B, magenta) (Movie S2) of 10 morphologically normal human blastocysts from 10 different patients. We acquired three Z planes for each channel every two hours, over a 36-hour period. To visualize the variations in metabolism of human blastocysts during development, we calculated the average photon arrival time of the segmented regions for both NAD(P)H (Figure 5C) and FAD+ (Figure 5D). Both signals showed complex spatial patterns which evolved over time as the embryos progressed through development. The FLIM parameters showed continual metabolic variations over time during blastocyst development, with some parameters increasing and some decreasing as the embryos progressed past the early blastocyst stage (Figure 5E).

The continual changes in FLIM parameters we observed with time-lapse imaging might reflect the endogenous evolution of blastocyst's metabolism or, alternatively, might be caused by artifacts due to the imaging procedure itself. To differentiate between these possibilities, we compared the results from time-lapse microscopy, in which embryos were on the microscopy and imaged for 36 hours, to the results from the single time point FLIM measurements described above, in which each embryo was only subject to a single measurement. The differences between day 5 and day 6 embryos in the single time-point measurements provides a proxy for the endogenous evolution of blastocysts over 24 hours, which we compared to the changes observed in time-lapse over a 24-hour period (Figure SI 4A). NAD(P)H long lifetime, NAD(P)H short lifetime, and FAD+ irradiance, long lifetime, and short lifetime, exhibited statistically indistinguishable ($FDR > 0.05$) changes in both single timepoint and time-lapse imaging, arguing that these are due to the endogenous evolution of blastocyst's metabolism. However, NAD(P)H irradiance, NAD(P)H fraction engaged, and the redox ratio displayed significant differences ($FDR p < 0.05$), suggesting that these FLIM parameters are altered by the time-lapse imaging procedure. There are two possibilities, subtle metabolic changes could either be induced by light exposure during FLIM measurements or by the blastocysts being on the microscope stage for an extended period (instead of being in a standard incubator). To differentiate between these possibilities, we cultured seven human blastocysts on the microscope stage for 36 hours subject only to individual FLIM measurements before and after the incubation period. We compared these blastocysts which were not exposed to FLIM measurements during incubation to ten human blastocysts that were subjected to FLIM measurements every two hours for the 36-hour incubation time. All FLIM parameters were statistically indistinguishable between the not exposed and the illuminated blastocysts ($FDR p > 0.05$, SI 4B) and both sets of embryos progressed through development, as assessed by a senior embryologist. Thus, we conclude that light exposure during FLIM measurements (at the level investigated here) does not induce significant changes in FLIM parameters, but culturing blastocysts on the microscope stage for extended periods can cause subtle changes in embryo metabolism. Furthermore, there are continual, endogenous changes in blastocyst's metabolism that take place over the course of development.

Discussion

In this study, we explored the use of FLIM of NAD(P)H and FAD+ for measuring the metabolic state of human blastocysts. First, we studied 215 human blastocysts at a single time point, two hours after thawing. We found that the metabolic state of these blastocysts varies based on both their time since fertilization and developmental stage. We also observed distinct metabolic states between cells in the ICM and the TE, and between cells inside and outside the zona pellucida. Using multilevel modeling of this data, we demonstrated that FLIM is sensitive enough to detect metabolic variations in individual blastocysts from the same patient and variations between patients. We next investigated the dynamics of blastocyst's metabolism using time-lapse FLIM imaging and found that the metabolic state of individual blastocysts change continuously over time.

Impaired metabolic activity results in decreased developmental capacity in oocytes and embryos, both in mouse (Wakefield et al., 2011; Harvey, 2019) and human (Wilding et al., 2001; Harvey, 2019).

To this end, several reports have focused on detecting metabolic biomarkers of embryo quality (Gardner and Leese, 1987; Brison et al., 2004; Dumollard et al., 2007; Vergouw et al., 2008; Heikal, 2010; Gardner et al., 2011; Gardner and Harvey, 2015; Harvey, 2019). In this study, we have demonstrated the use of FLIM imaging to detect the metabolic state of human discarded blastocysts. We observed that combining FLIM with SHG imaging (Campagnola and Loew, 2003; Hsieh et al., 2008; Yu et al., 2014) provides information on a range of cellular and subcellular structures in human blastocysts, including mitochondrial localization and physiology, spindle dynamics and mitotic divisions. Taken together, these results demonstrate that FLIM and SHG imaging can be used to obtain quantitative, non-invasive and biologically relevant information on live human blastocysts.

Metabolic shifts from the morula to the blastocyst stage have been described previously (Gardner et al., 2001; Leese, 2012, 2015; Thompson et al., 2016), including changes in redox state, and increasing levels of glucose uptake, oxygen consumption and lactate production (Houghton et al., 1996; Trimarchi et al., 2000; Harvey et al., 2002; Gardner, 2015). Our results extend these prior reports by showing continuous variations in metabolic state during human blastocyst development from the early blastocyst to hatching stages. These results are in line with previously reported dynamic changes in embryo metabolism throughout development (Leese, 2002; Gardner and Harvey, 2015; Thompson et al., 2016). In contrast with previous reports (Pais et al., 2020), we observed highly significantly different metabolic states in human blastocysts at day 5 vs day 6 post fertilization. Human embryos develop at different rates, and our results show that only a fraction of the metabolic differences between blastocysts at different days post fertilization can be explained by embryos tending to be at later developmental stages at later times. This implies an association between embryo developmental rate and metabolism, as has also been seen by other approaches (Leese, 2002; Gardner et al., 2011; Santos Monteiro et al., 2021). Taken together, these observations argue that the metabolism of human blastocysts are highly dynamic and flexible. It is an exciting future challenge to unravel the mechanistic basis of these metabolic variations in human embryos.

Our single timepoint measurements showing different metabolic state of cells in the ICM and TE are consistent with prior work indicating that they contain distinct mitochondrial physiology and function (Hewitson and Leese, 1993; Houghton, 2006; Van Blerkom, 2011; Gardner and Harvey, 2015). Thus, FLIM is sensitive enough to detect physiologically relevant changes in metabolism in human blastocysts, as has been previously seen for differentiation in *Caenorhabditis elegans* (Stringari et al., 2011) and mouse neuronal development (Stringari et al., 2012). We also observed differences in the metabolic state of trophoctoderm cells inside and outside of the zona pellucida during hatching. To our knowledge, this has not been reported previously. There seem to be two possibilities: 1) these metabolic differences may reflect differing microenvironments. Perhaps the increase in lactate production, release and associated pH change in the surroundings, observed during hatching (Gardner, 2015), results from the different energy expenditure needed of TE cells inside vs outside the zona pellucida; or reflects embryo plasticity to adapt to the culture media (de Lima et al., 2020)?; 2) the hatching process itself may also lead to metabolic changes, either due to specific signaling pathways or a general response to associated stresses (Brison et al., 2004). Future studies are planned to understand the nature of these variations.

In addition, by analyzing our data using multilevel modeling (Snijders and Bosker, 2011; Lorah, 2018), we found that blastocysts from the same patient have significantly different metabolic states. While some of this variation can be accounted for by time post fertilization and stage of development, a substantial variance between embryos remains even after accounting for these factors. It is unclear what causes these additional variations in metabolism between embryos. One possibility is that metabolism adjusts to respond to cellular or DNA damage, which are prevalent in preimplantation human embryos (Leese, 2002; Baumann et al., 2007; Sturmey et al., 2008). This provides an attractive explanation for the previously observed associations between blastocyst metabolism and viability (Gardner and Leese, 1987; Van Blerkom et al., 1995; Gardner et al., 2011). However, while embryo morphological scores are also associated with viability (Conaghan et al., 1993; Schoolcraft et al., 1999; Racowsky et al., 2003; Ahlström et al., 2011), we found no association between embryo metabolic state and morphological scores. This implies that multiple distinct processes impact embryo viability, some of which are associated with metabolism and others of which are associated with morphology. It will be of both fundamental interest and potential clinical import for future work to disentangle the contribution of specific pathways to embryo viability. Furthermore, the lack of association between metabolic state and morphology scores suggests that FLIM might provide synergistic information with conventional microscopy to aid in selecting the highest quality embryo for transfer in Assisted Reproductive Technologies (ART).

We found that FLIM illumination exposure during imaging did not induce significant changes in FLIM parameters but, culturing blastocysts on a FLIM microscope stage for extended periods can cause subtle variations in embryo metabolism. Thus, the on-stage microscope incubator and conventional incubator used in this study are not identical, though embryos successfully developed in both incubators. This highlights the need to critically evaluate the impact of on-stage microscope incubators, as has been previously pointed out in the context of conventional time-lapse imaging of embryos (Racowsky and Martins, 2017).

The present study demonstrates that FLIM is sensitive enough to detect endogenous variations in the metabolism of discarded human blastocysts, which suggests its promise as a research tool and as a potential means to aid in embryo selection. Before FLIM is used on human embryos that will be transferred back to patients, it will be crucial to perform extensive additional safety studies. Prior work has shown that FLIM imaging does not appear to disrupt the development or viability of mouse embryos (Sanchez et al., 2018; Seidler et al., 2020) and mouse embryos exposed to FLIM illumination do not show higher rates of reactive oxygen species than non-illuminated control (Sanchez et al., 2018). However, the results of safety studies in mice do not necessarily generalize to humans, so further studies focused on determining the impact of FLIM on human embryos are required.

There are also limitations to this study. First, the human blastocyst analysed were vitrified, thawed, and warmed for two hours prior to FLIM imaging. Whether vitrification causes metabolic distress in human blastocysts remains unknown, even though its clinical success has been well documented (Rienzi et al., 2017). In addition, it does not seem to alter mitochondrial potential or intracellular reactive oxygen species (Nohales-Córcoles et al., 2016). Additionally, the blastocysts used in this study were discarded material, and include both euploid and aneuploid embryos. Our

preliminary analysis indicates some associations between embryo metabolic state and ploidy(Shah et al., 2020), which will be reported on in a subsequent manuscript. Future studies should focus on addressing this important subject in more detail. Surprisingly, we did not observe a correlation between blastocyst metabolic state and maternal age or BMI, each of which have long been linked with embryo quality(Schoolcraft et al., 1999; Moragianni et al., 2012) and mitochondrial function(Leary et al., 2015; Morimoto et al., 2020). This result must be interpreted with caution as it may reflect a selection bias in the material used in this study: we only imaged embryos that were discarded, yet also reached the blastocyst stage. A clinical study using non-discarded embryos of all preimplantation developmental stages would provide a more complete view of the effect of maternal characteristics on embryo metabolic state. Finally, recent work has established a framework to relate FLIM parameters in oocytes to mitochondrial metabolic fluxes(Yang et al., 2021), but additional work is required to determine if this is applicable to the later stage embryos studied here.

In summary, non-invasive metabolic imaging via FLIM is a promising tool for quantitatively characterizing the metabolic state of human blastocysts. FLIM can sensitively detected metabolic variations associated with blastocyst development over 36h, the time post fertilization and blastocyst developmental stage. FLIM revealed differences in metabolic state between cells in the ICM and the TE, and between TE cells inside and outside the zona pellucida. The lack of an association between the metabolic state of human blastocyst and their morphological grading indicates that these two assessments may provide synergistic information to improve blastocyst selection. However, future work is required to determine the extent to which FLIM measurements are associated with the probability that a transferred human blastocyst will lead to a live birth.

Acknowledgments

We would like to acknowledge Becker and Hickl GmbH and Boston Electronics for the loaning of electronic equipment for this research. We also acknowledge the Boston IVF embryologists and clinicians for their assistance during the project, in particular Dr. Emily Seidler and Dr. Alan Penzias and the Needleman lab, at Harvard University especially Brian Leahy, PhD, for useful advice.

Author Contributions

M.V. contributed to the conceptualization of the idea of the experiment, contributed to data acquisition, analysis, and interpretation, and drafted the manuscript. J.S. contributed to data acquisition and critical revision of the manuscript. X.Y. contributed to data analysis and interpretation of the results and critical revision of the manuscript. T.S. contributed to the conceptualization of the idea of the experiment and critical revision of the manuscript. W.C. contributed to data analysis and critical revision of the manuscript. D.S. contributed to the conceptualization of the idea of the experiment and interpretation of the results and critical revision of the manuscript. D.J.N. contributed to the conceptualization of the idea of the experiment and interpretation of the results and critical revision of the manuscript.

Funding

Supported by the Blavatnik Biomedical Accelerator Grant at Harvard University. Becker and Hickl GmbH and Boston Electronics sponsored research with the loaning of equipment for FLIM.

Conflict of interest

DJN is an inventor on patent US20170039415A1.

References

- Ahlström A, Westin C, Reisner E, Wikland M, Hardarson T. Trophectoderm morphology: an important parameter for predicting live birth after single blastocyst transfer. *Human Reproduction* 2011;26:3289–3296.
- Ahlström A, Westin C, Wikland M, Hardarson T. Prediction of live birth in frozen–thawed single blastocyst transfer cycles by pre-freeze and post-thaw morphology. *Human Reproduction* 2013;28:1199–1209.
- Alm H, Torner H, Löhrike B, Viergutz T, Ghoneim IM, Kanitz W. Bovine blastocyst development rate in vitro is influenced by selection of oocytes by brilliant cresyl blue staining before IVM as indicator for glucose-6-phosphate dehydrogenase activity. *Theriogenology* 2005;63:2194–2205.
- Al-Zubaidi U, Liu J, Cinar O, Robker RL, Adhikari D, Carroll J. The spatio-temporal dynamics of mitochondrial membrane potential during oocyte maturation. *Mol Hum Reprod* 2019;25:695–705.
- Baumann CG, Morris DG, Sreenan JM, Leese HJ. The quiet embryo hypothesis: molecular characteristics favoring viability. *Mol Reprod Dev* 2007;74:1345–1353.
- Becker W. *Advanced Time-Correlated Single Photon Counting Techniques*. 2005; Available from: <https://link.springer.com/book/10.1007/3-540-28882-1>.
- Becker W. Fluorescence lifetime imaging--techniques and applications. *J Microsc* 2012;247:119–136.
- Berg S, Kutra D, Kroeger T, Straehle CN, Kausler BX, Haubold C, Schiegg M, Ales J, Beier T, Rudy M, et al. ilastik: interactive machine learning for (bio)image analysis. *Nat Methods* 2019;16:1226–1232.
- Brisson DR, Houghton FD, Falconer D, Roberts SA, Hawkhead J, Humpherson PG, Lieberman BA, Leese HJ. Identification of viable embryos in IVF by non-invasive measurement of amino acid turnover. *Hum Reprod* 2004;19:2319–2324.
- Campagnola PJ, Loew LM. Second-harmonic imaging microscopy for visualizing biomolecular arrays in cells, tissues and organisms. *Nat Biotechnol* 2003;21:1356–1360.
- Chi F, Sharpley MS, Nagaraj R, Roy SS, Banerjee U. Glycolysis-Independent Glucose Metabolism Distinguishes TE from ICM Fate during Mammalian Embryogenesis. *Dev Cell* 2020;53:9-26.e4.
- Cimadomo D, Fabozzi G, Vaiarelli A, Ubaldi N, Ubaldi FM, Rienzi L. Impact of Maternal Age on Oocyte and Embryo Competence. *Front Endocrinol (Lausanne)* [Internet] 2018;9:.
- Cinco R, Digman MA, Gratton E, Luderer U. Spatial Characterization of Bioenergetics and Metabolism of Primordial to Preovulatory Follicles in Whole Ex Vivo Murine Ovary. *Biol Reprod* [Internet] 2016;95:.
- Conaghan J, Hardy K, Handyside AH, Winston RM, Leese HJ. Selection criteria for human embryo transfer: a comparison of pyruvate uptake and morphology. *J Assist Reprod Genet* 1993;10:21–30.
- Coticchio G, Mignini Renzini M, Novara PV, Lain M, De Ponti E, Turchi D, Fadini R, Dal Canto M. Focused time-lapse analysis reveals novel aspects of human fertilization and suggests new parameters of embryo viability. *Hum Reprod* 2018;33:23–31.
- Cristianini N, Shawe-Taylor J. *An introduction to support Vector Machines: and other kernel-based learning methods*. 1999; Cambridge University Press: USA.
- Dumollard R, Carroll J, Duchon MR, Campbell K, Swann K. Mitochondrial function and redox state in mammalian embryos. *Semin Cell Dev Biol* 2009;20:346–353.
- Dumollard R, Marangos P, Fitzharris G, Swann K, Duchon M, Carroll J. Sperm-triggered [Ca²⁺] oscillations and Ca²⁺ homeostasis in the mouse egg have an absolute requirement for mitochondrial ATP production. *Development* 2004;131:3057–3067.
- Dumollard R, Ward Z, Carroll J, Duchon MR. Regulation of redox metabolism in the mouse oocyte and embryo. *Development* 2007;134:455–465.
- Gardner DK. Lactate production by the mammalian blastocyst: Manipulating the microenvironment for uterine implantation and invasion? *Bioessays* 2015;37:364–371.
- Gardner DK, Harvey AJ. Blastocyst metabolism. *Reprod Fertil Dev* 2015;27:638–654.
- Gardner DK, Lane M, Stevens J, Schlenker T, Schoolcraft WB. Blastocyst score affects implantation and pregnancy outcome: towards a single blastocyst transfer. *Fertil Steril* 2000;73:1155–1158.
- Gardner DK, Lane M, Stevens J, Schoolcraft WB. Noninvasive assessment of human embryo nutrient consumption as a measure of developmental potential. *Fertil Steril* 2001;76:1175–1180.
- Gardner DK, Leese HJ. Assessment of embryo viability prior to transfer by the noninvasive measurement of glucose uptake. *J Exp Zool* 1987;242:103–105.
- Gardner DK, Wale PL, Collins R, Lane M. Glucose consumption of single post-compaction human embryos is predictive of embryo sex and live birth outcome. *Hum Reprod* 2011;26:1981–1986.
- Gerris J, De Sutter P, De Neubourg D, Van Royen E, Vander Elst J, Mangelschots K, Vercruyssen M, Kok P, Elseviers M, Annemans L, et al. A real-life prospective health economic study of elective single embryo transfer versus two-embryo transfer in first IVF/ICSI cycles. *Hum Reprod* 2004;19:917–923.
- Ghukasyan VV, Heikal AA. *Natural Biomarkers for Cellular Metabolism: Biology, Techniques, and Applications*. 2014; CRC Press.
- Hardarson T, Ahlström A, Rogberg L, Botros L, Hillensjö T, Westlander G, Sakkas D, Wikland M. Non-invasive metabolomic profiling of Day 2 and 5 embryo culture medium: a prospective randomized trial. *Hum Reprod* 2012;27:89–96.

- Harvey AJ. Mitochondria in early development: linking the microenvironment, metabolism and the epigenome. *Reproduction* 2019;157:R159–R179.
- Harvey AJ, Kind KL, Thompson JG. REDOX regulation of early embryo development. *Reproduction* 2002;123:479–486.
- Heikal AA. Intracellular coenzymes as natural biomarkers for metabolic activities and mitochondrial anomalies. *Biomark Med* 2010;4:241–263.
- Hewitson LC, Leese HJ. Energy metabolism of the trophectoderm and inner cell mass of the mouse blastocyst. *J Exp Zool* 1993;267:337–343.
- Houghton FD. Energy metabolism of the inner cell mass and trophectoderm of the mouse blastocyst. *Differentiation* 2006;74:11–18.
- Houghton FD, Thompson JG, Kennedy CJ, Leese HJ. Oxygen consumption and energy metabolism of the early mouse embryo. *Mol Reprod Dev* 1996;44:476–485.
- Hsieh C-S, Chen S-U, Lee Y-W, Yang Y-S, Sun C-K. Higher harmonic generation microscopy of in vitro cultured mammal oocytes and embryos. *Opt Express* 2008;16:11574–11588.
- Jones GM, Trounson AO, Vella PJ, Thouas GA, Lolatgis N, Wood C. Glucose metabolism of human morula and blastocyst-stage embryos and its relationship to viability after transfer. *Reprod Biomed Online* 2001;3:124–132.
- Klaidman LK, Leung AC, Adams JD. High-performance liquid chromatography analysis of oxidized and reduced pyridine dinucleotides in specific brain regions. *Anal Biochem* 1995;228:312–317.
- Leary C, Leese HJ, Sturmev RG. Human embryos from overweight and obese women display phenotypic and metabolic abnormalities. *Human Reproduction* 2015;30:122–132.
- Leese HJ. Quiet please, do not disturb: a hypothesis of embryo metabolism and viability. *BioEssays* 2002;24:845–849.
- Leese HJ. Metabolism of the preimplantation embryo: 40 years on. *Reproduction* 2012;143:417–427.
- Leese HJ. History of oocyte and embryo metabolism. *Reprod Fertil Dev* 2015;27:567–571.
- Lima CB de, Santos ÉC dos, Ispada J, Fontes PK, Nogueira MFG, Santos CMD dos, Milazzotto MP. The dynamics between in vitro culture and metabolism: embryonic adaptation to environmental changes. *Sci Rep* 2020;10:15672.
- Lopes AS, Lane M, Thompson JG. Oxygen consumption and ROS production are increased at the time of fertilization and cell cleavage in bovine zygotes. *Hum Reprod* 2010;25:2762–2773.
- Lorah J. Effect size measures for multilevel models: definition, interpretation, and TIMSS example. *Large-scale Assessments in Education* 2018;6:8.
- Ma N, Mochele NR de, Pham PD, Yoo TY, Cho K WY, Digman MA. Label-free assessment of pre-implantation embryo quality by the Fluorescence Lifetime Imaging Microscopy (FLIM)-phasor approach. *Sci Rep* 2019;9:13206.
- Mertz J. Introduction to Optical Microscopy. Higher Education from Cambridge University Press [Internet] 2019; Cambridge University Press Available from: <https://www.cambridge.org/highereducation/books/introduction-to-optical-microscopy/F6C6318C87732519D7E07BA7A03F0B81>.
- Moragianni VA, Jones S-ML, Ryley DA. The effect of body mass index on the outcomes of first assisted reproductive technology cycles. *Fertil Steril* 2012;98:102–108.
- Morimoto N, Hashimoto S, Yamanaka M, Nakano T, Satoh M, Nakaoka Y, Iwata H, Fukui A, Morimoto Y, Shibahara H. Mitochondrial oxygen consumption rate of human embryos declines with maternal age. *J Assist Reprod Genet* 2020;37:1815–1821.
- Munné S, Kaplan B, Frattarelli JL, Child T, Nakhuda G, Shamma FN, Silverberg K, Kalista T, Handyside AH, Katz-Jaffe M, et al. Preimplantation genetic testing for aneuploidy versus morphology as selection criteria for single frozen-thawed embryo transfer in good-prognosis patients: a multicenter randomized clinical trial. *Fertility and Sterility* 2019;112:1071–1079.e7.
- Neapolitan RE. Probabilistic Methods for Bioinformatics. 2009; Available from: <https://www.elsevier.com/books/probabilistic-methods-for-bioinformatics/neapolitan/978-0-12-370476-4>.
- Nohales-Córcoles M, Sevillano-Almerich G, Di Emidio G, Tatone C, Cobo AC, Dumollard R, De Los Santos Molina MJ. Impact of vitrification on the mitochondrial activity and redox homeostasis of human oocyte. *Hum Reprod* 2016;31:1850–1858.
- Pais RJ, Sharara F, Zmuidinaite R, Butler S, Keshavarz S, Iles R. Bioinformatic identification of euploid and aneuploid embryo secretome signatures in IVF culture media based on MALDI-ToF mass spectrometry. *J Assist Reprod Genet* 2020;37:2189–2198.
- Patrizio P, Shoham G, Shoham Z, Leong M, Barad DH, Gleicher N. Worldwide live births following the transfer of chromosomally “Abnormal” embryos after PGT/A: results of a worldwide web-based survey. *J Assist Reprod Genet* 2019;36:1599–1607.
- Pearl J. Causal Inference in Statistics: A Primer. Wiley.com [Internet] 2016; Available from: <https://www.wiley.com/en-us/Causal+Inference+in+Statistics%3A+A+Primer-p-9781119186847>.
- Penzias A, Bendikson K, Butts S, Coutifaris C, Falcone T, Fossom G, Gitlin S, Gracia C, Hansen K, La Barbera A, et al. The use of preimplantation genetic testing for aneuploidy (PGT-A): a committee opinion. *Fertility and Sterility* 2018;109:429–436.
- Racowsky C, Combelles CMH, Nureddin A, Pan Y, Finn A, Miles L, Gale S, O’Leary T, Jackson KV. Day 3 and day 5 morphological predictors of embryo viability. *Reprod Biomed Online* 2003;6:323–331.
- Racowsky C, Martins WP. Effectiveness and safety of time-lapse imaging for embryo culture and selection: it is still too early for any conclusions? *Fertil Steril* 2017;108:450–452.
- Rienzi L, Gracia C, Maggiulli R, LaBarbera AR, Kaser DJ, Ubaldi FM, Vanderpoel S, Racowsky C. Oocyte, embryo and blastocyst cryopreservation in ART: systematic review and meta-analysis comparing slow-freezing versus vitrification to produce evidence for the development of global guidance. *Hum Reprod Update* 2017;23:139–155.
- Saha B, Ganguly A, Home P, Bhattacharya B, Ray S, Ghosh A, Rumi MAK, Marsh C, French VA, Gunewardena S, et al. TEAD4 ensures postimplantation development by promoting trophoblast self-renewal: An implication in early human pregnancy loss. *Proc Natl Acad Sci U S A* 2020;117:17864–17875.

- Sanchez T, Venturas M, Aghvami SA, Yang X, Fraden S, Sakkas D, Needleman DJ. Combined noninvasive metabolic and spindle imaging as potential tools for embryo and oocyte assessment. *Hum Reprod* 2019;34:2349–2361.
- Sanchez T, Wang T, Pedro MV, Zhang M, Esencan E, Sakkas D, Needleman D, Seli E. Metabolic imaging with the use of fluorescence lifetime imaging microscopy (FLIM) accurately detects mitochondrial dysfunction in mouse oocytes. *Fertil Steril* 2018;110:1387–1397.
- Santos Monteiro CA, Chow DJX, Leal GR, Tan TC, Reis Ferreira AM, Thompson JG, Dunning KR. Optical imaging of cleavage stage bovine embryos using hyperspectral and confocal approaches reveals metabolic differences between on-time and fast-developing embryos. *Theriogenology* 2021;159:60–68.
- Schoolcraft WB, Gardner DK, Lane M, Schlenker T, Hamilton F, Meldrum DR. Blastocyst culture and transfer: analysis of results and parameters affecting outcome in two in vitro fertilization programs. *Fertil Steril* 1999;72:604–609.
- Seidler EA, Sanchez T, Venturas M, Sakkas D, Needleman DJ. Non-invasive imaging of mouse embryo metabolism in response to induced hypoxia. *J Assist Reprod Genet* 2020;37:1797–1805.
- Seli E, Sakkas D, Scott R, Kwok SC, Rosendahl SM, Burns DH. Noninvasive metabolomic profiling of embryo culture media using Raman and near-infrared spectroscopy correlates with reproductive potential of embryos in women undergoing in vitro fertilization. *Fertil Steril* 2007;88:1350–1357.
- Shah JS, Venturas M, Sanchez TH, Penzias AS, Needleman D, Sakkas D. FLUORESCENCE LIFETIME IMAGING MICROSCOPY (FLIM) DETECTS DIFFERENCES IN METABOLIC SIGNATURES BETWEEN EUPLOID AND ANEUPLOID HUMAN BLASTOCYSTS. *Fertility and Sterility* 2020;114:e76–e77.
- Snijders TAB, Bosker RJ. *Multilevel Analysis: An Introduction to Basic and Advanced Multilevel Modeling*. 2011; SAGE.
- Stringari C, Cinquin A, Cinquin O, Digman MA, Donovan PJ, Gratton E. Phasor approach to fluorescence lifetime microscopy distinguishes different metabolic states of germ cells in a live tissue. *Proc Natl Acad Sci U S A* 2011;108:13582–13587.
- Stringari C, Nourse JL, Flanagan LA, Gratton E. Phasor Fluorescence Lifetime Microscopy of Free and Protein-Bound NADH Reveals Neural Stem Cell Differentiation Potential. *PLOS ONE* 2012;7:e48014. Public Library of Science.
- Sturmey RG, Brison DR, Leese HJ. Symposium: innovative techniques in human embryo viability assessment. Assessing embryo viability by measurement of amino acid turnover. *Reprod Biomed Online* 2008;17:486–496.
- Sutton-McDowall ML, Gosnell M, Anwer AG, White M, Purdey M, Abell AD, Goldys EM, Thompson JG. Hyperspectral microscopy can detect metabolic heterogeneity within bovine post-compaction embryos incubated under two oxygen concentrations (7% versus 20%). *Hum Reprod* 2017;32:2016–2025.
- Tejera A, Herrero J, Vilorio T, Romero JL, Gamiz P, Meseguer M. Time-dependent O₂ consumption patterns determined optimal time ranges for selecting viable human embryos. *Fertility and Sterility* 2012;98:849–857.e3.
- Thompson JG, Brown HM, Sutton-McDowall ML. Measuring embryo metabolism to predict embryo quality. *Reprod Fertil Dev* 2016;28:41–50.
- Tran D, Cooke S, Illingworth PJ, Gardner DK. Deep learning as a predictive tool for fetal heart pregnancy following time-lapse incubation and blastocyst transfer. *Hum Reprod* 2019;34:1011–1018.
- Trimarchi JR, Liu L, Porterfield DM, Smith PJS, Keefe DL. Oxidative Phosphorylation-Dependent and -Independent Oxygen Consumption by Individual Preimplantation Mouse Embryos¹. *Biology of Reproduction* 2000;62:1866–1874.
- Turner K, Martin KL, Woodward BJ, Lenton EA, Leese HJ. Comparison of pyruvate uptake by embryos derived from conception and non-conception natural cycles. *Hum Reprod* 1994;9:2362–2366.
- Urbanski JP, Johnson MT, Craig DD, Potter DL, Gardner DK, Thorsen T. Noninvasive Metabolic Profiling using Microfluidics for Analysis of Single Preimplantation Embryos. *Anal Chem* 2008;80:6500–6507.
- Van Blerkom J. Mitochondrial function in the human oocyte and embryo and their role in developmental competence. *Mitochondrion* 2011;11:797–813.
- Van Blerkom J, Davis PW, Lee J. ATP content of human oocytes and developmental potential and outcome after in-vitro fertilization and embryo transfer. *Hum Reprod* 1995;10:415–424.
- Vergouw CG, Botros LL, Roos P, Lens JW, Schats R, Hompes PGA, Burns DH, Lambalk CB. Metabolomic profiling by near-infrared spectroscopy as a tool to assess embryo viability: a novel, non-invasive method for embryo selection. *Hum Reprod* 2008;23:1499–1504.
- Wakefield SL, Lane M, Mitchell M. Impaired mitochondrial function in the preimplantation embryo perturbs fetal and placental development in the mouse. *Biol Reprod* 2011;84:572–580.
- Wilding M, Dale B, Marino M, Matteo L di, Alviggi C, Pisaturo ML, Lombardi L, De Placido G. Mitochondrial aggregation patterns and activity in human oocytes and preimplantation embryos. *Human Reproduction* 2001;16:909–917.
- Wong KM, Repping S, Mastenbroek S. Limitations of embryo selection methods. *Semin Reprod Med* 2014;32:127–133.
- Yang X, Ha G, Needleman DJ. A coarse-grained NADH redox model enables inference of subcellular metabolic fluxes from fluorescence lifetime imaging [Internet]. 2021;2020.11.20.392225 Available from: <https://www.biorxiv.org/content/10.1101/2020.11.20.392225v3>.
- Yu C-H, Langowitz N, Wu H-Y, Farhadifar R, Bragues J, Yoo TY, Needleman D. Measuring microtubule polarity in spindles with second-harmonic generation. *Biophys J* 2014;106:1578–1587.
- Zhu M, Zernicka-Goetz M. Living a Sweet Life: Glucose Instructs Cell Fate in the Mouse Embryo. *Dev Cell* 2020;53:1–2.

Figures and Tables

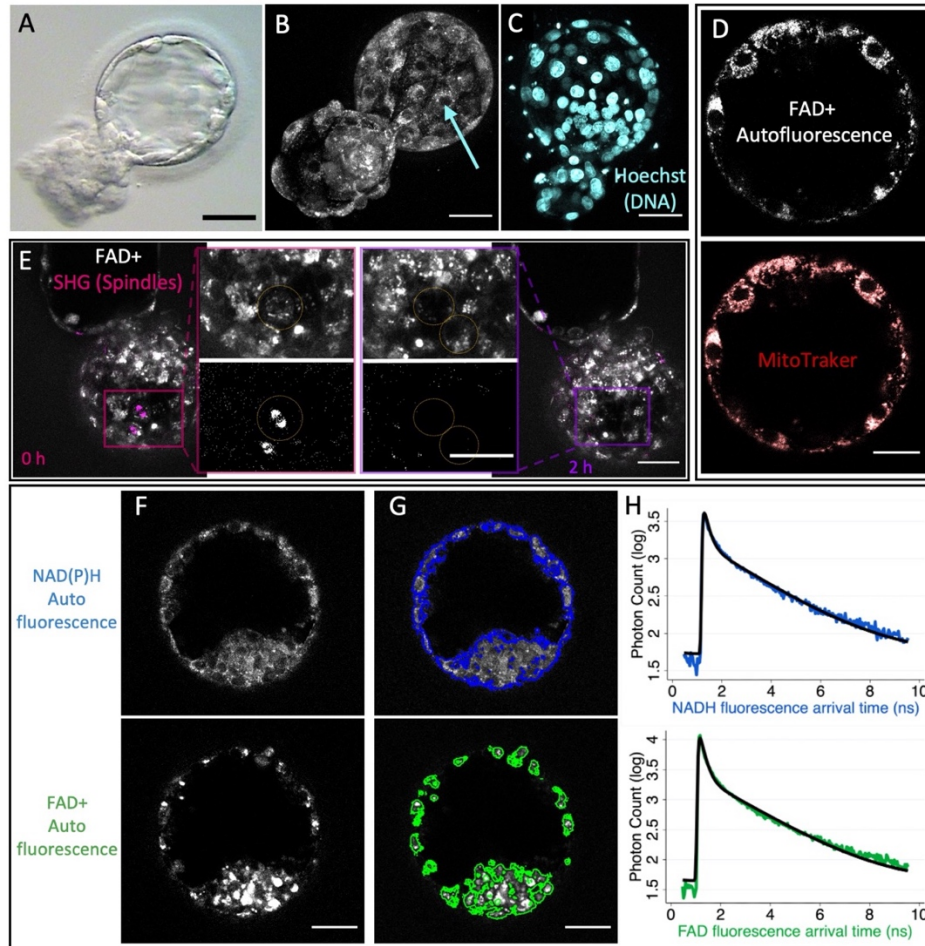


Fig 1. Two-photon fluorescence lifetime imaging microscopy (FLIM) and Second Harmonic Generation (SHG) enable visualization of cellular and subcellular structures. (A) Standard bright-field image of a human discarded blastocyst. (B) 3D reconstruction of two-photon NAD(P)H intensity images from multiple focal planes of the same blastocyst. Two-photon microscopy enables the detection of subcellular structures such as the nucleus (blue arrow). (C) 3-D reconstruction of DNA staining Hoechst showing cell nuclei. (D) Simultaneous FLIM FAD⁺ autofluorescence of a human blastocyst and mitochondria dye, MitoTracker Red CMXRos, demonstrate a high colocalization. (E) SHG spindle imaging (in magenta, false color), in combination with FLIM FAD⁺ autofluorescence imaging (in grey) enables detection of spindle formation capturing cellular mitotic divisions (also observed in Supplementary Figure 1 and Movies 1 and 2). A human blastocyst at time 0 hours with a cell in mitosis (left) showing a mitotic spindle in magenta. This cell then divides into two cells at time 2 hours (right). FLIM time-lapse imaging of the autofluorescence of NAD(P)H (F, top), and of FAD⁺ (F, bottom) of a human blastocyst. Supervised machine learning was applied to create masks to segment the fluorescence signal of NAD(P)H (G, upper) or FAD⁺ (G, lower). (H) All photon arrival times from a single embryo mask were combined to create a fluorescence decay for each fluorophore (NAD(P)H in blue and FAD⁺ in green). These curves were fitted to a two-exponential model (black curves) to obtain the quantitative parameters for characterizing the metabolic state of an embryo. Scale bars, 40 μm .

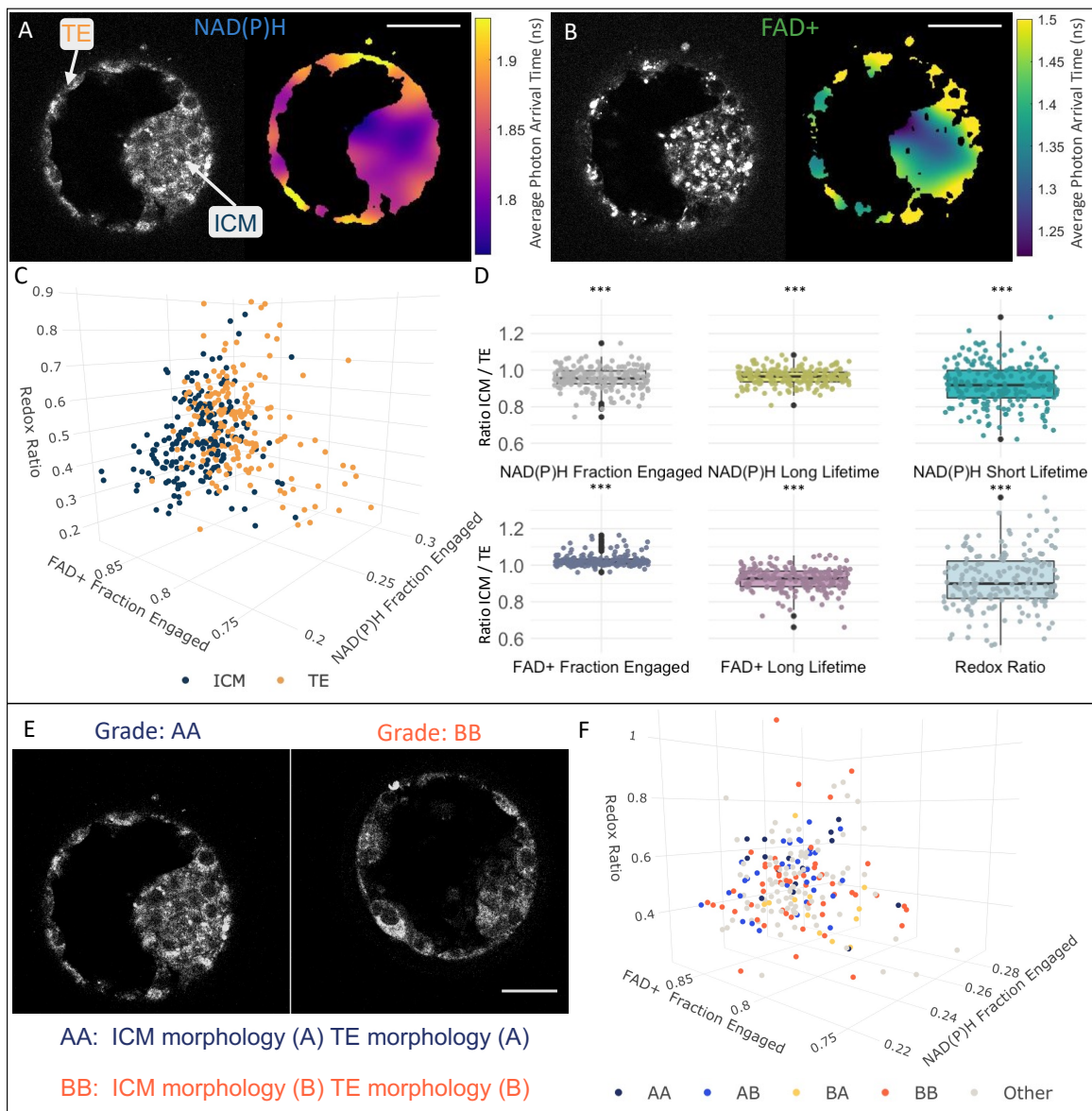


Fig. 2. Variations in metabolic signatures between inner cell mass (ICM) and trophoblast (TE) of human blastocysts. FLIM intensity image (left) and image of the average photon arrival time (right) of NAD(P)H (A) and of FAD+ (B) reveal spatial pattern of average photon arrival times, suggesting different metabolic state between the ICM and TE. Color bars show the average photon arrival times in nanoseconds. (C) FLIM parameters with the largest separation between ICM (blue) and TE (orange) were plotted in this 3D plot ($n=187$ from 125 patients, FDR $p < 0.001$). Each dot corresponds to the mean of 3Z images of the ICM or TE of single embryo. (D) Ratios of the FLIM parameters between the ICM and the TE. The box plots depict the interquartile range of the ratio, the center of the box represents the mean, the horizontal line in the box represents the median, and the vertical lines represent the 5 and 95% quartiles. Black dots represent points outside of the interquartile range. Color dots represent the average ratio per each individual embryo. ICM and TE morphology (22) of each embryo at the time of imaging.

(E) Example of NAD(P)H intensity images of two human discarded blastocysts with varying morphological grading (AA and BB). (F) FLIM parameters were compared between blastocysts of different morphological categories: AA (n=16 from 12 patients), AB (n=32 from 32 patients), BA (n=12 from 12 patients), BB (n=55 from 48 patients), and other (n=98 from 79 patients), this 3D plot shows no significant differences of metabolic signatures between embryo morphology grades (FDR $p > 0.05$). Each dot corresponds to the mean of an embryo. Scale bars, 40 μm . *** signifies FDR $p < 0.001$.

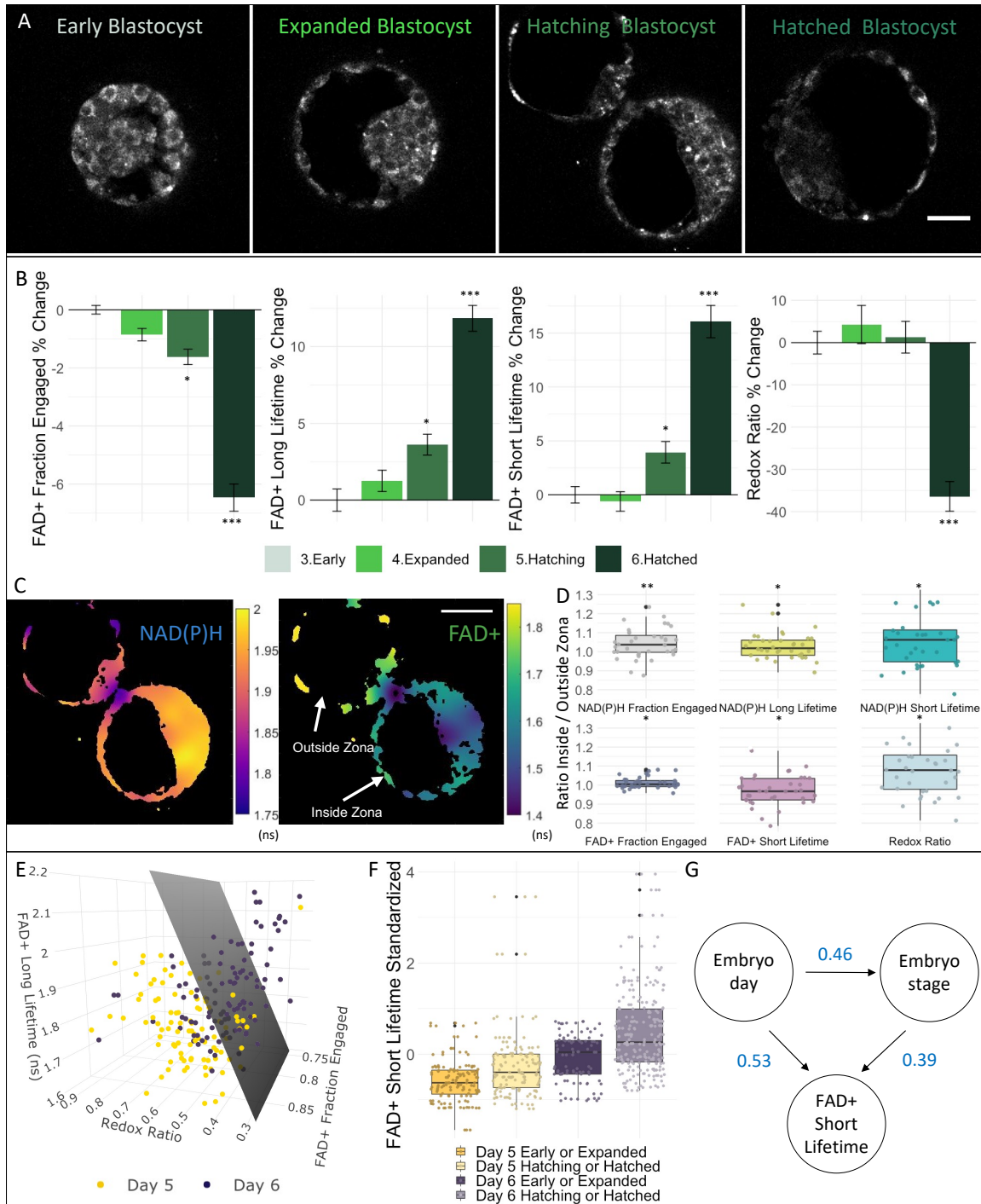


Figure 3. Human blastocyst metabolic state is associated with embryo day and embryo expansion stage. (A) NAD(P)H intensity images of four human blastocysts with varying expansion grade: early (n=25 from 25 patients), expanded (n=56 from 45 patients), hatching (n=101 from 74 patients) and hatched (n=31 from 29 patients) blastocysts. (B) Bar plots of the percentage change from early blastocysts of FAD+ fraction engaged, FAD+ long lifetime, FAD+ short lifetime and redox ratio with standard error bars displayed, showing a distinctive variation in these FLIM parameters between early and hatched blastocysts. (C) FLIM image of the photon arrival times (right) of NAD(P)H and of FAD+ (left) showing

variations in the metabolic state between the portion of the TE of a blastocyst inside and outside the zona pellucida. Color bars show the average photon arrival times in nanoseconds. (D) Of those embryos that were hatching (n=36), we computed the ratio of the FLIM parameters of the TE between the inside and outside of the zona pellucida. The box plots depict the interquartile range of the ratio, the center of the box represents the mean, the horizontal line in the box represents the median, and the vertical lines represent the 5 and 95% quartiles. Black dots represent data points outside of the interquartile range. Color dots represent the average ratio of each blastocyst. (E) FLIM parameters with largest separation between embryos of either day 5 or 6 after fertilization were plotted in a 3D plot. Each dot corresponds to the mean of a single blastocyst. Support vector machine was used to create a hyperplane that best separates day 5 (n=98 from 71 patients) and day 6 (n=111 from 77 patients) blastocysts (grey plane). (F) We subdivided the data in four categories: day 5 early/expanded (n= 47 from 41 patients), day 5 hatching/hatched (n=32 from 30 patients), day 6 early/expanded (n= 51 from 39 patients) or day 6 hatching/hatched (n=79 from 58 patients) embryos. This box plot displays the standardized FLIM FAD+ short lifetime of these four categories, showing that both day and stage impact FAD+ short lifetime. (G) DAG of FAD+ short lifetime showing that embryo day and stage are correlated and that embryo FAD+ short lifetime is dependent both on embryo day and stage. Numbers in blue represent the coefficient of the multilevel model. Scale bars, 40 μm . *** signifies FDR $p < 0.001$, **FDR $p < 0.01$ * signifies FDR $p < 0.05$.

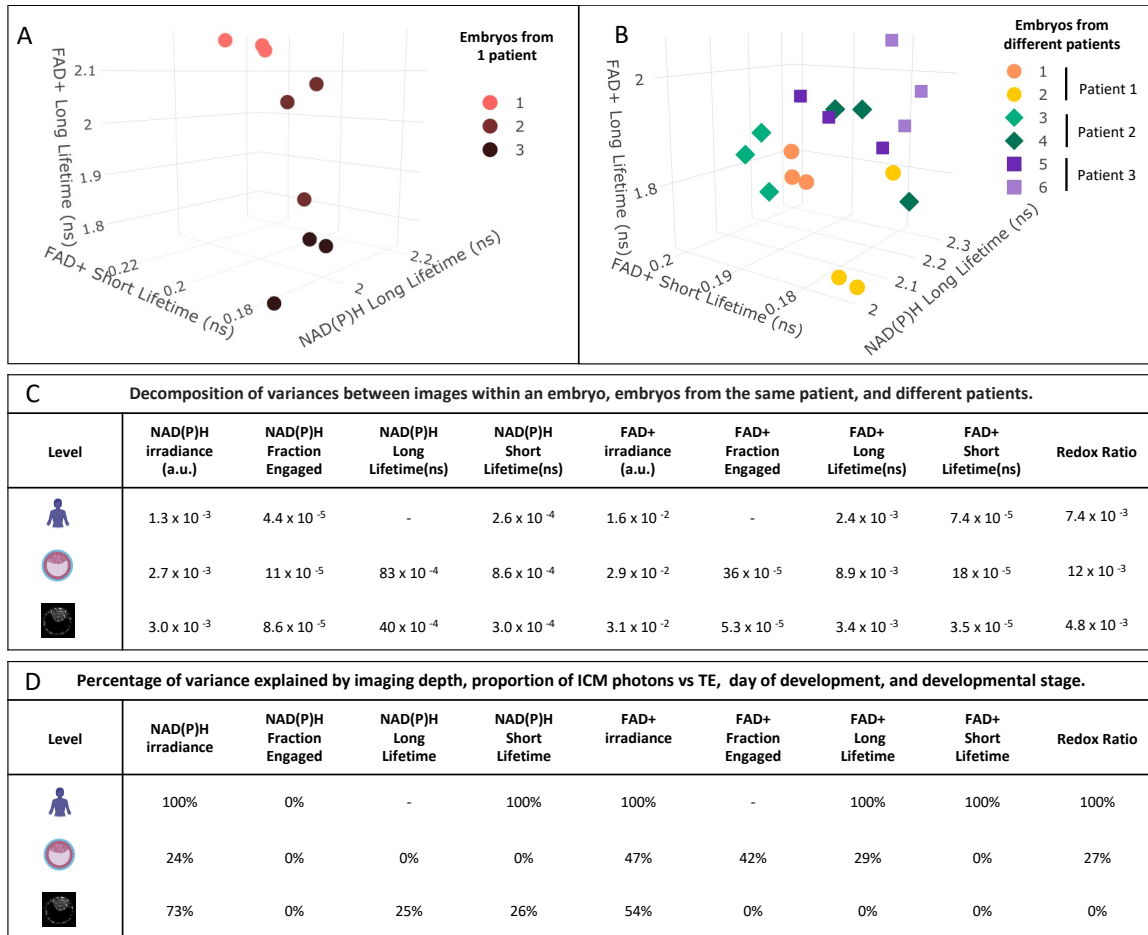


Figure 4. Variance of the metabolic parameters between patients, embryos, and images. Multilevel models encode information on the variance of each FLIM parameter between different patients, between different embryos from the same patient, and between different images from the same embryo (taken at different Z positions). (A) Example of a patient with three different blastocysts. Colors correspond to a different embryo and each dot corresponds to a different image, from a different Z position, within the embryo. (B) Example of three patients with two embryos each imaged. Symbols correspond to different patients; each color corresponds to a different embryo and each dot corresponds to a different Z position within each embryo. (C) The variance of each FLIM parameter associated with each level: patient (top), embryo (middle) and images (bottom). FLIM parameter variances between patients were significantly different from 0 (FDR p values ranging between 0.001 and 0.04), except NADH long lifetime and FAD+ fraction engaged. All variances associated with embryo level (FDR p values ranging between 1.1×10^{-6} and 9×10^{-9}) and all variances between images within embryos were significantly different from 0 (p values $< 1 \times 10^{-10}$). (D) The percentage of variance of each FLIM parameter associated with each level explained after controlling for embryo day, expansion stage, imaging depth and the proportion of photons coming from the ICM vs TE. 100% corresponds to no statistically significant variance remaining after controlling for the listed factors. 0% corresponds to the variances not being altered after controlling for the listed factors.

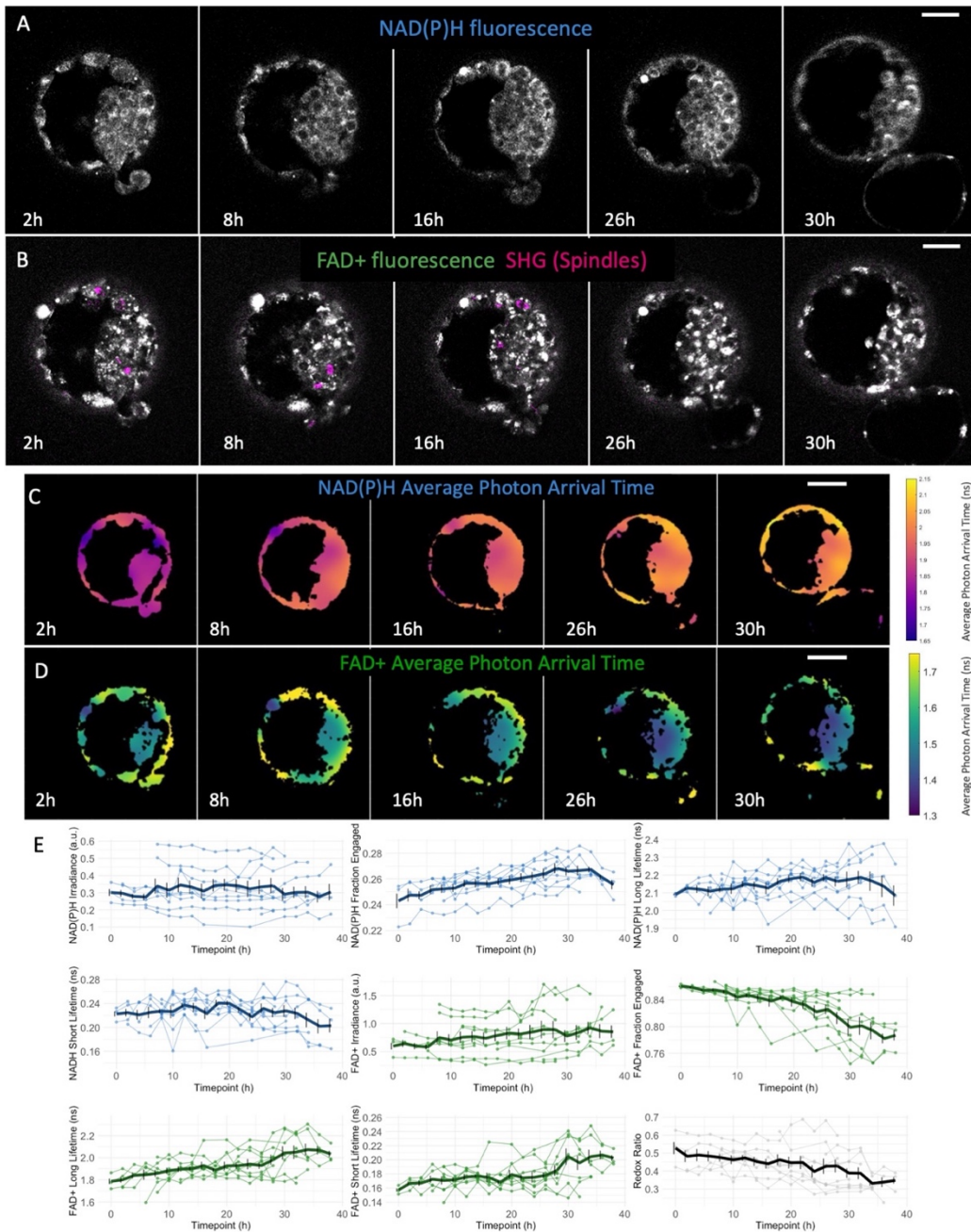
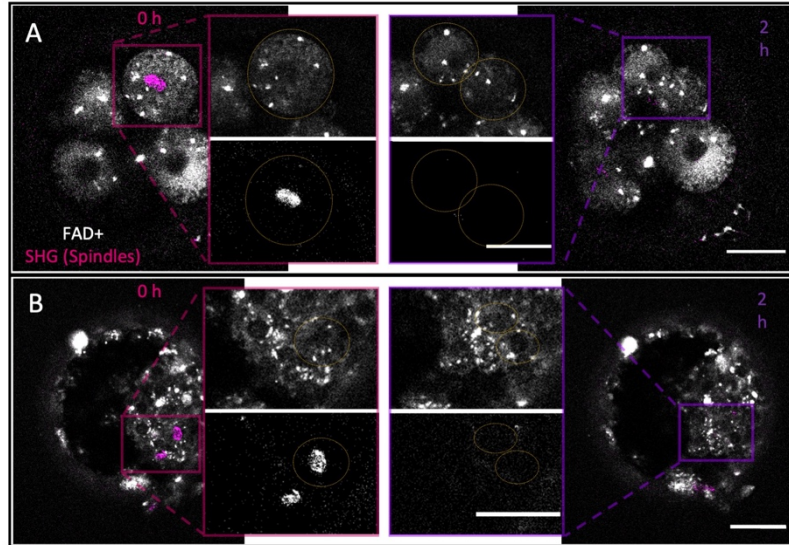
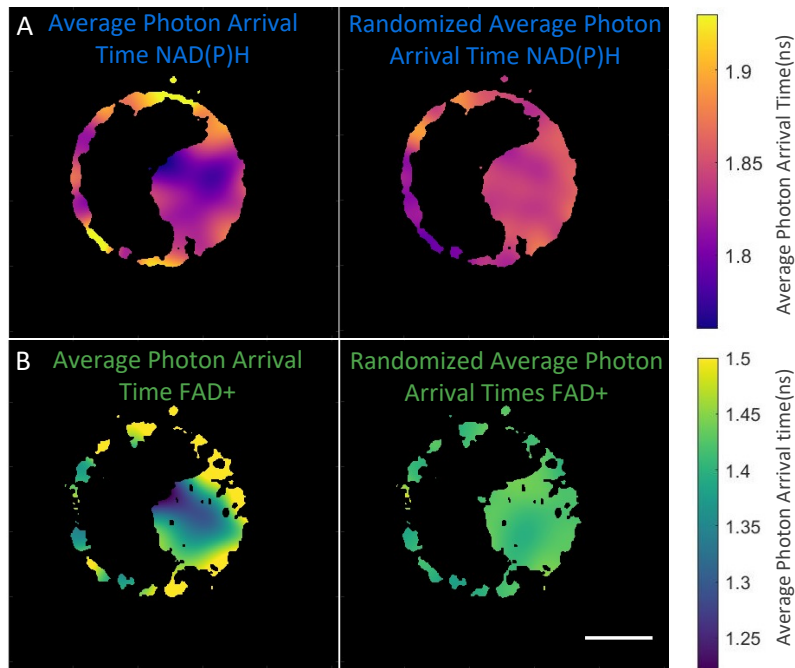


Figure 5. Non-invasive FLIM and SHG imaging detect metabolic variations during human blastocyst development. FLIM time-lapse imaging of the autofluorescence of NAD(P)H (A), and (B) of FAD+ (in grey) and SHG spindle imaging (in magenta) of a human blastocyst throughout 36h of incubation. (C) FLIM time-lapse imaging of the photon arrival times of NAD(P)H and (D) of FAD+ enable visualization of variations of metabolic state of human blastocysts throughout expansion and hatching. Color bars show the average photon arrival times in nanoseconds (Movie S1). (H) Time trajectory plots of individual embryos ($n=10$ from 10 patients) of four of the all the metabolic parameters produced. The average time curves from all the embryos are shown in thicker lines with SE bars, showing that these trends were reproducible among blastocysts. Scale bars, 40 μm .

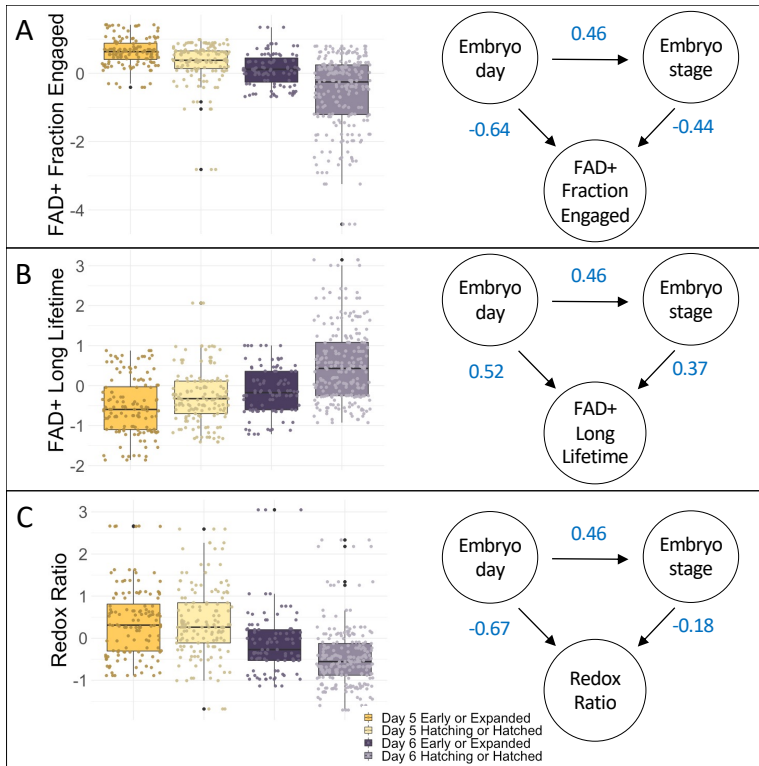
Supplementary Figures



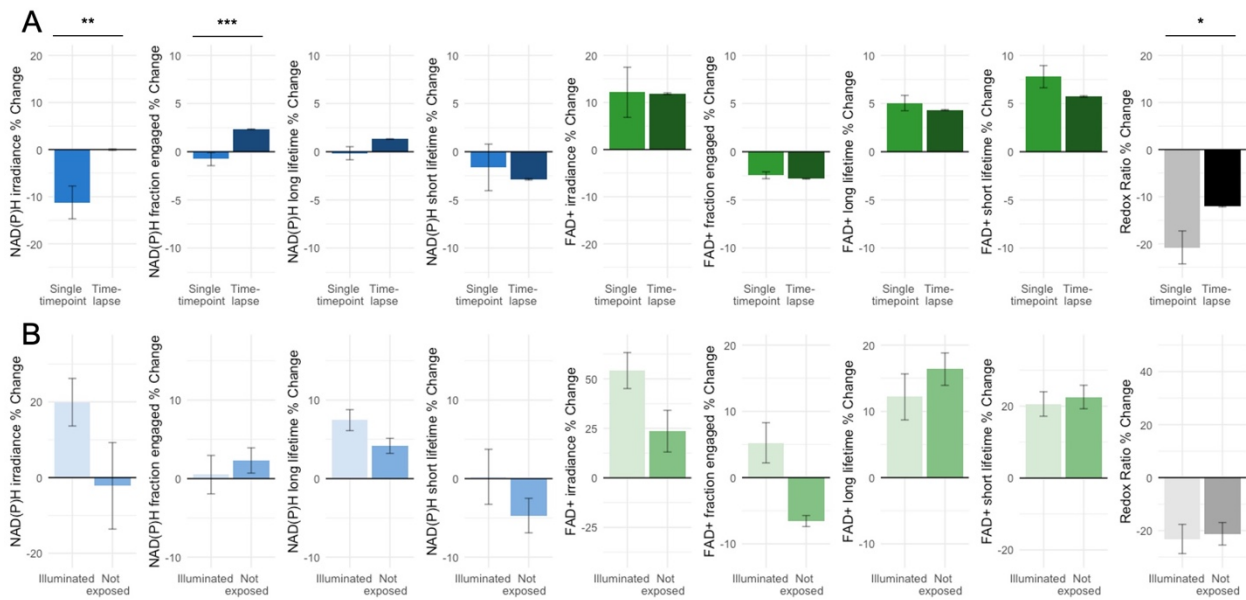
SI1. FLIM and SHG imaging enable spindle visualization. SHG spindle imaging (in magenta, false color), in combination with FLIM FAD+ autofluorescence imaging (in grey) enables detection of spindle formation capturing cellular mitotic divisions. (A) A human 4 cell embryo at time 0 hours containing a cell in mitosis (left) showing a mitotic spindle in magenta. This cell then divides into two cells after 2 hours (right) leading to a 6-cell embryo. (B) Example of a human blastocyst with an embryo with two cells in mitosis with a mitotic spindle in magenta (also in Movie S2). Scale bar, 40 μm .



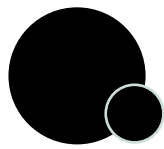
SI-2: FLIM average photon arrival time images. (A) Example of an average photon arrival time image of NAD(P)H and (B) FAD+ showing the spatial pattern of metabolic signatures between the inner cell mass and trophoctoderm (left images). In the right images, the randomized average photon arrival time demonstrate a homogeneous distribution, and do not show a characteristic spatial distribution. Color bars show the average photon arrival time for both NAD(P)H and FAD+ in nanoseconds. Scale bar, 40 μm .



SI-3. Directed acyclic graphical models of FLIM parameters of human blastocysts and embryo day and expansion stage. On the left side, the box plots display normalized FAD+ fraction engaged (A), FAD+ long lifetime (B) and redox ratio (C) of 4 categories (Day 5 early/expanded, Day 5 hatching/hatched, Day 6 early/expanded or Day 6 hatching/hatched embryos), showing that both day and stage impact the FLIM parameters. In order to explore the conditional dependencies between embryo day, stage and FLIM parameters we performed probabilistic graphical models. On the right side, DAG of FAD+ fraction engaged (A), FAD+ long lifetime (B) and redox ratio (C) showing that embryo day and stage are correlated and that embryo FLIM parameters are dependent both on embryo day and stage. Numbers in blue represent the β -coefficient of the multilevel model.



SI-4. Percentage change for each FLIM parameter. (A) Percentage change of each metabolic parameter over 24-hour period. The FLIM parameter change was calculated between day 5 and day 6 in the single time-point experiments and within 24 hours of development in the time-lapse experiment. Significant differences were observed in NAD(P)H irradiance, NAD(P)H fraction engaged, and redox ratio. (B) Percentage change of each metabolic parameter within 36 hours of development between embryos that were exposed to continual time-lapse illumination and embryos that were not exposed to illumination, both cultured in the same experimental conditions. No significant differences were observed between in any FLIM parameter (FDR $p > 0.05$, SI 4B). *** signifies FDR $p < 0.001$, **FDR $p < 0.01$ * signifies FDR $p < 0.05$.



Chapter 5. General Discussion

Correct metabolic function is essential for oocyte and embryo development (85,87,110). Additionally, mitochondrial dysfunction has been correlated with lower oocyte quality and embryo developmental competency (77,88,101,102). Hence, measures of the metabolic state of oocytes, cumulus cells and/or embryos are highly promising methods to be used as clinical assessments of quality. To this end, several studies have developed tools to measure cellular metabolism in order to assess developmental competency (17,101,109,123). However, these approaches are yet to be proven clinically useful as they can be invasive or require highly specialized skills (115,141). Two-photon FLIM to measure the autofluorescence of both NAD(P)H and FAD⁺, has been widely used in other fields (119,125,129) but its application in human ART yet to be studied. For this reason, this thesis has sought to determine the utility of FLIM in combination with SHG for imaging the metabolic state and spindle dynamics of oocytes, CCs and embryos, and to explore some potential applications of these techniques to be used in clinical IVF.

The first study of this thesis was focused on determining the feasibility, sensitivity, and safety of FLIM to measure the metabolic state of mouse oocytes and preimplantation embryos. FLIM could detect the fluorescence intensity of both NAD(P)H and FAD⁺, which correlate with their concentration and also offered measures of their fluorescence lifetimes, which varies whether these molecules are bound to an enzyme or free (128,134). Arguably, this proof-of-concept study found that FLIM is a highly promising alternative approach for non-invasively assessing metabolism at a cellular and even subcellular level. This approach provided quantitative and robust information of the metabolic state of both the mitochondrial and cytoplasmic regions, which can be related with the glycolytic and oxidative phosphorylation activities, respectively (119,125). These observations have been previously described in mouse oocytes (122,129).

Furthermore, SHG imaging can also be acquired simultaneously by using the same microscopic system than FLIM. SHG enabled images both meiotic and mitotic spindles, given their highly polarized structure (138,139,142). Associations between meiotic spindle morphology and oocyte quality have been previously observed (143–146). To this end, non-invasive imaging of meiotic and mitotic spindles in combination with measures of mitochondrial physiology and morphology, may provide new insights in the relationship between metabolic (dys)function, spindle morphology and chromosomal abnormalities.

Both techniques showed high sensitivity in measuring the variations that naturally occur during pre-implantation mouse embryo development (89,91). Furthermore, the addition of metabolic perturbators caused clear shifts FLIM parameters compared to oocytes not exposed to perturbations, further demonstrating the sensitivity of this technology. The addition of rotenone, which reduces the activity of the electron transport chain, or oxamate, that inhibits lactate dehydrogenase (147), caused significant changes in both the mitochondrial and cytoplasmic FLIM parameters. Furthermore, perturbing the metabolic state of mouse oocytes caused observable changes in spindle morphology. The relationship between metabolism and

spindle morphological characteristics has been previously described (148). Recent studies have been able to correlate embryo ploidy with metabolic state, using both FLIM and hyperspectral microscopy (123,149). These results argue that FLIM in combination with SHG imaging could be used to increase our knowledge of these correlations and may provide a further use of this technique for selecting higher quality oocytes and embryos.

Metabolic cooperation between oocytes and its surrounding CCs is essential for correct oocyte maturation and the acquisition of developmental competency (28,66,67). Hence, approaches to measure CC metabolism have potential utility in clinical ART. On this line, several CCs metabolic biomarkers haven been studied to determine oocyte developmental capacity (40,42,70,111). However, these studies are still preliminary, and their results have yet to be confirmed (68,83,84). The second study of this thesis, aimed to explore a potential application of FLIM to measure the metabolic state of CCs and to explore the associations between CCs metabolism and patient clinical factors and oocyte characteristics. FLIM provided quantitative information on the metabolic state of CCs, which showed distinct features between patients and oocytes. Maternal clinical factors like age, BMI and AMH levels are known to be associated with oocyte and embryo quality (5,11). CCs metabolic signatures also revealed associations with maternal clinical factors such as age, AMH levels, which have already been observed (42,83,112,113). Despite previous reports (112), no associations were found with maternal BMI.

Additionally, significant differences in CCs metabolic parameters were observed between CCs associated with MII oocytes or with immature oocytes. These findings provided further proof of the essential role of CC-oocyte communication (28) for oocyte quality (48,68). Therefore, this study is a step forward into the possible application of FLIM to measure CCs metabolic signatures to assess oocyte maturation and perhaps oocyte quality in clinical IVF. Whether variations in FLIM parameters will correlate with embryo viability and implantation potential is currently under investigation. Last, prediction models, including patient clinical characteristics and CCs metabolic signatures and embryo morphological characteristics will provide further validation of this application for clinical purposes.

Despite the widespread use of embryo morphology grading methods, they provide limited embryo information of embryo physiology or ploidy status (49). Given the essential role of metabolism in the acquisition of developmental competence (89,93,94,104,115), non-invasive methods to evaluate embryo metabolism may provide incredibly useful information to help improve embryo selection. The third study of this thesis aimed to explore a further use of FLIM to measure the metabolic state of human embryos at the blastocysts stage that were donated for research. FLIM in conjunction with SHG enabled quantitative information of the metabolic state of human blastocysts, spindle dynamics and cellular mitotic divisions.

Furthermore, spatial heterogeneity of the metabolic state of human blastocysts was observed between the ICM and TE. These observed findings are in line with previous studies (94,150,151) and perhaps can indicate that the ICM and TE have distinct mitochondrial activity or physiology that can be due to the high energy demands of the TE to maintain the blastocoele. Differences between the TE cells within and without the zona pellucida were also found during the hatching process. These observations may reflect the interaction with the different microenvironments observed during hatching (90) and the embryo metabolic plasticity to adapt to them (152), or perhaps may be a response to stress associated with the hatching process itself (153). These findings demonstrated the sensitivity of this method in measuring the metabolic state within human embryos at the subcellular level. Future experiments are planned to study the nature of this observed metabolic spatial distribution.

This study further demonstrated that human blastocyst's metabolism is incredibly dynamic and adaptative. Embryo metabolism varies throughout preimplantation development (85,110,154). Here, continuous changes in metabolic state were observed during development from the early blastocyst to hatching stages. Furthermore, blastocysts exhibited distinct metabolic parameters whether they were at day five or six after fertilization. Embryo metabolic state was also associated with the stage of expansion that blastocysts were at. These observations may imply an association between embryo developmental rate and metabolism, which as has also been discussed previously (93,103,104,155). Furthermore, the lack of association between metabolic state and morphology scores suggests that FLIM and morphological grading (49) offer distinct information yet together might help select the highest quality embryo for transfer.

The data in this thesis displayed a hierarchically organization: patients; oocytes, CCs or embryo; and FLIM images. This structured data was analyzed using multilevel models (156,157), to take into account the variance associated with each of this levels: variance associated with differences between patients, variance associated with differences between oocytes, CCs or embryos from the same patient, and variance associated with differences between individual images. In both studies, the variance of the metabolic parameters was greater within patients than between patients. These results suggest that the metabolic profiles of CC clusters or embryos with different characteristics is greater than the effect that the patient's clinical factors may have. These findings highlight the potential use of this approach to determine oocyte or embryo specific characteristics. Last, the variance between FLIM images was very small, which indicate the high reproducibility and robustness of this measurements.

Taken together, FLIM and SHG in oocytes, CCs and embryos are promising tools to non-invasively measure their metabolic state and spindle morphology. FLIM also enables metabolic

measurements with high spatial-temporal resolution, robustness, and sensitivity. We believe that this thesis provided new insights in CCs, oocytes and embryo metabolism and shed light into possible applications of FLIM and SHG in IVF. Future studies, combining FLIM imaging, patient clinical characteristics and embryo morphology with live birth, could help select oocytes and embryos with the highest success rates.

Limitations

Certain limitations of individual studies have been discussed in each manuscript, but some general limitations should be considered when interpreting this thesis. This thesis has led to the conclusion that FLIM imaging of the autofluorescence of NADH and FAD⁺ is robust and sensitive method capable of detecting the metabolic state of individual oocytes, CCs and embryos. Despite these findings, it remains a challenge to relate those variations in FLIM to the underlying metabolic pathways. Hence, understanding the implications of these observed variations in FLIM parameters will be our goal in future studies. Recent work has established a framework to relate FLIM parameters to mitochondrial metabolic fluxes (137). Nevertheless, these studies were performed in mouse MII oocytes, therefore additional studies are required to determine if these findings can generalize to human embryos and CCs.

Even though this technique is non-invasive, there is indeed a concern that the two-photon pulsed laser illumination could cause harm to the oocytes, CCs or embryos. Detrimental effects of light exposure have been previously detected after conventional microscopy or laser illumination used for biopsy, but only if used excessively (158,159). Despite prior work showing that the level of FLIM illumination does not cause measurable differences in intracellular reactive oxygen species nor blastocyst formation rates (73) and the promising findings of this thesis showing no disruption on mouse live birth rates or pup weights, or human FLIM parameters; it is essential to further investigate the safety of this assessment before its application in clinical IVF. To this end, large observational studies with complete safety assessments are planned to demonstrate the feasibility of this technique in assessing human oocytes or embryos.

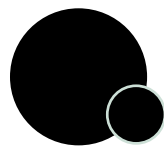
Finally, all samples used in these three studies were vitrified, thawed, and warmed prior to FLIM imaging. Despite the widespread use and clinical success of the vitrification method (160), and the fact that it does not appear to impact mitochondria nor cause oxidative stress (161), whether this technique alters the metabolic state of human CCs, oocytes or embryos remains unknown. Vitrification did not appear to induce significant changes on the FLIM parameters of CCs, nonetheless, larger studies in CCs and studies in human oocytes and preimplantation embryos are required to determine the effect of vitrification and warming on their metabolic parameters.

Future directions

Studies presented in this thesis have added valuable information on the literature of non-invasive methods to measure intracellular metabolism and potential applications of FLIM and SHG for ART. Nonetheless, a greater understanding of the correlations between metabolic variations and human oocyte and embryo growth could contribute to the development of more accurate selection tools for ART. Future large observational and later clinical trials are planned in order to understand these associations and will demonstrate the efficacy of FLIM and SHG for predicting live birth.

Oocyte quality is the primary driver of embryo viability and is the most important factor influencing the likelihood of successful IVF treatments (39). However, the biological mechanisms that determine oocyte quality are unclear and the exact cause of the decline of oocyte quality with increasing maternal age or BMI or in response to environmental toxins remains unknown. Additionally, oocyte mitochondrial health is crucial for correct development (75,162), but it is yet to be known if mitochondrial (dys)function contributes to clinically relevant reductions in human oocyte quality. Therefore, FLIM in combination with spindle imaging using SHG could provide important insights into the relationship between metabolism and chromosome segregation errors and its connection with oocyte quality.

Last, both nuclear and cytoplasmic maturation are essential for correct acquisition of oocyte developmental competence (24,40). However, whether metabolic disruption in oocytes or CCs, alters oocyte maturation remains unknown. Preliminary studies performed in our lab showed significant differences in mouse oocyte metabolic function of oocytes matured in vitro with or without CCs. The premise of our future work is to study whether metabolic function during oocyte maturation impacts nuclear or cytoplasmic maturation, or both. For this reason, studying the metabolic state and spindle dynamics of both denuded oocytes and entire COC throughout maturation will help gain fundamental insights into oocyte maturation and the importance of the bidirectional metabolic communication between CCs and oocytes.



Chapter 6. Conclusions

From the studies performed throughout this thesis, FLIM is a promising non-invasive approach to measure CC, oocytes, and embryo metabolic state and to gain global insights into the relation between the metabolic state of human CC, oocytes and embryos and their developmental competence. Specific conclusions were made:

- FLIM is a feasible and safe non-invasive technique that can quantitatively measure the metabolic state of live CCs, oocytes, and embryos.
- SHG imaging can provide information of meiotic and mitotic spindles morphology and location within the cells.
- FLIM illumination does not appear to disrupt live birth rates or pup weights.
- FLIM is sensitive enough to detect differences in CC metabolism and shows a greater variance in FLIM parameters among oocytes than between patients.
- Observed associations among clinically relevant patient factors, such as maternal age and levels of AMH, and the metabolic state of the cumulus masses, but not with BMI.
- Measures of the metabolic state of CC clusters are associated with the maturity of the oocyte they enclose.
- FLIM is also sensitive enough to detect differences in embryo metabolism and shows a greater variance in FLIM parameters among embryos within patients than between patients.
- FLIM can detect metabolic variations associated with blastocyst development over 36h, the time post fertilization and blastocyst developmental stage.
- This assessment revealed differences in metabolic state between cells in the ICM and the TE, and between TE cells inside and outside the zona pellucida.
- The lack of an association between the metabolic state of human blastocyst and their morphological grading indicates that these two assessments may provide synergistic information to improve blastocyst selection.

References

1. Zinaman MJ, Clegg ED, Brown CC, O'Connor J, Selevan SG. Estimates of human fertility and pregnancy loss. *Fertil Steril* 1996;65(3):503–9.
2. Assisted Reproductive Technology (ART) | Reproductive Health | CDC [Internet]. 2020 [cited 2021 Oct 1]; Available from: <https://www.cdc.gov/art/index.html>
3. Hull MG, Glazener CM, Kelly NJ, Conway DI, Foster PA, Hinton RA, et al. Population study of causes, treatment, and outcome of infertility. *Br Med J (Clin Res Ed)* 1985;291(6510):1693–7.
4. Cimadomo D, Fabozzi G, Vaiarelli A, Ubaldi N, Ubaldi FM, Rienzi L. Impact of Maternal Age on Oocyte and Embryo Competence. *Frontiers in Endocrinology* 2018;9:327.
5. Franiak JM, Forman EJ, Hong KH, Werner MD, Upham KM, Treff NR, et al. The nature of aneuploidy with increasing age of the female partner: a review of 15,169 consecutive trophectoderm biopsies evaluated with comprehensive chromosomal screening. *Fertil Steril* 2014;101(3):656–663.e1.
6. Gougeon A, Ecochard R, Thalabard JC. Age-related changes of the population of human ovarian follicles: increase in the disappearance rate of non-growing and early-growing follicles in aging women. *Biol Reprod* 1994;50(3):653–63.
7. Kotlyar AM, Seifer DB. Ethnicity/Race and Age-Specific Variations of Serum AMH in Women-A Review. *Front Endocrinol (Lausanne)* 2020;11:593216.
8. Munné S, Alikani M, Tomkin G, Grifo J, Cohen J. Embryo morphology, developmental rates, and maternal age are correlated with chromosome abnormalities. *Fertil Steril* 1995;64(2):382–91.
9. Erickson JD. Down syndrome, paternal age, maternal age and birth order. *Annals of Human Genetics* 1978;41(3):289–98.
10. Morris JK, Mutton DE, Alberman E. Revised estimates of the maternal age specific live birth prevalence of Down's syndrome. *J Med Screen* 2002;9(1):2–6.
11. Buratini J, Dellaqua TT, Dal Canto M, La Marca A, Carone D, Mignini Renzini M, et al. The putative roles of FSH and AMH in the regulation of oocyte developmental competence: from fertility prognosis to mechanisms underlying age-related subfertility. *Human Reproduction Update* 2021;dmab044.
12. Zheng D, Zeng L, Yang R, Lian Y, Zhu Y-M, Liang X, et al. Intracytoplasmic sperm injection (ICSI) versus conventional in vitro fertilisation (IVF) in couples with non-severe male infertility (NSMI-ICSI): protocol for a multicentre randomised controlled trial. *BMJ Open* 2019;9(9):e030366.
13. Dudenhausen JW, Maier RF. Perinatal Problems in Multiple Births. *Dtsch Arztebl Int* 2010;107(38):663–8.
14. Adashi EY, Barri PN, Berkowitz R, Braude P, Bryan E, Carr J, et al. Infertility therapy-associated multiple pregnancies (births): an ongoing epidemic. *Reprod Biomed Online* 2003;7(5):515–42.
15. Gardner DK, Lane M, Stevens J, Schlenker T, Schoolcraft WB. Blastocyst score affects implantation and pregnancy outcome: towards a single blastocyst transfer. *Fertil Steril* 2000;73(6):1155–8.
16. Urbanski JP, Johnson MT, Craig DD, Potter DL, Gardner DK, Thorsen T. Noninvasive Metabolic Profiling using Microfluidics for Analysis of Single Preimplantation Embryos. *Anal Chem* 2008;80(17):6500–7.
17. Gardner DK, Leese HJ. Assessment of embryo viability prior to transfer by the noninvasive measurement of glucose uptake. *J Exp Zool* 1987;242(1):103–5.
18. Gerris J, De Sutter P, De Neubourg D, Van Royen E, Vander Elst J, Mangelschots K, et al. A real-life prospective health economic study of elective single embryo transfer versus two-embryo transfer in first IVF/ICSI cycles. *Hum Reprod* 2004;19(4):917–23.
19. Rodrigues P, Limback D, McGinnis LK, Plancha CE, Albertini DF. Oogenesis: Prospects and challenges for the future. *J Cell Physiol* 2008;216(2):355–65.
20. Elder K, Dale B. *In-Vitro Fertilization* [Internet]. 3rd ed. Cambridge: Cambridge University Press; 2010 [cited 2021 Sep 24]. Available from: <https://www.cambridge.org/core/books/invitro-fertilization/8B2CE34C45A363F237C561B556841D60>
21. Durlinger AL, Kramer P, Karels B, de Jong FH, Uilenbroek JT, Grootegoed JA, et al. Control of primordial follicle recruitment by anti-Müllerian hormone in the mouse ovary. *Endocrinology* 1999;140(12):5789–96.
22. Durlinger ALL, Gruijters MJG, Kramer P, Karels B, Ingraham HA, Nachtigal MW, et al. Anti-Müllerian hormone inhibits initiation of primordial follicle growth in the mouse ovary. *Endocrinology* 2002;143(3):1076–84.
23. Mihajlović AI, FitzHarris G. Segregating Chromosomes in the Mammalian Oocyte. *Curr Biol* 2018;28(16):R895–907.
24. Li R, Albertini DF. The road to maturation: somatic cell interaction and self-organization of the mammalian oocyte. *Nat Rev Mol Cell Biol* 2013;14(3):141–52.
25. Coticchio G, Mignini Renzini M, Novara PV, Lain M, De Ponti E, Turchi D, et al. Focused time-lapse analysis reveals novel aspects of human fertilization and suggests new parameters of embryo viability. *Hum Reprod* 2018;33(1):23–31.
26. Anderson E, Albertini DF. Gap junctions between the oocyte and companion follicle cells in the mammalian ovary. *J Cell Biol* 1976;71(2):680–6.
27. El-Hayek S, Yang Q, Abbassi L, FitzHarris G, Clarke HJ. Mammalian Oocytes Locally Remodel Follicular Architecture to Provide the Foundation for Germline-Soma Communication. *Curr Biol* 2018;28(7):1124–1131.e3.

28. Eppig JJ. Intercommunication between mammalian oocytes and companion somatic cells. *Bioessays* 1991;13(11):569–74.
29. Albertini DF, Combelles CM, Benecchi E, Carabatsos MJ. Cellular basis for paracrine regulation of ovarian follicle development. *Reproduction* 2001;121(5):647–53.
30. Anderson SH, Glassner MJ, Melnikov A, Friedman G, Orynbayeva Z. Respiriometric reserve capacity of cumulus cell mitochondria correlates with oocyte maturity. *J Assist Reprod Genet* 2018;35(10):1821–30.
31. Eppig JJ. Oocyte control of ovarian follicular development and function in mammals. *Reproduction* 2001;122(6):829–38.
32. Sathananthan DH, Gunasheela S, Menezes J. Mechanics of human blastocyst hatching in vitro. *Reproductive BioMedicine Online* 2003;7(2):228–34.
33. Veeck LL. Extracorporeal Maturation: Norfolk, 1984. *Annals of the New York Academy of Sciences* 1985;442(1):357–67.
34. Wang Q, Sun Q-Y. Evaluation of oocyte quality: morphological, cellular and molecular predictors. *Reprod Fertil Dev* 2007;19(1):1–12.
35. Coticchio G, Sereni E, Serrao L, Mazzone S, Iadarola I, Borini A. What criteria for the definition of oocyte quality? *Ann N Y Acad Sci* 2004;1034:132–44.
36. Hammitt DG, Syrop CH, Van Voorhis BJ, Walker DL, Miller TM, Barud KM, et al. Prediction of nuclear maturity from cumulus-coronal morphology: Influence of embryologist experience. *J Assist Reprod Genet* 1992;9(5):439–46.
37. Balaban B, Urman B, Sertac A, Alatas C, Aksoy S, Mercan R. Oocyte morphology does not affect fertilization rate, embryo quality and implantation rate after intracytoplasmic sperm injection. *Hum Reprod* 1998;13(12):3431–3.
38. Heindryckx B, De Gheselle S, Lierman S, Gerris J, De Sutter P. Efficiency of polarized microscopy as a predictive tool for human oocyte quality. *Hum Reprod* 2011;26(3):535–44.
39. Keefe D, Kumar M, Kalmbach K. Oocyte competency is the key to embryo potential. *Fertil Steril* 2015;103(2):317–22.
40. Watson AJ. Oocyte cytoplasmic maturation: a key mediator of oocyte and embryo developmental competence. *J Anim Sci* 2007;85(13 Suppl):E1-3.
41. Krisher RL. The effect of oocyte quality on development^{1,2}. *Journal of Animal Science* 2004;82(suppl_13):E14–23.
42. Funsho Fagbohun C, Downs SM. Metabolic Coupling and Ligand-Stimulated Meiotic Maturation in the Mouse Oocyte-Cumulus Cell Complex¹. *Biology of Reproduction* 1991;45(6):851–9.
43. Assou S, Haouzi D, Mahmoud K, Aouacheria A, Guillemin Y, Pantesco V, et al. A non-invasive test for assessing embryo potential by gene expression profiles of human cumulus cells: a proof of concept study. *Molecular Human Reproduction* 2008;14(12):711–9.
44. Boucrot L, Chao de la Barca JM, Morinière C, Desquiere V, Ferré-L'Hôtelier V, Descamps P, et al. Relationship between diminished ovarian reserve and mitochondrial biogenesis in cumulus cells. *Hum Reprod* 2015;30(7):1653–64.
45. Gebhardt KM, Feil DK, Dunning KR, Lane M, Russell DL. Human cumulus cell gene expression as a biomarker of pregnancy outcome after single embryo transfer. *Fertility and Sterility* 2011;96(1):47-52.e2.
46. Huang Z, Wells D. The human oocyte and cumulus cells relationship: new insights from the cumulus cell transcriptome. *Mol Hum Reprod* 2010;16(10):715–25.
47. McKenzie LJ, Pangas SA, Carson SA, Kovanci E, Cisneros P, Buster JE, et al. Human cumulus granulosa cell gene expression: a predictor of fertilization and embryo selection in women undergoing IVF. *Hum Reprod* 2004;19(12):2869–74.
48. Uyar A, Torrealday S, Seli E. Cumulus and granulosa cell markers of oocyte and embryo quality. *Fertility and Sterility* 2013;99(4):979–97.
49. Schoolcraft WB, Gardner DK, Lane M, Schlenker T, Hamilton F, Meldrum DR. Blastocyst culture and transfer: analysis of results and parameters affecting outcome in two in vitro fertilization programs. *Fertil Steril* 1999;72(4):604–9.
50. Van Den Abbeel E, Balaban B, Ziebe S, Lundin K, Cuesta MJG, Klein BM, et al. Association between blastocyst morphology and outcome of single-blastocyst transfer. *Reproductive BioMedicine Online* 2013;27(4):353–61.
51. Gardner DK, Lane M, Stevens J, Schlenker T, Schoolcraft WB. Blastocyst score affects implantation and pregnancy outcome: Towards a single blastocyst transfer. *Fertility and Sterility* 2000;73(6):1155–8.
52. Ahlström A, Westin C, Reisner E, Wikland M, Hardarson T. Trophoctoderm morphology: An important parameter for predicting live birth after single blastocyst transfer. *Human Reproduction* 2011;26(12):3289–96.
53. Wong KM, Repping S, Mastenbroek S. Limitations of embryo selection methods. *Semin Reprod Med* 2014;32(2):127–33.
54. Hill MJ, Richter KS, Heitmann RJ, Graham JR, Tucker MJ, Decherney AH, et al. Trophoctoderm grade predicts outcomes of single-blastocyst transfers. *Fertility and Sterility* 2013;99(5):1283-1289.e1.
55. Irani M, Reichman D, Robles A, Melnick A, Davis O, Zaninovic N, et al. Morphologic grading of euploid blastocysts influences implantation and ongoing pregnancy rates. *Fertility and Sterility* 2017;107(3):664–70.
56. Yang L, Cai S, Zhang S, Kong X, Gu Y, Lu C, et al. Single embryo transfer by Day 3 time-lapse selection versus Day 5 conventional morphological selection: A randomized, open-label, non-inferiority trial. *Human Reproduction* 2018;33(5):869–76.
57. Armstrong S, Vail A, Mastenbroek S, Jordan V, Farquhar C. Time-lapse in the IVF-lab: How should we assess potential benefit? *Human Reproduction* 2015;30(1):3–8.

58. Goodman LR, Goldberg J, Falcone T, Austin C, Desai N. Does the addition of time-lapse morphokinetics in the selection of embryos for transfer improve pregnancy rates? A randomized controlled trial. *Fertility and Sterility* 2016;105(2):275–285.e10.
59. Fernandez EI, Ferreira AS, Cecilio MHM, Chéles DS, de Souza RCM, Nogueira MFG, et al. Artificial intelligence in the IVF laboratory: overview through the application of different types of algorithms for the classification of reproductive data. *Journal of Assisted Reproduction and Genetics* 2020;37(10):2359–76.
60. Scott RT, Upham KM, Forman EJ, Hong KH, Scott KL, Taylor D, et al. Blastocyst biopsy with comprehensive chromosome screening and fresh embryo transfer significantly increases in vitro fertilization implantation and delivery rates: A randomized controlled trial. *Fertility and Sterility* 2013;100(3):697–703.
61. Munné S, Kaplan B, Frattarelli JL, Child T, Nakhuda G, Shamma FN, et al. Preimplantation genetic testing for aneuploidy versus morphology as selection criteria for single frozen-thawed embryo transfer in good-prognosis patients: a multicenter randomized clinical trial. *Fertility and Sterility* 2019;112(6):1071–1079.e7.
62. Murphy LA, Seidler EA, Vaughan DA, Resetkova N, Penzias AS, Toth TL, et al. To test or not to test? A framework for counselling patients on preimplantation genetic testing for aneuploidy (PGT-A). *Human Reproduction* 2019;34(2):268–75.
63. Dumesic DA, Guedikian AA, Madrigal VK, Phan JD, Hill DL, Alvarez JP, et al. Cumulus Cell Mitochondrial Resistance to Stress In Vitro Predicts Oocyte Development During Assisted Reproduction. *J Clin Endocrinol Metab* 2016;101(5):2235–45.
64. Feuerstein P, Puard V, Chevalier C, Teusan R, Cadoret V, Guerif F, et al. Genomic Assessment of Human Cumulus Cell Marker Genes as Predictors of Oocyte Developmental Competence: Impact of Various Experimental Factors. *PLOS ONE* 2012;7(7):e40449.
65. Seli E, Babayev E, Collins SC, Nemeth G, Horvath TL. Minireview: Metabolism of Female Reproduction: Regulatory Mechanisms and Clinical Implications. *Mol Endocrinol* 2014;28(6):790–804.
66. Dumesic DA, Meldrum DR, Katz-Jaffe MG, Krisher RL, Schoolcraft WB. Oocyte environment: follicular fluid and cumulus cells are critical for oocyte health. *Fertility and Sterility* 2015;103(2):303–16.
67. Sutton ML, Cetica PD, Beconi MT, Kind KL, Gilchrist RB, Thompson JG. Influence of oocyte-secreted factors and culture duration on the metabolic activity of bovine cumulus cell complexes. *Reproduction* 2003;126(1):27–34.
68. Gilchrist RB, Lane M, Thompson JG. Oocyte-secreted factors: regulators of cumulus cell function and oocyte quality. *Hum Reprod Update* 2008;14(2):159–77.
69. Dalton CM, Szabadkai G, Carroll J. Measurement of ATP in single oocytes: impact of maturation and cumulus cells on levels and consumption. *J Cell Physiol* 2014;229(3):353–61.
70. Downs SM, Humpherson PG, Leese HJ. Pyruvate utilization by mouse oocytes is influenced by meiotic status and the cumulus oophorus. *Mol Reprod Dev* 2002;62(1):113–23.
71. Stojkovic M, Machado SA, Stojkovic P, Zakhartchenko V, Hutzler P, Gonçalves PB, et al. Mitochondrial distribution and adenosine triphosphate content of bovine oocytes before and after in vitro maturation: correlation with morphological criteria and developmental capacity after in vitro fertilization and culture. *Biol Reprod* 2001;64(3):904–9.
72. Hoshino Y. Updating the markers for oocyte quality evaluation: intracellular temperature as a new index. *Reprod Med Biol* 2018;17(4):434–41.
73. Sanchez T, Wang T, Pedro MV, Zhang M, Esencan E, Sakkas D, et al. Metabolic imaging with the use of fluorescence lifetime imaging microscopy (FLIM) accurately detects mitochondrial dysfunction in mouse oocytes. *Fertil Steril* 2018;110(7):1387–97.
74. Zhao J, Li Y. Adenosine triphosphate content in human unfertilized oocytes, undivided zygotes and embryos unsuitable for transfer or cryopreservation. *J Int Med Res* 2012;40(2):734–9.
75. Eichenlaub-Ritter U, Vogt E, Yin H, Gosden R. Spindles, mitochondria and redox potential in ageing oocytes. *Reprod Biomed Online* 2004;8(1):45–58.
76. Bentov Y, Yavorska T, Esfandiari N, Jurisicova A, Casper RF. The contribution of mitochondrial function to reproductive aging. *J Assist Reprod Genet* 2011;28(9):773–83.
77. Wilding M, Dale B, Marino M, di Matteo L, Alviggi C, Pisaturo ML, et al. Mitochondrial aggregation patterns and activity in human oocytes and preimplantation embryos. *Human Reproduction* 2001;16(5):909–17.
78. Boucrot L, Bris C, Seegers V, Goudenège D, Desquret-Dumas V, Domin-Bernhard M, et al. Deep sequencing shows that oocytes are not prone to accumulate mtDNA heteroplasmic mutations during ovarian ageing. *Hum Reprod* 2017;32(10):2101–9.
79. Lan Y, Zhang S, Gong F, Lu C, Lin G, Hu L. The mitochondrial DNA copy number of cumulus granulosa cells may be related to the maturity of oocyte cytoplasm. *Hum Reprod* 2020;35(5):1120–9.
80. Nagano M, Katagiri S, Takahashi Y. ATP content and maturational/developmental ability of bovine oocytes with various cytoplasmic morphologies. *Zygote* 2006;14(4):299–304.
81. Fontana J, Martínková S, Petr J, Žalmanová T, Trnka J. Metabolic cooperation in the ovarian follicle. *Physiol Res* 2020;69(1):33–48.
82. Ogino M, Tsubamoto H, Sakata K, Oohama N, Hayakawa H, Kojima T, et al. Mitochondrial DNA copy number in cumulus cells is a strong predictor of obtaining good-quality embryos after IVF. *J Assist Reprod Genet* 2016;33(3):367–71.
83. Desquret-Dumas V, Clément A, Seegers V, Boucrot L, Ferré-L'Hotellier V, Bouet PE, et al. The mitochondrial DNA content of cumulus granulosa cells is linked to embryo quality. *Hum Reprod* 2017;32(3):607–14.

84. Cinco R, Digman MA, Gratton E, Luderer U. Spatial Characterization of Bioenergetics and Metabolism of Primordial to Preovulatory Follicles in Whole Ex Vivo Murine Ovary. *Biol Reprod* [Internet] 2016 [cited 2021 Mar 23];95(6). Available from: <https://www.ncbi.nlm.nih.gov/pmc/articles/PMC5315427/>
85. Gardner DK, Lane M, Stevens J, Schoolcraft WB. Noninvasive assessment of human embryo nutrient consumption as a measure of developmental potential. *Fertil Steril* 2001;76(6):1175–80.
86. Leese HJ. Metabolism of the preimplantation embryo: 40 years on. *Reproduction* 2012;143(4):417–27.
87. Leese HJ. History of oocyte and embryo metabolism. *Reprod Fertil Dev* 2015;27(4):567–71.
88. Harvey AJ. Mitochondria in early development: linking the microenvironment, metabolism and the epigenome. *Reproduction* 2019;157(5):R159–79.
89. Chason RJ, Csokmay J, Segars JH, DeCherney AH, Armant DR. Environmental and epigenetic effects upon preimplantation embryo metabolism and development. *Trends in Endocrinology & Metabolism* 2011;22(10):412–20.
90. Gardner DK. Lactate production by the mammalian blastocyst: Manipulating the microenvironment for uterine implantation and invasion? *Bioessays* 2015;37(4):364–71.
91. Houghton FD, Thompson JG, Kennedy CJ, Leese HJ. Oxygen consumption and energy metabolism of the early mouse embryo. *Mol Reprod Dev* 1996;44(4):476–85.
92. Trimarchi JR, Liu L, Porterfield DM, Smith PJS, Keefe DL. Oxidative Phosphorylation-Dependent and -Independent Oxygen Consumption by Individual Preimplantation Mouse Embryos1. *Biology of Reproduction* 2000;62(6):1866–74.
93. Gardner DK, Wale PL, Collins R, Lane M. Glucose consumption of single post-compactation human embryos is predictive of embryo sex and live birth outcome. *Hum Reprod* 2011;26(8):1981–6.
94. Gardner DK, Harvey AJ. Blastocyst metabolism. *Reprod Fertil Dev* 2015;27(4):638–54.
95. Lane M, Gardner DK. Lactate Regulates Pyruvate Uptake and Metabolism in the Preimplantation Mouse Embryo1. *Biology of Reproduction* 2000;62(1):16–22.
96. Chi F, Sharpley MS, Nagaraj R, Roy SS, Banerjee U. Glycolysis-Independent Glucose Metabolism Distinguishes TE from ICM Fate during Mammalian Embryogenesis. *Dev Cell* 2020;53(1):9-26.e4.
97. Kaneko KJ, DePamphilis ML. TEAD4 establishes the energy homeostasis essential for blastocoel formation. *Development* 2013;140(17):3680–90.
98. Kumar RP, Ray S, Home P, Saha B, Bhattacharya B, Wilkins HM, et al. Regulation of energy metabolism during early mammalian development: TEAD4 controls mitochondrial transcription. *Development* [Internet] 2018 [cited 2021 Feb 18];145(19). Available from: <https://dev.biologists.org/content/145/19/dev162644>
99. Zhu M, Zernicka-Goetz M. Living a Sweet Life: Glucose Instructs Cell Fate in the Mouse Embryo. *Dev Cell* 2020;53(1):1–2.
100. Saha B, Ganguly A, Home P, Bhattacharya B, Ray S, Ghosh A, et al. TEAD4 ensures postimplantation development by promoting trophoblast self-renewal: An implication in early human pregnancy loss. *Proc Natl Acad Sci U S A* 2020;117(30):17864–75.
101. Van Blerkom J, Davis PW, Lee J. ATP content of human oocytes and developmental potential and outcome after in-vitro fertilization and embryo transfer. *Hum Reprod* 1995;10(2):415–24.
102. Wakefield SL, Lane M, Mitchell M. Impaired mitochondrial function in the preimplantation embryo perturbs fetal and placental development in the mouse. *Biol Reprod* 2011;84(3):572–80.
103. Leese HJ. Quiet please, do not disturb: a hypothesis of embryo metabolism and viability. *BioEssays* 2002;24(9):845–9.
104. Brison DR, Houghton FD, Falconer D, Roberts SA, Hawkhead J, Humpherson PG, et al. Identification of viable embryos in IVF by non-invasive measurement of amino acid turnover. *Hum Reprod* 2004;19(10):2319–24.
105. Lopes AS, Lane M, Thompson JG. Oxygen consumption and ROS production are increased at the time of fertilization and cell cleavage in bovine zygotes. *Hum Reprod* 2010;25(11):2762–73.
106. Turner K, Martin KL, Woodward BJ, Lenton EA, Leese HJ. Comparison of pyruvate uptake by embryos derived from conception and non-conception natural cycles. *Hum Reprod* 1994;9(12):2362–6.
107. Tejera A, Herrero J, Vilorio T, Romero JL, Gamiz P, Meseguer M. Time-dependent O₂ consumption patterns determined optimal time ranges for selecting viable human embryos. *Fertility and Sterility* 2012;98(4):849-857.e3.
108. Jones GM, Trounson AO, Vella PJ, Thouas GA, Lolatgis N, Wood C. Glucose metabolism of human morula and blastocyst-stage embryos and its relationship to viability after transfer. *Reprod Biomed Online* 2001;3(2):124–32.
109. Ahlström A, Westin C, Wikland M, Hardarson T. Prediction of live birth in frozen–thawed single blastocyst transfer cycles by pre-freeze and post-thaw morphology. *Human Reproduction* 2013;28(5):1199–209.
110. Thompson JG, Brown HM, Sutton-McDowall ML. Measuring embryo metabolism to predict embryo quality. *Reprod Fertil Dev* 2016;28(1–2):41–50.
111. Gilchrist RB, Ritter LJ, Armstrong DT. Oocyte–somatic cell interactions during follicle development in mammals. *Animal Reproduction Science* 2004;82–83:431–46.
112. Gorshinova VK, Tsvirkun DV, Sukhanova IA, Tarasova NV, Volodina MA, Marey MV, et al. Cumulus cell mitochondrial activity in relation to body mass index in women undergoing assisted reproductive therapy. *BBA Clin* 2017;7:141–6.

113. Taugourdeau A, Desquiret-Dumas V, Hamel JF, Chupin S, Boucret L, Ferré-L'Hotellier V, et al. The mitochondrial DNA content of cumulus cells may help predict embryo implantation. *J Assist Reprod Genet* 2019;36(2):223–8.
114. Gardner DK, Wale PL, Collins R, Lane M. Glucose consumption of single post-compaction human embryos is predictive of embryo sex and live birth outcome. *Human Reproduction* 2011;26(8):1981–6.
115. Vergouw CG, Botros LL, Roos P, Lens JW, Schats R, Hompes PGA, et al. Metabolomic profiling by near-infrared spectroscopy as a tool to assess embryo viability: a novel, non-invasive method for embryo selection. *Hum Reprod* 2008;23(7):1499–504.
116. Alm H, Torner H, Löhrke B, Viergutz T, Ghoneim IM, Kanitz W. Bovine blastocyst development rate in vitro is influenced by selection of oocytes by brilliant cresyl blue staining before IVF as indicator for glucose-6-phosphate dehydrogenase activity. *Theriogenology* 2005;63(8):2194–205.
117. Al-Zubaidi U, Liu J, Cinar O, Robker RL, Adhikari D, Carroll J. The spatio-temporal dynamics of mitochondrial membrane potential during oocyte maturation. *Mol Hum Reprod* 2019;25(11):695–705.
118. Conaghan J, Hardy K, Handyside AH, Winston RM, Leese HJ. Selection criteria for human embryo transfer: a comparison of pyruvate uptake and morphology. *J Assist Reprod Genet* 1993;10(1):21–30.
119. Heikal AA. Intracellular coenzymes as natural biomarkers for metabolic activities and mitochondrial anomalies. *Biomark Med* 2010;4(2):241–63.
120. Chance B, Williams GR. RESPIRATORY ENZYMES IN OXIDATIVE PHOSPHORYLATION: I. KINETICS OF OXYGEN UTILIZATION. *Journal of Biological Chemistry* 1955;217(1):383–93.
121. Klaidman LK, Leung AC, Adams JD. High-performance liquid chromatography analysis of oxidized and reduced pyridine dinucleotides in specific brain regions. *Anal Biochem* 1995;228(2):312–7.
122. Dumollard R, Marangos P, Fitzharris G, Swann K, Duchon M, Carroll J. Sperm-triggered [Ca²⁺] oscillations and Ca²⁺ homeostasis in the mouse egg have an absolute requirement for mitochondrial ATP production. *Development* 2004;131(13):3057–67.
123. Tan TCY, Mahbub SB, Campbell JM, Habibalahi A, Campugan CA, Rose RD, et al. Non-invasive, label-free optical analysis to detect aneuploidy within the inner cell mass of the preimplantation embryo. *Human Reproduction* 2022;37(1):14–29.
124. Ghukasyan VV, Heikal AA. *Natural Biomarkers for Cellular Metabolism: Biology, Techniques, and Applications*. CRC Press; 2014.
125. Skala MC, Riching KM, Bird DK, Gendron-Fitzpatrick A, Eickhoff J, Eliceiri KW, et al. In vivo multiphoton fluorescence lifetime imaging of protein-bound and free nicotinamide adenine dinucleotide in normal and precancerous epithelia. *J Biomed Opt* 2007;12(2):024014.
126. Dumollard R, Carroll J, Duchon MR, Campbell K, Swann K. Mitochondrial function and redox state in mammalian embryos. *Semin Cell Dev Biol* 2009;20(3):346–53.
127. Stein LR, Imai S. The dynamic regulation of NAD metabolism in mitochondria. *Trends Endocrinol Metab* 2012;23(9):420–8.
128. Becker W. Fluorescence lifetime imaging—techniques and applications. *J Microsc* 2012;247(2):119–36.
129. Ma N, Mochele NR de, Pham PD, Yoo TY, Cho KWY, Digman MA. Label-free assessment of pre-implantation embryo quality by the Fluorescence Lifetime Imaging Microscopy (FLIM)-phasor approach. *Sci Rep* 2019;9(1):13206.
130. Suhling K, Siegel J, Lanigan PMP, Lévêque-Fort S, Webb SED, Phillips D, et al. Time-resolved fluorescence anisotropy imaging applied to live cells. *Opt Lett* 2004;29(6):584–6.
131. Lakowicz JR. *Principles of Fluorescence Spectroscopy* [Internet]. 3rd ed. Springer US; 2006 [cited 2021 Aug 27]. Available from: <https://www.springer.com/gp/book/9780387312781>
132. Alberts B, Johnson A, Lewis J, Raff M, Roberts K, Walter P. *Molecular Biology of the Cell*. 4th ed. Garland Science; 2002.
133. Bird DK, Yan L, Vrotsos KM, Eliceiri KW, Vaughan EM, Keely PJ, et al. Metabolic Mapping of MCF10A Human Breast Cells via Multiphoton Fluorescence Lifetime Imaging of the Coenzyme NADH. *Cancer Res* 2005;65(19):8766–73.
134. Becker W. *Advanced Time-Correlated Single Photon Counting Techniques* [Internet]. 2005 [cited 2020 Dec 1]; Available from: <https://link.springer.com/book/10.1007/3-540-28882-1>
135. Mertz J. *Introduction to Optical Microscopy* [Internet]. Higher Education from Cambridge University Press. 2019 [cited 2021 Apr 26]; Available from: <https://www.cambridge.org/highereducation/books/introduction-to-optical-microscopy/F6C6318C87732519D7E07BA7A03F0B81>
136. Gadella TWJ, Jovin TM, Clegg RM. Fluorescence lifetime imaging microscopy (FLIM): Spatial resolution of microstructures on the nanosecond time scale. *Biophysical Chemistry* 1993;48(2):221–39.
137. Yang X, Needleman DJ. Coarse-grained model of mitochondrial metabolism enables subcellular flux inference from fluorescence lifetime imaging of NADH. *bioRxiv* 2021;2020.11.20.392225.
138. Hsieh C-S, Chen S-U, Lee Y-W, Yang Y-S, Sun C-K. Higher harmonic generation microscopy of in vitro cultured mammal oocytes and embryos. *Opt Express* 2008;16(15):11574–88.
139. Yu C-H, Langowitz N, Wu H-Y, Farhadifar R, Bragues J, Yoo TY, et al. Measuring microtubule polarity in spindles with second-harmonic generation. *Biophys J* 2014;106(8):1578–87.
140. Sanchez T, Venturas M, Aghvami SA, Yang X, Fraden S, Sakkas D, et al. Combined noninvasive metabolic and spindle imaging as potential tools for embryo and oocyte assessment. *Hum Reprod* 2019;34(12):2349–61.

141. Hardarson T, Ahlström A, Rögberg L, Botros L, Hillensjö T, Westlander G, et al. Non-invasive metabolomic profiling of Day 2 and 5 embryo culture medium: a prospective randomized trial. *Hum Reprod* 2012;27(1):89–96.
142. Campagnola PJ, Loew LM. Second-harmonic imaging microscopy for visualizing biomolecular arrays in cells, tissues and organisms. *Nat Biotechnol* 2003;21(11):1356–60.
143. Guo J, Shi L, Gong X, Jiang M, Yin Y, Zhang X, et al. Oocyte-dependent activation of MTOR in cumulus cells controls the development and survival of cumulus-oocyte complexes. *J Cell Sci* 2016;129(16):3091–103.
144. Mogessie B, Scheffler K, Schuh M. Assembly and Positioning of the Oocyte Meiotic Spindle. *Annual Review of Cell and Developmental Biology* 2018;34(1):381–403.
145. Thomas C, Cavazza T, Schuh M. Aneuploidy in human eggs: contributions of the meiotic spindle. *Biochem Soc Trans* 2021;49(1):107–18.
146. Howe K, FitzHarris G. Recent Insights into Spindle Function in Mammalian Oocytes and Early Embryos¹. *Biology of Reproduction* [Internet] 2013 [cited 2021 Feb 9];89(71, 1–9). Available from: <https://doi.org/10.1095/biolreprod.113.112151>
147. Dumollard R, Ward Z, Carroll J, Duchen MR. Regulation of redox metabolism in the mouse oocyte and embryo. *Development* 2007;134(3):455–65.
148. Zhang X, Wu XQ, Lu S, Guo YL, Ma X. Deficit of mitochondria-derived ATP during oxidative stress impairs mouse MII oocyte spindles. *Cell Res* 2006;16(10):841–50.
149. Shah JS, Venturas M, Sanchez TH, Penzias AS, Needleman D, Sakkas D. FLUORESCENCE LIFETIME IMAGING MICROSCOPY (FLIM) DETECTS DIFFERENCES IN METABOLIC SIGNATURES BETWEEN EUPLOID AND ANEUPLOID HUMAN BLASTOCYSTS. *Fertility and Sterility* 2020;114(3):e76–7.
150. Houghton FD. Energy metabolism of the inner cell mass and trophectoderm of the mouse blastocyst. *Differentiation* 2006;74(1):11–8.
151. Hewitson LC, Leese HJ. Energy metabolism of the trophectoderm and inner cell mass of the mouse blastocyst. *J Exp Zool* 1993;267(3):337–43.
152. de Lima CB, dos Santos EC, Ispada J, Fontes PK, Nogueira MFG, dos Santos CMD, et al. The dynamics between in vitro culture and metabolism: embryonic adaptation to environmental changes. *Sci Rep* 2020;10(1):15672.
153. Brison DR, Sturmey RG, Leese HJ. Metabolic heterogeneity during preimplantation development: the missing link? *Hum Reprod Update* 2014;20(5):632–40.
154. Leese HJ. Metabolic control during preimplantation mammalian development. *Hum Reprod Update* 1995;1(1):63–72.
155. Santos Monteiro CA, Chow DJX, Leal GR, Tan TC, Reis Ferreira AM, Thompson JG, et al. Optical imaging of cleavage stage bovine embryos using hyperspectral and confocal approaches reveals metabolic differences between on-time and fast-developing embryos. *Theriogenology* 2021;159:60–8.
156. Snijders TAB, Bosker RJ. *Multilevel Analysis: An Introduction to Basic and Advanced Multilevel Modeling*. SAGE; 2011.
157. Lorah J. Effect size measures for multilevel models: definition, interpretation, and TIMSS example. *Large-scale Assessments in Education* 2018;6(1):8.
158. Bradley CK, Livingstone M, Traversa MV, McArthur SJ. Impact of multiple blastocyst biopsy and vitrification-warming procedures on pregnancy outcomes. *Fertil Steril* 2017;108(6):999–1006.
159. *Handbook of Biomedical Nonlinear Optical Microscopy* - Barry R. Masters; Peter So - Oxford University Press [Internet]. [cited 2022 Jan 20]; Available from: <https://global.oup.com/academic/product/handbook-of-biomedical-nonlinear-optical-microscopy-9780195162608?cc=us&lang=en&>
160. Rienzi L, Gracia C, Maggiulli R, LaBarbera AR, Kaser DJ, Ubaldi FM, et al. Oocyte, embryo and blastocyst cryopreservation in ART: systematic review and meta-analysis comparing slow-freezing versus vitrification to produce evidence for the development of global guidance. *Hum Reprod Update* 2017;23(2):139–55.
161. Nohales-Córcoles M, Sevillano-Almerich G, Di Emidio G, Tatone C, Cobo AC, Dumollard R, et al. Impact of vitrification on the mitochondrial activity and redox homeostasis of human oocyte. *Hum Reprod* 2016;31(8):1850–8.
162. Moragianni VA, Jones S-ML, Ryley DA. The effect of body mass index on the outcomes of first assisted reproductive technology cycles. *Fertil Steril* 2012;98(1):102–8.

Annex

Compendia of publications acceptance



Departament de Biologia Cel·lular
Fisiologia i Immunologia

RESOLUCIÓ DE PRESENTACIÓ DE LA TESI COM A COMPENDI DE PUBLICACIONS

En la reunió del dia 10 de gener de 2022 de la Comissió Acadèmica del Programa de Doctorat en Biologia Cel·lular, d'acord amb la normativa Acadèmica de la Universitat Autònoma de Barcelona aplicable als Estudis universitaris regulats de conformitat amb el RD 1393/2007, de 29 d'octubre, modificat pel RD 861/2010, de 2 de juliol.

Ha resultat,

- Autoritzar
- No autoritzar

la presentació de la tesi de la Sra. **Marta Venturas Pedro** de títol "*Non-invasive imaging of the metabolic state of human cumulus cells and embryos*" en forma de compendi de publicacions a la Universitat Autònoma de Barcelona.

Ignasi Roig
Coordinador del programa de
Doctorat en Biologia Cel·lular

Bellaterra (Cerdanyola del Vallès), a 10 de gener de 2022

CÒPIA PER A LA PERSONA INTERESSADA

Rights for publication of content in Paper 1

Order Completed

Thank you for your order.

This Agreement between MARTA venturas ("You") and Oxford University Press ("Oxford University Press") consists of your license details and the terms and conditions provided by Oxford University Press and Copyright Clearance Center.

Your confirmation email will contain your order number for future reference.

License Number 5235390378432

[Printable Details](#)

License date Jan 24, 2022

Licensed Content

Licensed Content Publisher Oxford University Press
Licensed Content Publication Human Reproduction
Licensed Content Title Combined noninvasive metabolic and spindle imaging as potential tools for embryo and oocyte assessment
Licensed Content Author Sanchez, Tim; Venturas, Marta
Licensed Content Date Dec 8, 2019
Licensed Content Volume 34
Licensed Content Issue 12

Order Details

Type of Use Thesis/Dissertation
Requestor type Author of this OUP content
Format Print and electronic
Portion Text Extract
Number of pages requested 18
Will you be translating? No

About Your Work

Title Combined noninvasive metabolic and spindle imaging as potential tools for embryo and oocyte assessment
Institution name Universitat autonoma de barcelona
Expected presentation date Mar 2022

Additional Data

Order reference number 1
Portions full manuscript

Requestor Location

MARTA venturas
42 glenwood road apt 2

Tax Details

Publisher Tax ID GB125506730

Requestor Location

SOMERVILLE, MA 02145
United States
Attn: Universitat autonoma de barcelona

Price

Total 0.00 USD

Thank you for your order.

This Agreement between MARTA venturas ("You") and Oxford University Press ("Oxford University Press") consists of your license details and the terms and conditions provided by Oxford University Press and Copyright Clearance Center.

Your confirmation email will contain your order number for future reference.

License Number 5235390488335

[Printable Details](#)

License date Jan 24, 2022

Licensed Content

Licensed Content Publisher Oxford University Press
Licensed Content Publication Human Reproduction
Licensed Content Title Combined noninvasive metabolic and spindle imaging as potential tools for embryo and oocyte assessment
Licensed Content Author Sanchez, Tim; Venturas, Marta
Licensed Content Date Dec 8, 2019
Licensed Content Volume 34
Licensed Content Issue 12

Order Details

Type of Use Thesis/Dissertation
Requestor type Author of this OUP content
Format Print and electronic
Portion Figure/table
Number of figures/tables 6
Will you be translating? No

About Your Work

Title Combined noninvasive metabolic and spindle imaging as potential tools for embryo and oocyte assessment
Institution name Universitat autonoma de barcelona
Expected presentation date Mar 2022

Additional Data

Order reference number 2
Portions all figures

Requestor Location

MARTA venturas
42 glenwood road apt 2

Tax Details

Publisher Tax ID GB125506730

Requestor Location

SOMERVILLE, MA 02145
United States
Attn: Universitat autonoma de barcelona

Price

Total 0.00 USD

Rights for publication of content in Paper 2



Metabolic imaging of human cumulus cells reveals associations among metabolic profiles of cumulus cells, patient clinical factors, and oocyte maturity

Author: Marta Venturas, Xingbo Yang, Kishlay Kumar, Dagan Wells, Catherine Racowsky, Daniel J. Needleman

Publication: Fertility and Sterility

Publisher: Elsevier

Date: December 2021

©2021 Published by Elsevier Inc. on behalf of the American Society for Reproductive Medicine

Journal Author Rights

Please note that, as the author of this Elsevier article, you retain the right to include it in a thesis or dissertation, provided it is not published commercially. Permission is not required, but please ensure that you reference the journal as the original source. For more information on this and on your other retained rights, please visit: <https://www.elsevier.com/about/our-business/policies/copyright#Author-rights>

BACK

CLOSE WINDOW

Rights for publication of content in Paper 3

Order Completed

Thank you for your order.

This Agreement between MARTA venturas ("You") and Oxford University Press ("Oxford University Press") consists of your license details and the terms and conditions provided by Oxford University Press and Copyright Clearance Center.

Your confirmation email will contain your order number for future reference.

License Number 5235390245493

[Printable Details](#)

License date Jan 24, 2022

Licensed Content

Licensed Content Publisher Oxford University Press
Licensed Content Publication Human Reproduction
Licensed Content Title Metabolic state of human blastocysts measured by fluorescence lifetime imaging microscopy
Licensed Content Author Venturas, Marta; Shah, Jaimin S
Licensed Content Date Jan 6, 2022

Order Details

Type of Use Thesis/Dissertation
Requestor type Author of this OUP content
Format Print and electronic
Portion Text Extract
Number of pages requested 20
Will you be translating? No

About Your Work

Title Metabolic state of human blastocysts measured by fluorescence lifetime imaging microscopy
Institution name Universitat autonoma de barcelona
Expected presentation date Mar 2022

Additional Data

Order reference number 1
Portions full manuscript

Requestor Location

MARTA venturas
42 glenwood road apt 2

Tax Details

Publisher Tax ID GB125506730

Requestor Location

SOMERVILLE, MA 02145
United States
Attn: Universitat autonoma de barcelona

\$ Price

Total 0.00 USD

Thank you for your order.

This Agreement between MARTA venturas ("You") and Oxford University Press ("Oxford University Press") consists of your license details and the terms and conditions provided by Oxford University Press and Copyright Clearance Center.

Your confirmation email will contain your order number for future reference.

License Number 5235390576286

[Printable Details](#)

License date Jan 24, 2022

Licensed Content

Licensed Content Publisher Oxford University Press
Licensed Content Publication Human Reproduction
Licensed Content Title Metabolic state of human blastocysts measured by fluorescence lifetime imaging microscopy
Licensed Content Author Venturas, Marta; Shah, Jaimin S
Licensed Content Date Jan 6, 2022

Order Details

Type of Use Thesis/Dissertation
Requestor type Author of this OUP content
Format Print and electronic
Portion Figure/table
Number of figures/tables 8
Will you be translating? No

About Your Work

Title Metabolic state of human blastocysts measured by fluorescence lifetime imaging microscopy
Institution name Universitat autonoma de barcelona
Expected presentation date Mar 2022

Additional Data

Order reference number 4
Portions all figures

Requestor Location

MARTA venturas
42 glenwood road apt 2

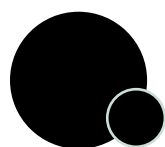
Requestor Location
SOMERVILLE, MA 02145
United States
Attn: Universitat autonoma de barcelona

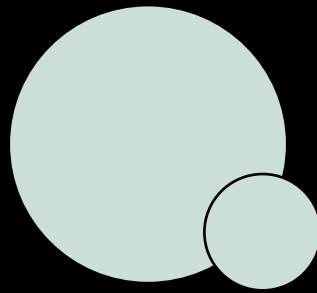
Tax Details

Publisher Tax ID GB125506730

Price

Total 0.00 USD





DOCTORAL THESIS
Non-invasive imaging of the
metabolic state of oocytes, cumulus
cells and embryos

MARTA VENTURAS PEDRO